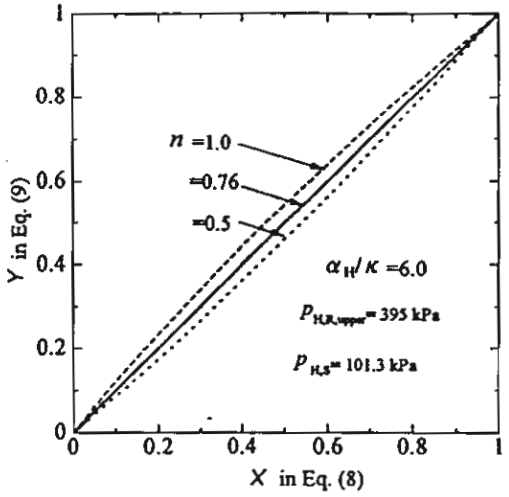

Fig. 1 Linearity of order for PC mode

$$Q_H = \kappa\left\{\left(p_{H,R}/p_0\right)-\left(p_{H,M}/p_0\right)\right\} = \alpha_H\left\{\left(p_{H,M}/p_0\right)^{1/2}-\left(p_{H,S}/p_0\right)^{1/2}\right\} \quad (2)$$

where α_H is the permeability coefficient of hydrogen through the palladium film and κ is the diffusion coefficient of hydrogen through the ceramic support.

From Eq. (2), the pressure of hydrogen at the interface between the palladium film and the membrane support can be solved as

$$\frac{p_{H,M}}{p_0} = \frac{1}{4}\left(\sqrt{\left(\frac{\alpha_H}{\kappa}\right)^2+4\left(\frac{p_{H,R}}{p_0}+\frac{\alpha_H}{\kappa}\left(\frac{p_{H,S}}{p_0}\right)^{1/2}\right)}-\frac{\alpha_H}{\kappa}\right)^2 \quad (3)$$

Hence

$$Q_H\left(p_{H,R},p_{H,S}\right) = \alpha_H\left(\frac{1}{2}\left(\sqrt{\left(\frac{\alpha_H}{\kappa}\right)^2+4\left(\frac{p_{H,R}}{p_0}+\frac{\alpha_H}{\kappa}\left(\frac{p_{H,S}}{p_0}\right)^{1/2}\right)}-\frac{\alpha_H}{\kappa}\right)-\left(\frac{p_{H,S}}{p_0}\right)^{1/2}\right) \quad (4)$$

1.2 PC mode

The material balance for PC mode can be carried out using the same manner as that of CP mode. The hydrogen permeation rate can be expressed as

$$Q_H = \alpha_H\left\{\left(p_{H,R}/p_0\right)^{1/2}-\left(p_{H,M}/p_0\right)^{1/2}\right\} = \kappa\left\{\left(p_{H,M}/p_0\right)-\left(p_{H,S}/p_0\right)\right\} \quad (5)$$

From Eq. (5), the pressure of hydrogen at the interface between the palladium film and the membrane support can be solved as

$$\frac{p_{H,M}}{p_0} = \frac{1}{4}\left(\sqrt{\left(\frac{\alpha_H}{\kappa}\right)^2+4\left(\frac{p_{H,S}}{p_0}+\frac{\alpha_H}{\kappa}\left(\frac{p_{H,R}}{p_0}\right)^{1/2}\right)}-\frac{\alpha_H}{\kappa}\right)^2 \quad (6)$$

Hence

$$Q_H\left(p_{H,R},p_{H,S}\right) = \alpha_H\left(\left(\frac{p_{H,S}}{p_0}\right)^{1/2}-\frac{1}{2}\left(\sqrt{\left(\frac{\alpha_H}{\kappa}\right)^2+4\left(\frac{p_{H,S}}{p_0}+\frac{\alpha_H}{\kappa}\left(\frac{p_{H,R}}{p_0}\right)^{1/2}\right)}-\frac{\alpha_H}{\kappa}\right)\right) \quad (7)$$

2. Results and Discussions

Figure 1 shows one typical result for the PC mode. The parameters were derived from a set of data in the conditions of Umemiya *et al.* (1991). In their study, the pressure of hydrogen in the reaction side was varied from 145 to 395 kPa while the pressure of hydrogen in the sweep side was fixed at 101.3 kPa.

X-axis and Y-axis represent as follows:

$$X = \frac{\left(\frac{p_{H,R}}{p_0}\right)^n-\left(\frac{p_{H,S}}{p_0}\right)^n}{\left(\frac{p_{H,R,upper}}{p_0}\right)^n-\left(\frac{p_{H,S}}{p_0}\right)^n} \quad (8)$$

$$Y = \frac{Q_H\left(p_{H,R},p_{H,S}\right)}{Q_H\left(p_{H,R,upper},p_{H,S}\right)} \quad (9)$$

where $p_{H,R,upper}$ is the upper limit of the pressure of hydrogen in the reaction side (=395 kPa) and $p_{H,S}$ is fixed at 101.3 kPa. $Q_H(p_{H,R}, p_{H,S})$ in the Y-axis can be calculated from Eq. (7) for PC mode.

Three lines in Fig. 1 are drawn by changing the pressure of hydrogen in the reaction side, $p_{H,R}$ from 101.3 to 395 kPa for the order, $n = 0.5$, 0.76 and 1.0, at the relative resistance, $\alpha_H/\kappa = 6.0$. It is seen from Fig. 1 that when the resistance through the ceramic support is six times higher than the resistance through the palladium film, the linearity can hold at $n = 0.76$, which was the value reported by Umemiya *et al.* (1991) who used a composite membrane consisting of thin palladium film (the thickness, 20 μm) supported on the outer surface of a porous glass cylinder (the thickness, 800

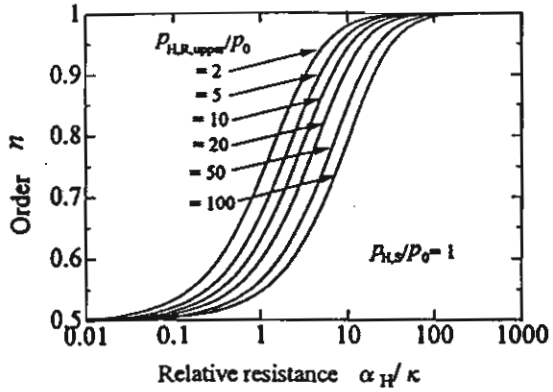

Fig. 2 Relation of order and the relative resistance for CP mode

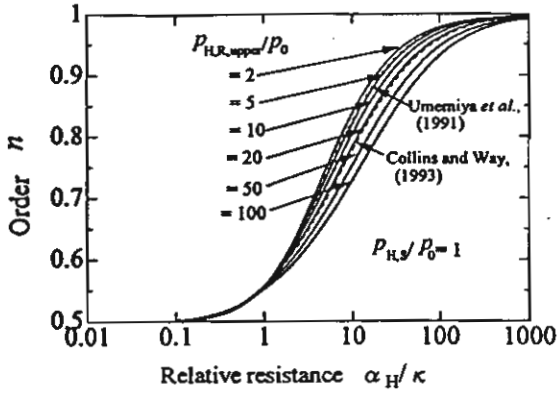

Fig. 3 Relation of order and the relative resistance for PC mode

μm). Here, the presence of resistance from the ceramic support is proposed to be one explanation why the order in some composite membranes may be higher than 0.5. However, measurements of respective resistances may be required to confirm them. Another possibility for the deviation of the apparent order is due to the presence of pinholes on the palladium film or leakage through sealing (Collins and Way, 1993). However, this should be carefully checked by permeation tests with helium gas, and its contribution should be excluded from the experimental results. Therefore, it will not be considered in this paper.

It should be noted that the dependency of pressure of hydrogen on the permeation of hydrogen through the composite membrane can be expressed in Eqs. (4) and (7) for CP and PC modes, respectively. However, the expressions are rather complicated, and it is usually approximated by correlating the experimental results with Eq. (1). The apparent order, n, only shows the best fit parameter for a certain range of experimental results.

The square deviation, Δ, is introduced to determine the linearity.

$$\Delta = \int_{p_{H,S}}^{p_{H,R,upper}} (Y - X)^2 \, dp_{H,R} \qquad (10)$$

where Y and X can be calculated from Eqs. (8) and (9).

The apparent order, n, can be obtained by minimizing the square deviation, Δ, at the specified value of the relative resistance, α_H/κ, within the specified range of pressure of hydrogen. The all-purpose equation solver, EQUATRAN-G (Omega Simulation Co. Ltd) is useful to solve these equations.

Figures 2 and 3 show the relation between n and α_H/κ for CP and PC modes, respectively, for the ranges of interest from $p_{H,S}/p_0$ of 1 to $p_{H,R,upper}/p_0$ at various values of 2, 5, 10, 20, 50 and 100. Two dotted lines in Fig. 3 show the results for experimental conditions of Umemiya *et al.* (1991) and Collins and Way (1993).

In the palladium film controlling region ($\alpha_H/\kappa < 0.01$), the order is naturally 0.5. On the other hand, in the ceramic support controlling region ($\alpha_H/\kappa > 1000$), the order becomes 1.0.

In the transition region ($0.01 < \alpha_H/\kappa < 1000$), the order varies between 0.5 and 1.0. In this region, the pressure of hydrogen at the interface, $p_{H,M}$ in Eq. (3) for CP mode is higher than that in Eq. (6) for PC mode as indicated in Goto *et al.* (to be submitted). This makes the contribution of permeation in ceramic membrane (first order) for CP mode greater than that for PC mode. Therefore, the order n for CP mode is higher than that for PC mode at the same value of α_H/κ.

The relation between n and α_H/κ is dependent on the upper limit of the pressure of hydrogen in the reaction side, $p_{H,R,upper}$.

Once the order can be determined from the linearity of the experimental data at the known range pressure of hydrogen, we can estimate the relative resistance by using Figs. 2 or 3. For example, the relative resistance, α_H/κ may be within 0.95 and 2.5 in the case of Collins and Way (1993), who obtained the apparent order in PC mode, n, in the range of 0.526 and 0.622 for the $p_{H,R,upper}$ of 2445 kPa.

Conclusion

The apparent order of hydrogen pressure on the hydrogen permeation rate through the composite membrane is related to the relative resistance of palladium film and ceramic support. Once the apparent order can be determined from the linearity of experimental data, we can estimate the relative resistance. However, the relation is dependent on the operating conditions.

Acknowledgment

The authors would like to thank NGK INSULATOR LTD, TJTTP-OECF and the Thailand Research Fund.

Nomenclature

$p_{H,M}$	=	pressure of hydrogen at interface between palladium film and ceramic support	[Pa]
$p_{H,R}$	=	pressure of hydrogen in reaction side	[Pa]
$p_{H,S}$	=	pressure of hydrogen in sweep side	[Pa]
p_0	=	standard pressure (=101.3 kPa)	[Pa]
Q_H	=	permeation rate of hydrogen	[mol/s]
α_H	=	permeation rate constant through palladium film	[mol/s]
κ	=	diffusion rate constant through ceramic support	[mol/s]

Literature Cited

Collins, J. P. and J. D. Way; "Preparation and Characterization of a Composite Palladium-Ceramic Membrane," *Ind. Eng. Chem. Res.*, 32, 3006–3013 (1993)

DeRosset, A. J.; "Diffusion of Hydrogen through Palladium Membranes," *Ind. Eng. Chem.*, 52, 525–528 (1960)

Dittmeyer, R., V. Hollein, P. Quicker, G. Emig, G. Hausinger and F. Schmidt; "Factors Controlling the Performance of Catalytic Dehydrogenation of Ethylbenzene in Palladium Composite Membrane Reactors," *Chem. Eng. Sci.*, 54, 1431–1440 (1999)

Goto, S., S. Assabumrungrat, T. Tagawa and P. Praserthdam; "Permeation of Hydrogen through a Composite Palladium Membrane," *J. Membr. Sci.* (to be submitted)

Hurlbert, R. C. and J. O. Konecny; "Diffusion of Hydrogen through Palladium," *J. Chem. Phys.*, 34, 655–658 (1961)

Umemiya, S., N. Sato, H. Ando and E. Kikuchi; "The Water Gas Shift Reaction Assisted by a Palladium Membrane Reactor," *Ind. Eng. Chem. Res.*, 30, 585–589 (1991)

Journal of Chemical Engineering of Japan, Vol. 33, No. 2, pp. 333–336, 2000 **Short Communication**

Application of a Zeolite A Membrane to Reverse Osmosis Process

IZUMI KUMAKIRI, TAKEO YAMAGUCHI AND SHIN-ICHI NAKAO

Department of Chemical System Engineering, The University of Tokyo, Tokyo 113-8656, Japan

Keywords: Zeolite Membrane, Reverse Osmosis (RO), Pervaporation (PV), Liquid Separation

The reverse osmosis process needs no phase transformation during separation, and thus it has a potential in saving energy for liquid mixture separations. Application of reverse osmosis to organic liquid is limited, owing to the lower stability of polymer membranes against organic liquid. Zeolites are inorganic materials having durability against organic liquid and heat, and they show good separation ability in pervaporation. In this study, zeolite membrane was firstly applied to the reverse osmosis process. Zeolite A membrane, having thickness around 5 μm, showed 0.44 rejection from 10wt% ethanol water mixture. The membrane was stable to applied pressures up to 50 kgf cm^{-2}.

Introduction

For liquid mixture separation, much attention has been paid to membrane separation technology because of energy saving. For this purpose, reverse osmosis (RO) and pervaporation (PV) processes can be used. In the RO process, a membrane is placed between liquid feed and liquid permeate. Since the driving force is mainly pressure gradient, high applied pressure should be used to cancel the osmotic pressure effect. In the PV process, on the other hand, liquid feed is vaporized while passing through the membrane and the process thus includes a phase change. This means that the PV process needs additional energy for vaporization. Nakao (1994) showed the advantages of the RO system in energy saving compared with PV and distillation systems in ethanol/water separation.

However, the application of RO to organic mixture separation has been limited because of two problems. One issue is that most RO membranes are made of organic materials, and most of them do not have much resistance to organic liquid. The application of RO is, thus, limited to the separation of aqueous solutions (Ohya *et al.*, 1981). The other is the durability at high pressures. If an inorganic membrane could be applied to RO processes, it will significantly improve the application range of RO separation.

Zeolites are inorganic materials having good stability against organic liquids. The application of zeolite membranes in PV processes has been reported this

Received on October 22, 1999. Correspondence concerning this article should be addressed to I. Kumakiri (E-mail address: izumi@nakao1.t.u-tokyo.ac.jp).

ELSEVIER

Journal of Membrane Science 175 (2000) 19–24

journal of MEMBRANE SCIENCE

www.elsevier.nl/locate/memsci

The effect of direction of hydrogen permeation on the rate through a composite palladium membrane

Shigeo Goto[a,*], Suttichai Assabumrungrat[b], Tomohiko Tagawa[a], Piyasan Praserthdam[b]

[a] *Department of Chemical Engineering, Nagoya University, Chikusa, Nagoya 464-8603, Japan*

[b] *Department of Chemical Engineering, Faculty of Engineering, Chulalongkorn University, Bangkok 10330, Thailand*

Received 1 June 1999; accepted 15 March 2000

Abstract

This paper reports the effect of direction of hydrogen permeation on the rate through a composite palladium membrane. Palladium film is coated on the outer surface of a tubular ceramic support. Permeation rates of hydrogen through the palladium membrane were measured at 573, 673 and 773 K under two modes. The first one is called 'CP mode' in which hydrogen permeates at first through the ceramic support and then through the palladium film. The other mode is called 'PC mode' in which hydrogen permeates in the opposite manner. It was found from the measurements that the permeation rate of hydrogen increased with the increase of temperature and that the permeation rate under CP mode was higher than that under PC mode.

Mathematical models taking into account the combined resistances of both palladium film and ceramic support were developed to describe the hydrogen permeation rate through the composite palladium membrane tube under both modes of permeation. In addition, the mathematical models were used to predict the relative contributions of two resistances for both CP mode and PC mode.

Keywords: Composite palladium membrane; Permeation rate; Hydrogen permeation; Membrane reactor; Resistance model

1. Introduction

Palladium-based membranes have been studied extensively due to their extremely high hydrogen permselectivity and the applications to many reactions [1]. Although the palladium-based membrane reactors have shown the promising improvement of reaction selectivity and yield, the process is still not economically attractive because of high cost, low hydrogen permeation and low chemical stability. Recent studies [2,3] have focused on the use of composite palladium membrane in which a thin film of palladium layer is coated on a porous support such as vycor glass, alumina and stainless steel. The support provides the mechanical strength for the membrane. Since the palladium film in the composite membrane is much thinner than the normal dense membrane, the resulting permeation rate may be significantly improved. An extensive review on the development of composite metal membranes, especially for hydrogen separation was presented by Uemiya [4].

There are two directions of hydrogen permeation through the composite palladium membrane, that is, CP mode (at first through the ceramic support and then

* Corresponding author. Tel.: +81-52-789-3261; fax: +81-52-789-3261.
E-mail address: goto@park.nuce.nagoya-u.ac.jp (S. Goto)

0376-7388/00/$ – see front matter
PII: S0376-7388(00)00405-1

through the palladium film) and PC mode (opposite manner). However, according to our knowledge, no publications have been found on these topics.

In this study, a composite palladium membrane prepared by NGK Insulators Ltd. in Japan was used to investigate the hydrogen permeation rate at 573, 673 and 773 K under these two modes.

Mathematical models taking into account the combined resistances of both palladium film and ceramic support were developed to describe the hydrogen permeation rate through the composite membrane.

2. Experiment

The membrane employed in this study was a tubular configuration. The outer part of ceramic membrane was coated with palladium film. Fig. 1 shows the schematic composition of the membrane supplied by NGK Insulators Ltd. The inner and outer diameters are 6 and 10.6 mm, respectively. The total length of the membrane is 156 mm. The supporting tube made of alumina with 2 mm thickness and 5.0 μm pore size was coated with two alumina layers with pore sizes of 1.0 and 0.5 μm with 0.3 and 0.02 mm thickness, respectively. At the outer surface of the support, palladium film of 0.02 mm thickness was plated. The district interfaces were observed from SEM photographs. The porosity in ceramic layers was about 0.3 independently of pore sizes.

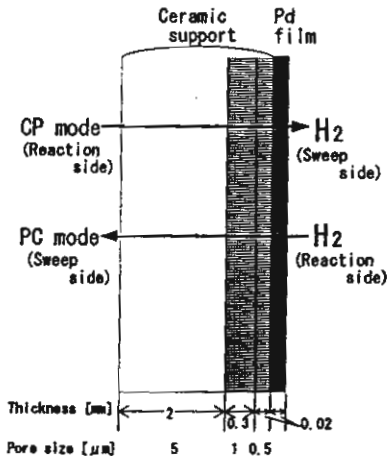

Fig. 1. Schematics of a composite Pd/ceramic membrane.

A needle valve was used to control the inlet gas flow, which was monitored by an orifice meter. The membrane tube was placed in an electric furnace to control the operation temperature. Quartz sand (13.0 g) was packed inside the membrane tube. The outlet flow rate was measured using a soap film meter. There are two modes of operation as shown in Fig. 1. The first one is named 'CP mode' where hydrogen flows inside the membrane tube packed with quartz sand while the pressure in the shell side is reduced by using an aspirator. Therefore, hydrogen can permeate at first through the ceramic support and then through the palladium film. The other is named 'PC mode' where hydrogen is fed into the shell side while the pressure inside the membrane tube is reduced.

The inlet molar flow rate of pure hydrogen in the feed side (reaction side) is $F_{H,R,0}$ and the pressure in the sweep side is $p_{H,S}$. The outlet molar flow rate of hydrogen in the reaction side is $F_{H,R}$. Then, the molar flow rate of permeated hydrogen, Q_H is equal to $F_{H,R,0}-F_{H,R}$.

3. Permeation rate expressions

The mathematical expressions of hydrogen permeation through a composite palladium membrane can be developed using the resistance model taking into account of the combined resistances through both the ceramic support and the palladium film. The expressions for two modes of hydrogen permeation are different and can be formulated as follows.

3.1. CP mode

Let $p_{H,M}$ be the pressure of hydrogen at the membrane interface between the palladium film and ceramic support. Since the transport through the support is mainly governed by the first order with respect to the pressure of hydrogen according to Knudsen diffusion and that through the palladium film is governed by the half order with respect to the pressure of hydrogen, the permeation rate ($Q_{H,CP}$) can be expressed as

$$Q_{H,CP} = \kappa_{CP}\left\{\left(\frac{p_{H,R}}{p_0}\right) - \left(\frac{p_{H,M}}{p_0}\right)\right\} = \alpha_H\left\{\left(\frac{p_{H,M}}{p_0}\right)^{1/2} - \left(\frac{p_{H,S}}{p_0}\right)^{1/2}\right\} \quad (1)$$

where α_H is the permeability coefficient of hydrogen though the palladium film and κ_{CP} is the diffusion coefficient of hydrogen through the ceramic support.

From Eq. (1), the pressure of hydrogen at the interface between the palladium film and the membrane support can be solved as

$$\frac{p_{H,M}}{p_0} = \frac{1}{4}\left(\sqrt{\left(\frac{\alpha_H}{\kappa_{CP}}\right)^2 + 4\left(\left(\frac{p_{H,R}}{p_0}\right) + \frac{\alpha_H}{\kappa_{CP}}\left(\frac{p_{H,S}}{p_0}\right)^{1/2}\right)} - \frac{\alpha_H}{\kappa_{CP}}\right)^2 \quad (2)$$

hence

$$Q_{H,CP} = \alpha_H\left(\frac{1}{2}\left(\sqrt{\left(\frac{\alpha_H}{\kappa_{CP}}\right)^2 + 4\left(\left(\frac{p_{H,R}}{p_0}\right) + \frac{\alpha_H}{\kappa_{CP}}\left(\frac{p_{H,S}}{p_0}\right)^{1/2}\right)} - \frac{\alpha_H}{\kappa_{CP}}\right) - \left(\frac{p_{H,S}}{p_0}\right)^{1/2}\right). \quad (3)$$

3.2. PC mode

The expression for PC mode can be carried out using the same manner as that of CP mode. The hydrogen permeation rate can be expressed as

$$Q_{H,PC} = \alpha_H\left\{\left(\frac{p_{H,R}}{p_0}\right)^{1/2} - \left(\frac{p_{H,M}}{p_0}\right)^{1/2}\right\} = \kappa_{PC}\left\{\left(\frac{p_{H,M}}{p_0}\right) - \left(\frac{p_{H,S}}{p_0}\right)\right\}. \quad (4)$$

From Eq. (4), the pressure of hydrogen at the interface between the palladium film and the membrane support can be solved as

$$\frac{p_{H,M}}{p_0} = \frac{1}{4}\left(\sqrt{\left(\frac{\alpha_H}{\kappa_{PC}}\right)^2 + 4\left(\left(\frac{p_{H,S}}{p_0}\right) + \frac{\alpha_H}{\kappa_{PC}}\left(\frac{p_{H,R}}{p_0}\right)^{1/2}\right)} - \frac{\alpha_H}{\kappa_{PC}}\right)^2 \quad (5)$$

hence

$$Q_{H,PC} = \alpha_H\left(\left(\frac{p_{H,R}}{p_0}\right)^{1/2} - \frac{1}{2}\left(\sqrt{\left(\frac{\alpha_H}{\kappa_{PC}}\right)^2 + 4\left(\left(\frac{p_{H,S}}{p_0}\right) + \frac{\alpha_H}{\kappa_{PC}}\left(\frac{p_{H,R}}{p_0}\right)^{1/2}\right)} - \frac{\alpha_H}{\kappa_{PC}}\right)\right). \quad (6)$$

3.3. Comparison between CP and PC modes

Fig. 2 shows one typical result with $p_{H,R}/p_0=1$, $p_{H,S}/p_0=0.2$ and $\alpha_H=\kappa_{CP}=\kappa_{PC}$. The relative pressure of hydrogen at the interface between the palladium film and the ceramic support, $p_{H,M}/p_0$ can be calculated as 0.64 and 0.50 by using Eqs. (2) and (5) for CP and PC modes, respectively. The ratio of permeation rate for CP mode to PC mode, $Q_{H,CP}/Q_{H,PC}$, can be calculated as 1.20 by using Eqs. (3) and (6). Therefore, the permeation rate for CP mode is higher by 20% than that for PC mode in this case. This is due to the difference in the pressure dependence of the permeation rates between the palladium film (half order) and the ceramic support (first order).

4. Results and discussion

4.1. Permeation rate of hydrogen

Fig. 3 shows experimental data of permeation rate on various relative pressures in the sweep side, $p_{H,S}/p_0$ at three different temperatures, T=573, 673 and 773 K.

As the pressure in the sweep side decreases and the temperature increases, the permeation rate of hydrogen increases. The permeation rate for CP mode is always higher than that for PC mode as expected from Fig. 2.

Solid and broken lines are the results calculated by using Eqs. (3) and (6), respectively, and the values of parameters determined in the next section for CP and PC modes, respectively. Although no replications of

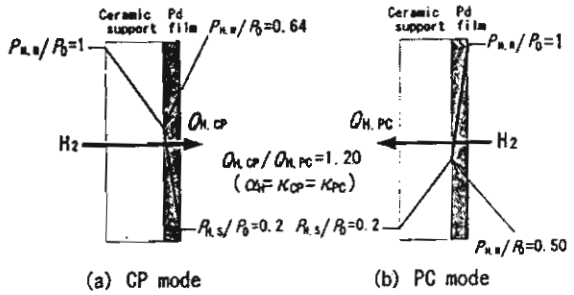

Fig. 2. Comparison between CP and PC modes.

experimental data have been made, these are almost on lines of calculated results.

4.2. Determination of parameters

The permeability coefficient of hydrogen through the palladium film, α_H is given as

$$\alpha_H = D_H C_0 \frac{\pi dz_t}{t_m} \quad (\mathrm{mol/s}) \tag{7}$$

The diffusivity of hydrogen, D_H and the concentration of dissolved hydrogen, C_0 are adopted from Adballa and Elnashaie [5] and Hermann et al. [3].

$$D_H = 2.30 \times 10^{-7} \exp\left(\frac{-21700}{R_g T}\right) \quad (\mathrm{m^2/s}) \tag{8}$$

$$C_0 = 3.03 \times 10^5 T^{1.0358} \quad (\mathrm{mol/m^3}) \tag{9}$$

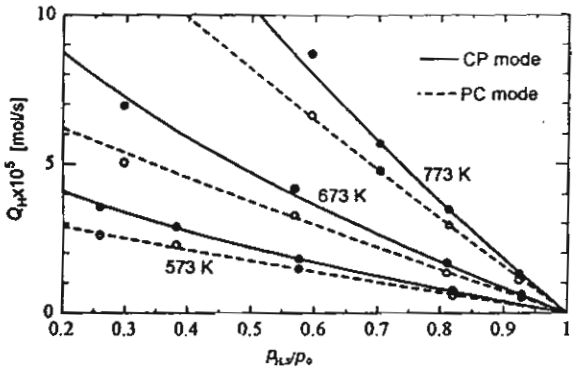

Fig. 3. Permeation rate of hydrogen for CP and PC modes.

Table 1
Determined values of parameters

T (K)	$\alpha_H \times 10^4$ (mol/s)	$\kappa_{CP} \times 10^4$ (mol/s)	$\kappa_{PC} \times 10^4$ (mol/s)	α_H/κ_{PC}	κ_{CP}/κ_{PC}
573	2.63	0.623	0.498	5.28	1.25
673	4.38	1.45	1.08	4.06	1.34
773	6.10	5.36	3.56	1.71	1.51

The diffusion of hydrogen through the ceramic support may include both Knudsen diffusion and viscous bulk flow. Since the structure of the ceramic support is complicated as shown in Fig. 1, the estimation of diffusion coefficient may be difficult. Therefore, the diffusion coefficients of hydrogen through the ceramic support for CP and PC modes, κ_{CP} and κ_{PC} are adjusted by curve fittings of Fig. 3 with Eqs. (3) and (6) for CP and PC modes, respectively.

Table 1 summarizes the determined values of parameters. The ratio, α_H/κ_{PC} is greater than unity. This means that the diffusion resistance through the ceramic support is higher than that through the palladium film. The ratio, κ_{CP}/κ_{PC} is also greater than unity. The difference between κ_{CP} and κ_{PC} may be explained by the asymmetric configuration of the ceramic support as shown in Fig. 1. The direction of permeation should affect the permeation rate through the asymmetric ceramic support. It is suggested from our preliminary estimation that the direction from coarse to fine pores has higher permeation rates than the opposite direction when both Knudsen diffusion and viscous bulk flow dominate.

4.3. The effect of the relative resistance on the relative permeation rate

Fig. 4 shows the effect of the ratio of rate constants, α_H/κ_{PC} on the ratio of permeation rates, $Q_{H,CP}/Q_{H,PC}$ for the values of κ_{CP}/κ_{PC}=1.0 and 1.2. The relative pressure in the sweep side, $p_{H,S}/p_0$ is changed from 0 to 0.8. The lower pressure in the sweep side enhances the effect of the direction of permeation.

When both resistances through the palladium film and the ceramic support are comparative ($0.1 < \alpha_H/\kappa_{PC} < 10$), the effect of the relative pressure in the sweep side, $p_{H,S}/p_0$ on the ratio of $Q_{H,CP}/Q_{H,PC}$

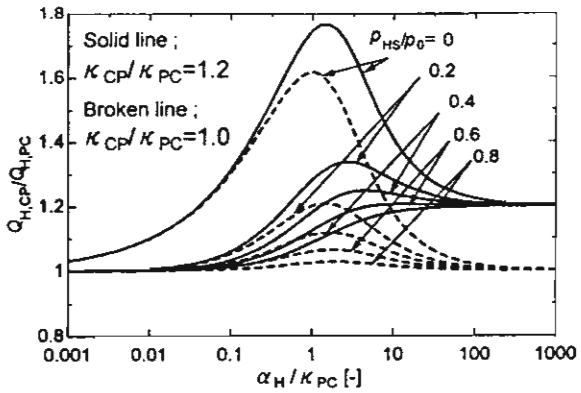

Fig. 4. The effect of the relative resistance on the relative permeation rate at κ_{CP}/κ_{PC}=1.0 and 1.2.

is significant. CP mode is always superior to PC mode.

When the resistance through the palladium film is much greater than that through the ceramic support ($\alpha_H/\kappa_{PC}<0.01$), the permeation through palladium membrane dominates and $Q_{H,CP}/Q_{H,PC}$ value reached to unity. In this case, the direction of permeation is not important.

On the other hand, when the resistance through the ceramic support is much greater than that through the palladium film ($\alpha_H/\kappa_{PC}>100$), the permeation rate of hydrogen is controlled by the resistance through the ceramic support. Therefore, the $Q_{H,CP}/Q_{H,PC}$ value reached to the value of κ_{CP}/κ_{PC}.

5. Conclusions

The permeation rate through a composite palladium membrane was affected by the direction of hydrogen permeation. The first one is 'CP mode'. The other mode is 'PC mode'. It was found from the experimental results that the permeation rate of hydrogen increased with the increase of temperature and that the permeation rate under the CP mode in which hydrogen permeates at first through the ceramic support and then through palladium film was higher than the permeation rate under the PC mode in which hydrogen permeates in the opposite manner. The difference in the permeation rate between two modes indicated the effect of resistance of the support on the hydrogen permeation through the asymmetric composite palladium membrane.

The mathematical model was used to predict the relative resistances of palladium film and ceramic support for both CP mode and PC mode.

6. Nomenclature

C_0	concentration of dissolved hydrogen (mol/m^3)
D_H	diffusivity of hydrogen (m^2/s)
d	outer diameter of membrane tube (m)
$F_{H.R.0}$	molar flow rate of hydrogen in the feed (mol/s)
$F_{H.R}$	molar flow rate of hydrogen in the exit (mol/s)
$p_{H.M}$	pressure at the interface between palladium film and ceramic support (Pa)
$p_{H.R}$	pressure in the reaction side (Pa)
$p_{H.S}$	pressure in the sweep side (Pa)
p_0	standard pressure (=1.013×10^5 Pa) (Pa)
$Q_{H.CP}$	permeation rate of hydrogen for CP mode (mol/s)
$Q_{H.PC}$	permeation rate of hydrogen for PC mode (mol/s)
R_g	gas constant (=8.314 J/(mol K)) (J/(mol K))
T	temperature (K)
t_m	thickness of palladium film (m)
z_t	total length of membrane tube (m)

Greek symbols

α_H	permeation rate constant through palladium film (mol/s)
κ_{CP}	diffusion rate constant through ceramic support for CP mode (mol/s)
κ_{PC}	diffusion rate constant through ceramic support for PC mode (mol/s)

Acknowledgements

The authors would like to thank NGK Insulator Ltd., JSPS, TJTTP-OECF and the Thailand Research Fund for the support and Mr. Isao Takakuwa and Mr. Hajime Itoh for their experimental help.

References

[1] J. Hu, B.P.A. Grandjean, A. Van Neste, S. Kaliaguine, Catalytic palladium-based membrane reactors: a review, Can. J. Chem. Eng. 69 (1991) 1036.

[2] J.P. Collins, J.D. Way, Preparation and characterization of a composite palladium-ceramic membrane, Ind. Eng. Chem. Res. 32 (1993) 3006.

[3] C. Hermann, P. Quicker, R. Dittmer, Mathematical simulation of catalytic dehydrogenation of ethylbenzene to styrene in a composite palladium membrane reactor, J. Membr. Sci. 136 (1997) 161.

[4] S. Uemeya, State of the art of supported metal membranes for gas separation, Sep. Purif. Method 28 (1999) 51.

[5] B.K. Adballa, S.S.H. Elnashaie, Catalytic dehydrogenation of ethylbenzene in membrane reactor, AIChE J. 40 (1994) 2055.

Submission of papers: Papers may be submitted in quadruplicate to the following Editors on the basis of geographic location or area of expertise:

W.J. Koros – gas separation, membrane formation, vapor and reverse osmosis
K.W. Böddeker – liquid separation, bioseparations, dialysis, pervaporation
A.G. Fane – micro-, ultra- and nanofiltration, fouling, porous membranes, engineering
S. Nakao – inorganic membranes, micro- and ultrafiltration, fouling

Electronic manuscripts: Electronic manuscripts have the advantage that there is no need for the rekeying of text, thereby avoiding the possibility of introducing errors and resulting in reliable and fast delivery of proofs.

For the initial submission of manuscripts for consideration, hardcopies are sufficient. For the processing of *accepted papers*, electronic versions are preferred. After *final acceptance*, your disk plus one final and exactly matching printed version should be submitted together. Double density (DD) or high density (HD) diskettes (3.5 or 5.25 inch) are acceptable. It is important that the file saved is in the native format of the wordprocessor program used. Label the disk with the name of the computer and wordprocessing package used, your name, and the name of the file on the disk.

For detailed instructions to authors (including submission of manuscripts on floppy disks) contact one of the editors or the publisher. The instructions can be found in *Journal of Membrane Science*, Vol. 163, pp. 155–157, and also on the World Wide Web: access under http://www.elsevier.nl or http://www.elsevier.com.

Proofs and reprints: Authors will receive **proofs,** which they are requested to correct and return as soon as possible. No new material may be inserted in the text at the time of proofreading. A total of **50 reprints** of each paper will be supplied free of charge to the author(s). Additional copies can be ordered at prices shown on the reprint order form.

All questions arising after acceptance of the manuscript, especially those relating to proofs, should be directed to *Journal of Membrane Science*, Elsevier Science Ireland Ltd., Elsevier House, Brookvale Plaza, East Park, Shannon, Co.Clare, Ireland, Tel. (+353-61) 709600, Fax (+353-61) 709100/709101, E-mail: r.sweeney@elsevier.ie

Journal of Membrane Science **has no page charges.**

Publication information: *Journal of Membrane Science* (ISSN 0376-7388). For 2000, volumes 163–177 are scheduled for publication. Subscription prices are available upon request from the Publisher or from the Regional Sales Office nearest you or from this journal's website (http://www.elsevier.nl/locate/memsci). Further information is available on this journal and other Elsevier Science products through Elsevier's website: (http://www.elsevier.nl). Subscriptions are accepted on a prepaid basis only and are entered on a calendar year basis. Issues are sent by standard mail (surface within Europe, air delivery outside Europe). Priority rates are available upon request. Claims for missing issues should be made within six months of the date of dispatch.

Orders, claims, and product enquiries: please contact the Customer Support Department at the Regional Sales Office nearest you:
New York: Elsevier Science, PO Box 945, New York, NY 10159-0945. USA; phone: (+1) (212) 633 3730 [toll free number for North American customers: 1-888-4ES-INFO (437-4636)]; fax: (+1) (212) 633 3680; e-mail: usinfo-f@elsevier.com
Amsterdam: Elsevier Science, PO Box 211, 1000 AE Amsterdam, The Netherlands; phone: (+31) 20 4853757; fax: (+31) 20 4853432; e-mail: nlinfo-f@elsevier.nl
Tokyo: Elsevier Science, 9-15, Higashi-Azabu 1-chome, Minato-ku, Tokyo 106-0044, Japan; phone: (+81) (3) 5561 5033; fax: (+81) (3) 5561 5047; e-mail: info@elsevier.co.jp
Singapore: Elsevier Science, No. 1 Temasek Avenue, #17-01 Millenia Tower, Singapore 039192; phone: (+65) 434 3727; fax: (+65) 337 2230; e-mail: asiainfo@elsevier.com.sg
Rio de Janeiro: Elsevier Science, Rua Sete de Setembro 111/16 Andar, 20050-002 Centro, Rio de Janeiro - RJ, Brazil; phone: (+55) (21) 509 5340; fax: (+55) (21) 507 1991; e-mail: elsevier@campus.com.br [Note (Latin America): for orders, claims and help desk information, please contact the Regional Sales Office in New York as listed above]

Advertising Information: Advertising orders and enquiries can be sent to: **USA, Canada and South America:** Mr Tino DeCarlo, The Advertising Department, Elsevier Science Inc., 655 Avenue of the Americas, New York, NY 10010-5107, USA; phone: (+1) (212) 633 3815; fax: (+1) (212) 633 3820; e-mail: t.decarlo@elsevier.com. **Japan:** The Advertising Department, Elsevier Science K.K., 9-15 Higashi-Azabu 1-chome, Minato-ku, Tokyo 106-0044, Japan; phone: (+81) (3) 5561 5033; fax: (+81) (3) 5561 5047. **Europe and ROW:** Rachel Leveson-Gower, The Advertising Department, Elsevier Science Ltd., The Boulevard, Langford Lane, Kidlington, Oxford OX5 1GB, UK; phone: (+44) (1865) 843565; fax: (+44) (1865) 843976; e-mail: r.leveson-gower@elsevier.co.uk.

USA mailing notice: *Journal of Membrane Science* (ISSN 0376-7388) is published semi-monthly with additional issues in January, April, July and October by Elsevier Science B.V. (P.O. Box 211, 1000 AE Amsterdam, The Netherlands). Annual subscription price in the USA US$ 4574.00 (valid in North, Central and South America), including air speed delivery. Application to mail at periodical postage rate is pending at Jamaica, NY 11431.
USA POSTMASTER: Send address changes to *Journal of Membrane Science*, Publications Expediting Inc., 200 Meacham Avenue, Elmont, NY 11003.
AIRFREIGHT AND MAILING in the USA by Publications Expediting Inc., 200 Meacham Avenue, Elmont, NY 11003.

♾ The paper used in this publication meets the requirements of ANSI/NISO Z39.48-1992 (Permanence of Paper).

PRINTED IN THE NETHERLANDS

JOURNAL OF MATERIALS SCIENCE LETTERS 19, 2000, 1439–1443

Synthesis of large-surface area silica-modified titania ultrafine particles by the glycothermal method

S. IWAMOTO
Department of Energy and Hydrocarbon Chemistry, Graduate School of Engineering, Kyoto University, Sakyo-ku, Kyoto 606-8501, Japan

W. TANAKULRUNGSANK
Department of Chemical Technology, Rajamangala Institute of Technology, 2 Nanglinchee RD, Yannawa Bangkok 10120, Thailand

M. INOUE
Department of Energy and Hydrocarbon Chemistry, Graduate School of Engineering, Kyoto University, Sakyo-ku, Kyoto 606-8501, Japan

K. KAGAWA
The Kansai Electric Power Company, INC., 3-11-20 Nyakuoji, Amagasaki 661, Japan

P. PRASERTHDAM
Department of Chemical Engineering, Faculty of Engineering, Chulalongkorn University, Phayathai RD, Bangkok 10330, Thailand

The preparation of titania is the subject of considerable interest because this material is widely used as catalyst supports for the selective catalytic reduction (SCR) of NOx with ammonia [1] and the selective oxidation of hydrocarbons [2], and as photocatalysts for various reactions [3]. Besides catalytic applications, it also has many uses such as pigment, filler, more recently, membrane and anti-reflection coating. Surface area is one of the important factors for the use of titania as catalyst materials. However, large-surface area materials have high tendency for sintering because of their surface energies. Amorphous titania having extremely large surface area has been prepared by sol-gel methods [4–6]; however, it crystallizes into anatase at around 500 °C, which is accompanied by a marked decrease in surface area [6–8]. Since thermal stability seriously affects the catalyst life, titania having large surface area with reasonable thermal stability has been sought. Thus, many studies have been devoted to improve the thermal stability of titania using additives such as Al [8, 9], Si [10, 11], La [12, 13] and others [14–16]. The effects of these additives are quite different by the procedures of the doping and the amounts of the additives, and the mechanisms for the stabilization effects of these dopants are not yet fully elucidated. One possible method for the preparation of thermally stable titania seems to be direct synthesis of well-crystallized materials. One of the authors has examined the thermal reaction of metal alkoxides in glycols (glycothermal reaction) or other organic media and demonstrated that a number of novel or characteristic crystalline products can be obtained directly without bothersome procedures such as purification of the reactants or handling in inert atmosphere to exclude the effect of moisture [17–21]. By applying this method, nanocrystalline anatases having large surface areas (>50 m^2/g after calcination at 550 °C) were obtained by the reaction of $TiO(acac)_2$ in toluene [22, 23]. Further optimization of the reaction conditions and careful choice of the titanium source and organic solvent provided anatase nanocrystals having an extremely large surface area (>100 m^2/g after calcination at 550 °C) [24]. However, transformation of anatase into rutile took place in the temperature range of 600–1000 °C resulting in drastic decrease in surface area. To improve the thermal stability of titania, we prepared the silica-modified titanias by the glycothermal method and found that these materials had quite large surface areas and exhibited high thermal stabilities.

Titanium tetraisopropoxide (TIP; 25 g) and an appropriate amount of tetraethyl orthosilicate (TEOS, Si/Ti atomic ratio of 0–0.50) were added to 100 ml of 1,4-butanediol, and this mixture was placed in a 300 ml autoclave. After the atmosphere inside the autoclave was replaced with nitrogen, the mixture was heated at a rate of 2.3 °C/min to a desired temperature (200–300 °C) and kept at that temperature for 2 h. After the assembly was cooled, the resulting powders were collected by centrifugation, washed with methanol or ammoniacal methanol and air-dried. The calcination of the thus-obtained product was carried out in a box furnace in air: the product was heated at a rate of 10 °C/min to a desired temperature and kept at that temperature for 30 min. Powder X-ray diffraction (XRD) patterns were recorded on a Shimadzu XD-D1 diffractometer using CuK_α radiation and a carbon-monochrometer. The crystallite size was calculated by the Scherrer equation from the half-height width of the (101) diffraction peak of anatase after correction for the instrumental broadening. Simultaneous thermogravimetric and differential thermal analyses (TGA and DTA) were performed on a Shimadzu DTG-50 thermal analyzer at a heating rate

0261–8028

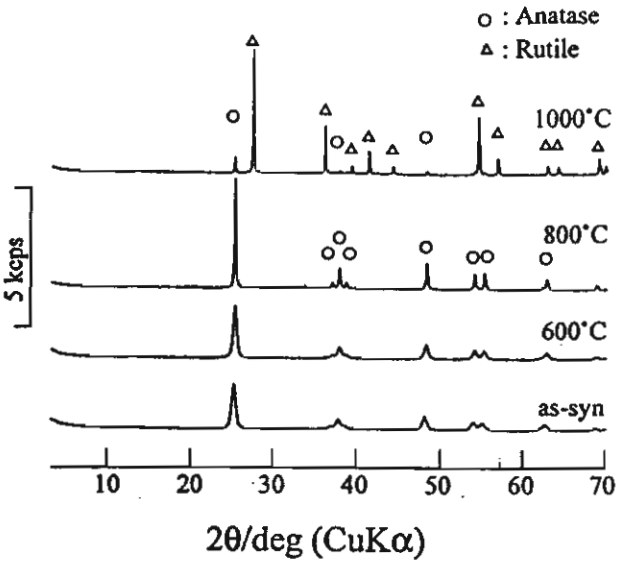

Figure 1 XRD patterns of the product obtained by the reaction of titanium tetraisopropoxide in 1,4-butanediol at 300 °C and the samples obtained by calcination thereof at the temperatures specified in the figure.

of 10 °C/min in a 40 ml/min flow of dried air. The specific surface area was calculated using the BET single-point method on the basis of the nitrogen uptake measured at 77 K using a Micromeritics Flowsorb II 2300. X-ray photoelectron spectroscopy (XPS) measurement was performed on an ULVAC-PHI Model 5500 spectrometer with 15 kV–400 W MgK_α emission as the X-ray source. NH_3 temperature-programmed desorption (NH_3-TPD) profiles were obtained on a Bel Japan TPD-1-AT with a Q-MASS detector.

The XRD pattern of the product obtained by the reaction of TIP alone at 300 °C (Fig. 1) showed that anatase was directly crystallized by the reaction. The crystallite size calculated by the XRD broadening was 17 nm. The average particle size determined from the transmission electron micrograph of the product (Fig. 2) was 17 nm, which is in good agreement with the crystallite size, indicating that each primary particle observed by TEM is a single crystal of anatase. BET surface area of the product was 91.5 m^2/g. When one assumes that each particle is truly spherical, the surface area calculated from the particle size is 90.5 m^2/g, suggesting that each particle of the product exposes its outer surface to the adsorbate, nitrogen. The product preserved relatively large surface area even after calcination at high temperatures. The anatase-rutile transformation began at around 1000 °C. This transformation temperature is much higher than that of the titania prepared by the hydrazine method [25], and as high as that of the titania prepared by the non-hydrous sol-gel method [26], suggesting that the product prepared by the glycothermal method has high crystallinity.

The XRD patterns of the products obtained with addition of TEOS revealed that all the products had the anatase structure (Fig. 3) and that the peak intensities were not affected by the TEOS content in the reaction mixture. This result shows a sharp contrast against the titanias synthesized by other methods, where the peak intensities of anatase decreased with the increase in the silica content due to formation of amorphous phases [25, 27]. The surface areas and crystallite sizes of the products are summarized in Table I. With the increase of the amounts of TEOS added, the surface area increased and the crystallite size decreased.

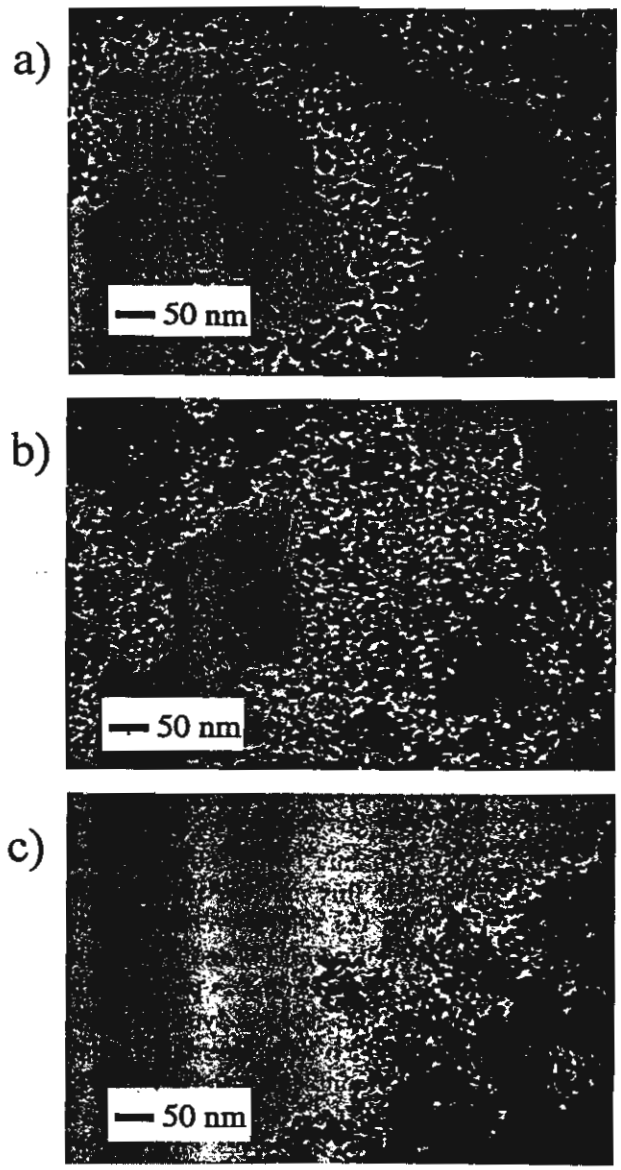

Figure 2 TEM images of products synthesized by the glycothermal reaction of titanium tetraisopropoxide and tetraethyl orthosilicate with the charged ratio of: a) Si/Ti = 0, b) Si/Ti = 0.01, c) Si/Ti = 0.10.

The effect of the reaction temperature was examined by fixing the Si/Ti ratio at 0.10. The reaction at 230–250 °C also afforded products having the anatase structure. The products had larger surface areas as well as smaller crystallite sizes than the product obtained by the 300 °C reaction. When these products were calcined, however, surface areas decreased drastically as compared with the 300 °C product. When the reaction was carried out at 200 °C, a transparent viscous solution was obtained without formation of any solid product. On addition of drops of water into the solution, white precipitates immediately formed. Therefore, this solution contained titanium and silicon in the form of alkoxides or more probably glycoxides.

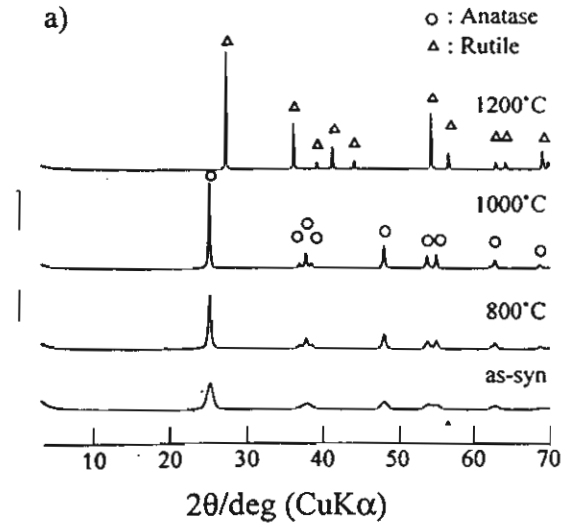

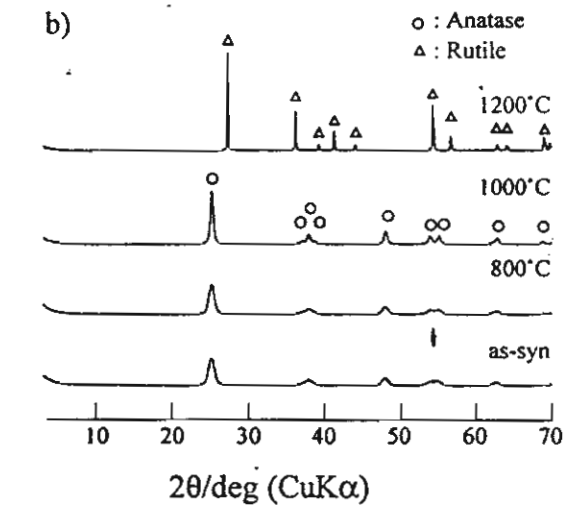

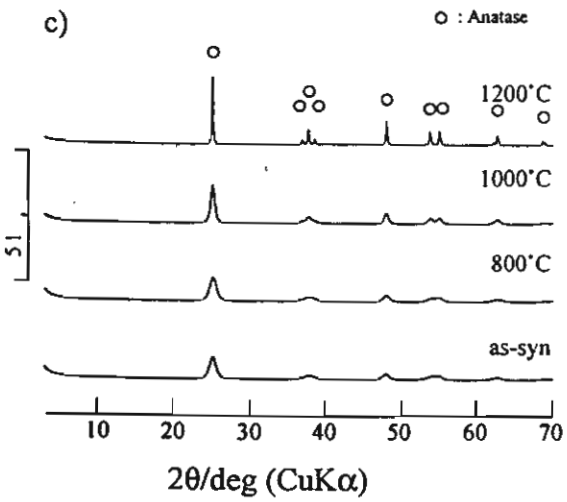

3 XRD patterns of the products by the reaction of titanium isopropoxide and tetraethyl orthosilicate with the charged ratio of: i/Ti = 0.02; b) Si/Ti = 0.10; c) Si/Ti = 0.20; in 1,4-butanediol at and the samples obtained by calcination thereof at the temperaecified in the figure.

; 4 shows the relation between surface area and stallite size of all the samples prepared in this work. surface area was inversely proportional to the allite size. Because the datum for the titania sample

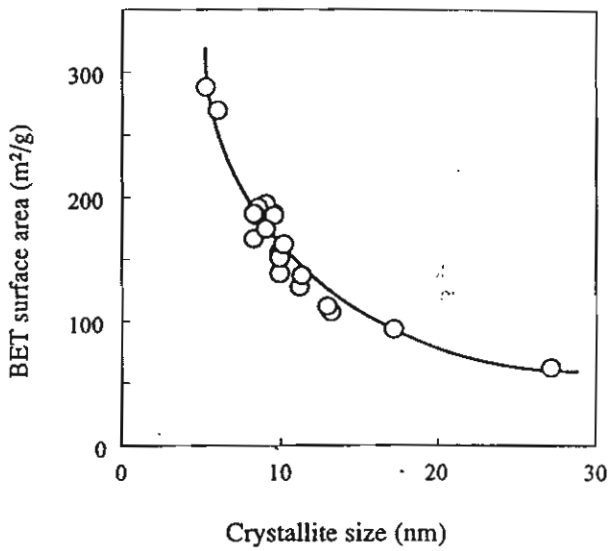

Figure 4 Relation between surface area and crystallite size of the samples obtained by the glycothermal method.

prepared without the addition of TEOS is also included in the plot, the relation indicates that all the crystallites of the products are well dispersed.

The XRD patterns of the products after calcination are shown in Fig. 3. A small amount of TEOS added to the reaction mixture caused the anatase-rutile phase transformation to shift markedly toward higher temperatures, and the samples with the silica content higher than 0.20 preserved the anatase structure even after calcination at 1200 °C for 30 min. Changes in BET surface area and crystallite size by calcination are also shown in Table I. Apparently, the grain growth of anatase was retarded with increasing the amount of TEOS added. Even after calcination at 1000 °C, the products with the Si/Ti >0.20 maintained BET surface areas of >70 m^2/g and crystallite size of <20 nm. To the best of our knowledge, the present product maintained the highest surface area at higher temperatures of the titania-based materials reported so far.

Thermal analysis of the product obtained without the TEOS addition showed 1.5% weight loss from 200 to 600 °C which is associated with an exothermic peak in DTA. This peak is attributed to the combustion of the organic species on the surface of the product. The TG-DTA profiles of the products with the Si/Ti ratio of 0.01–0.06 were similar to that of the product obtained without the TEOS addition. However, this exothermic peak was not observed for the products with Si/Ti of >0.10. This result indicates the decrease of the amount of the surface organic species and suggests the change of surface property. The XPS analysis revealed that the surface compositions of the samples calcined at 600 °C were rich in Si as compared with the charged Si/Ti ratios. With increasing the calcination temperature, the surface composition became more Si-rich. This indicates that Si ions in the products migrate towards the surface of the particles by calcination at high temperatures.

Fig. 5 shows NH_3-TPD profiles of the products. With the increase of Si content, the total amount of adsorbed ammonia increased, but acid-site population based on

TABLE I BET surface area and crystallite size of product synthesized by the glycothermal method and the sample calcined at various temperatures

Charged Si/Ti ratio	Reaction temperature (°C)	S_{BET}[a] (m^2/g)				d_{101}[b] (nm)			
		300 °C	600 °C	800 °C	1000 °C	300 °C	600 °C	800 °C	1000 °C
0	300	91.5	62.1	12.3	2.3	17	22	95	320
0.01	300	138	102	44.6	13.8	10	13	37	120
0.02	300	154	128		16.8	10	11	28	85
0.04	300	150	145	96.0	29.5	10	10	16	48
0.06	300	174	169	112	36.4	9.1	9.1	12	37
0.10	300	161	157	124	49.5	10		11	26
0.15	300	186		111	54.5	9.7		10	21
0.20	300	194	189	168	71.9	9.1		9.2	17
0.30	300	191	185	168	83.8	8.7		8.8	14
0.50	300	166	168	151	79.3	8.4		8.6	16
0.10	270	185			39.0	9.6		11	33
0.10	250	288	240	117	34.4	5.4		10	33
0.10	230	268	200	95.9	14.7	6.1		11	44
0.10	200	—				—			

[a]BET surface area.
[b]Crystallite size of anatase calculated from the 101 diffraction peak.

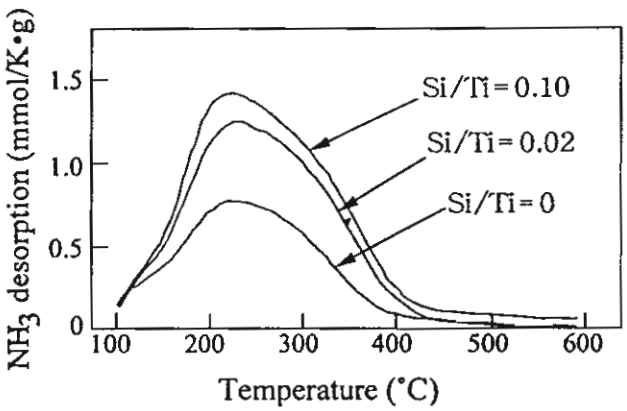

Figure 5 NH_3-TPD profiles of the silica-modified titanias synthesized by the glycothermal method.

a unit surface area rather decreased. Silica modification did not alter the acid strength. These results show a sharp contrast against the acid properties of amorphous TiO_2-SiO_2. Tanabe *et al.* reported that amorphous TiO_2-SiO_2 samples prepared by a coprecipitation method had higher acid strength and much larger number of acid sites than TiO_2. Therefore, the results of Figure 5 suggest the absence of amorphous TiO_2-SiO_2 layer in the present sample. TEM images (Fig. 2b, c) of the silica-modified titania samples as well did not show any indication of the amorphous phase. The presence of Si in the titania lattice seems to contribute to the deceleration of the grain growth of anatase and the suppression of anatase-rutile transformation. Further experiments are in progress to elucidate the mechanism of the surface stabilization of titania by the silica modification.

In conclusion, silica-modified titanias with various silica contents were directly synthesized by the reaction of TIP and TEOS in 1,4-butanediol. The products possessed significantly large surface areas with small crystallite sizes, and exhibited remarkable thermal stabilities.

Acknowledgment

This work was funded in part by The Thailand Research Fund.

References

1. H. BOSCH and F. JANSSEN, *Catal. Today* **2** (1988) 369.
2. I. E. WACHS, R. Y. SALEH, S. S. CHAN and C. CHERSICH, *Chemtech* (1985) 756.
3. M. R. HOFFMANN, S. T. MARTIN, W. CHOI and D. W. BAHNEMANN, *Chem. Rev.* **95** (1995) 69.
4. M. ZAHARESCU and M. CRISAN, *J. Sol-Gel Sci. Technol.* **8** (1997) 249.
5. G. DAGAN and M. TOMKIEWICZ, *J. Non-Crystl. Solids* **175** (1994) 294.
6. I. A. MONTOYA, T. VIVEROS, J. M. DOMÍNGUEZ, L. A. CANALES and I. SCHIFTER, *Catal. Lett.* **15** (1992) 207.
7. A. HESS and E. KEMNITZ, *Appl. Catal. A: General* **149** (1997) 373.
8. X. DING, L. LIU, X. MA, Z. QI and Y. HE, *J. Mater. Sci. Lett.* **13** (1994) 462.
9. K. P. KUMAR, *Appl. Catal. A: General* **119** (1994) 163.
10. B. M. REDDY, S. MEHDI and E. P. REDDY, *Catal. Lett.* **20** (1993) 317.
11. J. E. SWAIN, M. V. JUSKELIS, J. P. SLANGA, J. G. MILLER, M. UBEROI and N. D. SPENCER, *Appl. Catal. A: General* **139** (1996) 175.
12. R. GOPALAN and Y. S. LIN, *Ind. Eng. Chem. Res.* **34** (1995) 1189.
13. C. A. LEDUC, J. M. CAMPBELL and J. A. ROSSIN, *ibid.* **35** (1996) 2473.
14. G. OLIVERI, G. RAMIS, G. BUSCA and V. S. ESCRIBANO, *J. Mater. Chem.* **3** (1993) 1239.
15. M. K. AKHTAR and S. E. PRATSINIS, *J. Am. Ceram. Soc.* **75** (1992) 3408.
16. A. KUROSAKI and S. OKAZAKI, *Nippon Kagaku Kaishi* (1976) 1821.
17. M. INOUE, H. TANINO, Y. KONDO and T. INUI, *J. Am. Ceram. Soc.* **72** (1989) 352.
18. M. INOUE, H. OTSU, H. KOMINAMI and T. INUI, *J. Mater. Sci. Lett.* **11** (1992) 269.
19. M. INOUE, T. NAKAMURA, H. OTSU, H. KOMINAMI and T. INUI, *Nippon Kagaku Kaishi* (1993) 612.
20. M. INOUE, H. OTSU, H. KOMINAMI and T. INUI, *J. Alloys Comp.* **226** (1995) 146.
21. M. INOUE, T. NISHIKAWA, T. NAKAMURA and T. INUI, *J. Am. Ceram. Soc.* **80** (1997) 2157.

22. M. INOUE, H. KOMIMAMI, H. OTSU and T. INUI, *Nippon Kagaku Kaishi* (1991) 1364.
23. H. KOMINAMI, Y. TAKADA, H. YAMAGIWA, Y. KERA, M. INOUE and T. INUI, *J. Mater. Sci. Lett.* 15 (1996) 197.
24. H. KOMINAMI, J. KATO, Y. TAKADA, Y. DOUSHI, B. OHTANI, S. NISHIMOTO, M. INOUE, T. INUI and Y. KERA, *Catal. Lett.* 46 (1997) 235.
25. M. YOSHINAKA, K. HIROTA and O. YAMAGUCHI, *J. Am. Ceram. Soc.* 80 (1997) 2749.
26. P. ARNAL, R. J. P. CORRIU, D. LECLERCQ, P. H. MUTIN and A. VIOUX, *J. Mater. Chem.* 6 (1996) 1925.
27. M. ITOH, H. HATTORI and K. TANABE, *J. Catal.* 35 (1974) 225.

Received 13 October 1999
and accepted 26 January 2000

Selective Oxidation of Ethanol and 1-Propanol over V-Mg-O/TiO_2 catalyst

Tharathon Mongkhonsi*, Purida Pimanmas, and Piyasan Praserthdam
Department of Chemical Engineering, Faculty of Engineering, Chulalongkorn University, Bangkok 10330 THAILAND.

Ethanol and 1-propanol can be selectively oxidized to ethanal and propanal, respectively, by V-Mg-O catalyst supported on TiO_2 (anatase). Aldehyde yields up to 73% and 66% for ethanal and propanal, respectively, were achieved in the temperature range 573-623 K. The catalyst was rather inactive for the further oxidation of aldehyde products to carboxylic acids.

In the last decade, much attention has been devoted to produce olefins and oxygenates by direct oxidation of light paraffins. There are three main motivations behind these researches. The first one is paraffins are less toxic than aromatics. The second one is paraffins are cheaper than olefins. And the last one is the oxidation reaction is thermodynamically more favorable at lower reaction temperature than dehydrogenation reaction which requires high temperature. Only few, however, could achieve industrial application. An example is the replacement of benzene by butane in maleic anhydride production. The future of the oxidative dehydrogenation of paraffins to olefins is still in doubt since a suitable catalyst has yet to be found. The main problem is the fact that paraffin is rather in active than its respective olefin. A catalyst capable to oxidize paraffin is usually very reactive for the olefin product formed.[1]

Using an alcohol as reactant is another alternative. C_1-C_4 alcohols can be produced by fermentation of agricultural products. Although the alcohol obtained from fermetation process has low concentration, the possibility to convert this low concentration feed to a more expansive product exists. In this study the gas phase oxidation process is selected since this process operates at low reactant concentration to avoid explosive mixture.

V-Mg-O catalyst system has found some limited success in the oxidative dehydrogenation reaction.[2-6] To the best of our knowledge, there is no published information about supported V-Mg-O catalyst. V_2O_5 has been known to have strong interaction with MgO and TiO_2(anatase). Therefore, in our research we experimentally supported V-Mg-O on TiO_2 (anatase) and applied this new catalyst system to the gas phase oxidation of alcohols.

The catalyst studied 9V2MgTi (8.7 wt% V_2O_5, 2 wt% Mg, surface area, BET method, 9.27 m^2g^{-1}) was prepared by wet impregnation method. TiO_2 was added to an aqueous solution of NH_4VO_3 and dried at 353 K until achieving a thick paste. The obtained paste was calcined in air at 823 K for 6 hours to convert the paste into V_2O_5/TiO_2. Then, Mg was introduced into V_2O_5/TiO_2 by impregnation from $Mg(NO_3)_2$ solution. The suspension was dried and calcined again at the conditions mentioned above. The XRD pattern of the obtained V-Mg-O catalyst showed only the peaks of TiO_2(anatase).

The catalytic performance test was performed in a quartz fixed-bed reactor (6 mm ID) packed with 0.3 gram of catalyst

(100-150 mesh). Alcohols (ethanol and 1-propanol) were fed via a saturator. Pure dry air was used as oxygen source and nitrogen was used as balancing gas. The feed contained 8 vol% alcohol and 5 vol% oxygen, total flow rate 100 ml min^{-1}. The reaction was studied in the temperature range 473-773 K. Combustion products (CO, CO_2, and H_2O) were analyzed using a gas chromatograph Shimadzu GC 8A equipped with a TCD and a MS-5A Porapak-Q column. Hydrocarbons were analyzed using a gas chromatograph Shimadzu GC 14A equipped with a FID and a VZ-10 column. Oxygenate compounds were analyzed using a gas chromatograph Shimadzu GC 14B equipped with a FID and a capillary column. Total carbon balance in product stream was with in the range 100±5% The selectivity towards products was calculated from the following expression:

$$\%S = \frac{\text{mole product formed}}{\text{mole alcohol converted}} \times \frac{\text{no of C atom of product}}{\text{no of C atom of alcohol}} \times 100$$

The result obtained from ethanol oxidation is shown in Figure 1. Between 473-623 K, ethanol conversion rapidly increased up to a maximum about 86% while selectivity to ethanal was still higher than 80%. The other observed products were mainly CO_2, with traces of CH_4, C_2H_4, and C_3H_6. No CO appeared in the product stream. The maximum ethanal yield, 73%, occurred at 623 K. Beyond 623 K, both ethanol conversion and ethanal selectivity slightly decreased.

1-Propanol conversion and product selectivities are shown in Figure 2. The conversion of 1-propanol increased rapidly between 473-573 K, reaching a maximum conversion about 85%. Beyond 573 K, the conversion was quite constant. The main products observed were propanal and CO_2. Methanal, CH_4, C_2H_4, and C_3H_6 also appeared in the product stream. No CO was detected in the product stream. The maximum propanal yield (about 66%) was achieved at 573 K.

The mass balance of O_2 showed that O_2 was nearly completely consumed at 623 K for ethanol and 573 K for 1-propanol. This is the reason why beyond these temperatures, ethanol and 1-propanol conversions were quite constant. For ethanol oxidation, the slight decrease of ethanol conversion when the reaction temperature was higher than 623 K was the result of the competitive reaction between ethanol/ethanal with O_2. At high temperature, part of oxygen reacted with ethanal rather than ethanol. This reaction caused the decrease in ethanal selectivity as well as ethanol conversion.

It is known that on MgO support, vanadium ion can form bridging oxygen structure, V-O-V, apart from V=O species. This V-O-V species plays role as selective oxidation site. For the oxidation of ethanol, the reaction mechanism shown in Figure 3 is purposed.

The mechanism shown in figure 3 was based on the studies on the selective oxidation and combustion of light hydrocarbons at metal oxide surfaces.[7,8] Ethanol is adsorbed on V-O-V sites to

produce an adsorbed alkoxide species (step 1). H-atom of the alcohol hydroxyl group is eliminated in the form of hydroxyl group by an O anion on the catalyst surface. The surface hydroxyl group further subtracts a H atom of the C atom attaches to the O atom to form water and ethanal (step 2). Desorption of water causes a vacant oxygen site, V-□-V, on the catalyst surface. Finally, the V-□-V site is reoxidized by an oxygen molecule from the gas phase to form V-O-V again (step 3). 1-Propanol is believed to react in the same way as ethanol.

This work was supported by Thai Research Fund (TRF).

References

1. F. Cavani, F. Trifiró, *Catal. Today*, **36**, 431 (1997).
2. M.A. Charr, D. Patel, M.C. Kung, and H.H. Kung, *J. Catal.*, **105**, 483 (1987).
3. M.A. Charr, D. Patel, and H.H. Kung, *J. Catal.*, **109**, 463 (1988).
4. O.S. Owen, M.C. Kung, and H.H. Kung, *Catal. Lett.*, **12**, 45 (1992).
5. X. Gao, P. Ruiz, Q. xin, X. Guo, and B. Delmon, *Catal. Lett.*, **23**, 321 (1994).
6. F. Cavani, F. Trifiró, *Catal. Today*, **24**, 307 (1995).
7. M.M. Bettahar, G. Costentin, L. Savary, and J.C. Lavalley, *Appl. Catal. A*, **145**, 1 (1996).
8. E. Finocchio, R.J. Willey, G. Busca, and V. Lorenzelli, *J. Chem. Soc. Faraday Trans.*, **93**, 175 (1997).

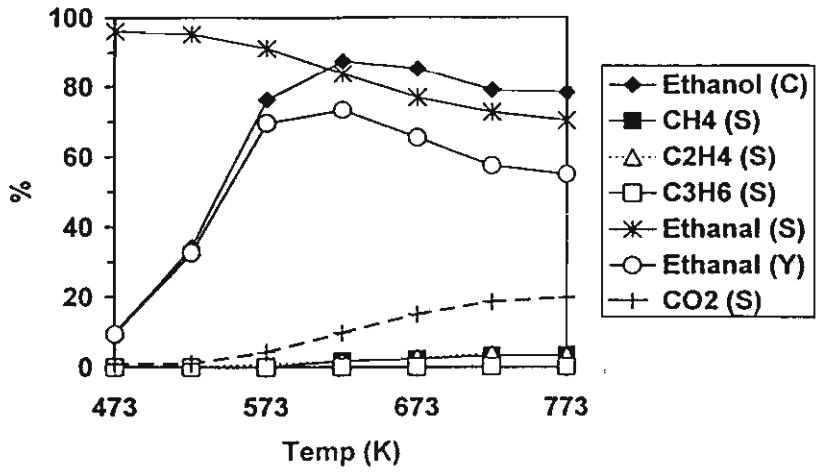

Figure 1 Ethanol oxidation : C - conversion, S - selectivity, Y - Yield

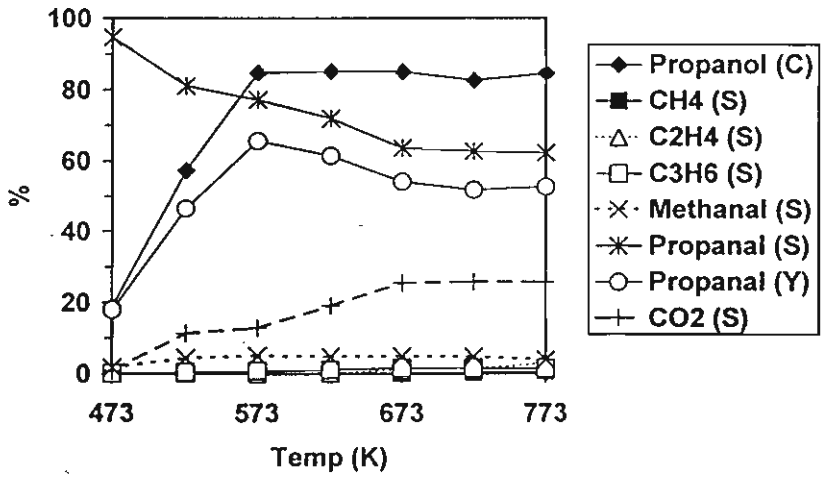

Figure 2 1-Propanol oxidation : C - conversion, S - selectivity, Y - Yield

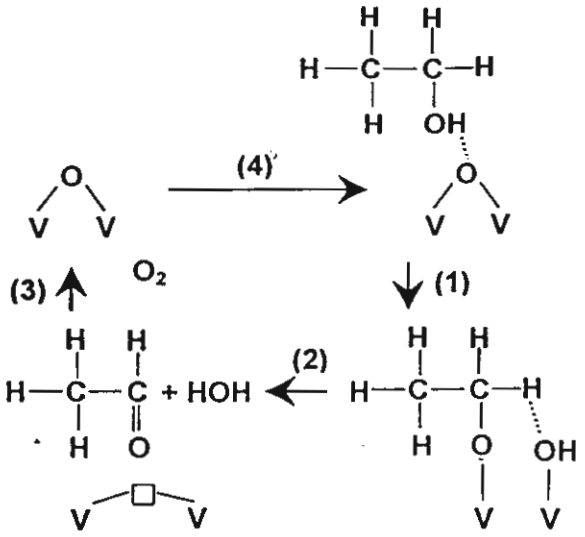

Figure 3 Proposed scheme for ethanol oxidation to ethanal

Inbox

From: gseo <gseo@chonnam.chonnam.ac.kr> Save Address - Block Sender
To: sunee srihiranpullop <sunee11@hotmail.com> Save Address
Subject: Acceptance
Date: Fri, 07 Jul 2000 14:04:14 +0900

Ms Sunee Srihiranpullop
Petrochemical Laboratory
Department of Chemical Engineering
Chulalongkorn University,Bangkok 10330
Thailand
Fax: (662)-218-6769

July 7, 2000

RE:" Deactivation of The Metal and Acidic Functions for Pt, Pt-Sn and Pt-Sn-K using Physically Mixed Catalysts" (ARTICLE NO: 00-05CCE)

Dear Ms Srihiranpullop,

I am pleased to inform the acceptance of your paper to the Korean Journal of Chemical Engineering. I sent your paper to the Office. Your will receive a formal acceptance letter from Chief-of-Editor. I appreciate your contribution.

Sincerely yours,

Gon Seo
Editor of The Korean Journal of Chemical Engineering
Chonnam National University
300, Yongbong-dong, Buk-gu
Kwangju 500-757
Korea

DEACTIVATION OF THE METAL AND ACIDIC FUNCTIONS FOR Pt, Pt-Sn AND Pt-Sn-K USING PHYSICALLY MIXED CATALYSTS

Sunee Srihiranpullop*, Piyasan Praserthdam and Tharathon Mongkhonsi

Department of Chemical Engineering, Chulalongkorn University, 10330 Thailand

Abstract- The effect of K addition on the amount and dispersion of carbon deposition on the metal sites and the support sites was investigated on a physical mixture for hexane dehydrogenation. TPO, BET and ESR experiments were used for characterization. The K addition significantly decreases catalyst deactivation involving the amount of coke deposits and the density of carbon radicals on the metal and support sites because of the ensemble and electronic effects, especially on the metal sites. Coke on the metal sites associated with carbonaceous species rich in hydrogen is less polymerized than coke on the support sites corresponded to a more graphitic-like carbon.

Running title: Deactivation of the Physically Mixed Catalysts

Keywords: deactivation, Pt-based catalyst, Pt-based catalyst modified with Sn and/or K, physically mixed catalyst

***To whom correspondence should be addressed**

TEL: +662-218-6710

FAX: +662-218-6769

E-mail: sunee11@hotmail.com

INTRODUCTION

Catalytic processing of many industrial feedstocks is frequently accompanied by the deposition of carbonaceous deposits. For metal catalysts, the supported mono- and multi-metal Pt containing catalysts are widely used for dehydrogenation in the petroleum and other industries. The addition of the modifiers such as K and/or Sn into Pt-containing catalysts may change the selectivity of catalysts and can increase the resistance of carbon deposition [1-3]. It has been reported that coking on the catalyst surface is a dynamic process [4-7]. Carbon deposition takes place on both the active metal sites and the support surface for supported metal catalysts. Numerous species of carbon are observed to be deposited or formed on the surface of coked catalysts, ranging from carbides or microcrystalline and amorphous species to highly aromatic/ graphitic carbons apparently through polymerization reaction and rearrangement for the polymer formed to be stabilized [3,5,8]. Additionally, analysis by temperature programmed oxidation (TPO) generally indicates two types of coke; the first one burns at low temperatures (polymeric carbon), which is associated with the metal phase and the second type burns at high temperatures (amorphous/graphitized carbon), associated with the support [9,10]. Although catalyst deactivation has been studied for many years, coke growth completely separated between coke on the metal and coke on the support sites has not been investigated sufficiently so far. In order to shed some light on this matter, the physically mixed Pt/SiO_2 and Al_2O_3 was used in this work as a representative catalyst of Pt/Al_2O_3. Since the SiO_2 support in Pt/SiO_2 has a very low acidity, its contribution to the acidic function is, therefore, negligible. The mesh sizes of Al_2O_3 and SiO_2 selected for the physically mixed catalyst are based on ones that give approximately

the conversion of hexane similar to that obtained from the conventional Pt/Al_2O_3 catalyst [7,11,12]. With this simulated catalyst associated with the presence of K and /or Sn, much debate about how the additive metal brings about the enhancement in catalytic properties should be better conceived.

Thus, this work involved a detailed study of coke deposition on Pt, Pt-Sn and Pt-Sn-K catalysts employed in a physically mixed system where silica-supported platinum, Pt/SiO_2, represents the metal sites and acidic alumina, Al_2O_3, represents the support sites. The dehydrogenation of n-hexane was adopted to cause coked catalysts with the carefully selected reaction conditions so that the thermal cracking effect may be negligible. The main goal was to determine the effect of K and/or Sn on coke distribution over the metal sites and support sites in order to better understand the deactivation process of the catalysts.

EXPERIMENTAL

Catalyst preparation

The alumina used in this study was obtained from Sumitomo Alumina Smelting (type NKH-3) and the silica was manufactured by Merck. They were ground and then sieved to retain particles with sizes between 60-80 mesh and 100-120 mesh, respectively. Three types of catalyst, namely, 0.3wt% Pt/SiO_2, 0.3wt%Pt-0.3wt%Sn/SiO_2 and 0.3wt%Pt-0.3wt%Sn-0.6wt%K/SiO_2 were employed in this work. The catalysts were prepared by impregnation method using H_2PtCl_6, $SnCl_2$ and KNO_3 as salt precursors. All chemicals used were normally analytical grade. After drying at 110°C overnight, the catalysts were calcined in an air flow at 500°C for 3 h.

RESULTS AND DISCUSSION

Carbon deposition on the metal sites and the acidic sites of the Pt, Pt-Sn and Pt-Sn-K catalysts

Carbon depositions on Pt-based catalysts were investigated by temperature programmed oxidation (TPO). On the active metal sites of various catalysts, Fig. 1A shows TPO profiles of Pt, Pt-Sn and Pt-Sn-K catalysts, respectively. It is observed that two peaks appear at 300°C and 425°C in every TPO profile. This indicates that carbon depositions on these catalysts can be divided into two types: (i) coke deposited directly on metal and (ii) coke in the vicinity of metal centers, which correspond to the report somewhere else [4,13]. In addition, it is obvious that coke is depositing on different sites on the different catalysts and affecting deactivation to deferring extents. From Fig. 1A, the difference of the modified catalysts is that, for Pt and Pt-Sn catalysts, the area of the first peak at lower temperature is less than that of the second peak at higher temperature. For the Pt-Sn-K catalyst, the situation is just opposite. Interestingly, the peak of the K-doped catalyst decreased more than any other catalysts, especially in the position at 425°C. In previous studies [4-10], it was speculated that the active metal site was linked with the originally generated coke precursors. Consequently, K addition dramatically inhibits the production of coke intermediates resulting in the lower area of carbonaceous compounds. It is seen that the order of their TPO areas is as follows: Pt > Pt-Sn > Pt-Sn-K. Furthermore, the total carbon accumulate on the metal sites of different catalysts listed in Table 1 was determined from the areas under the TPO profiles. The order of decreasing amount of carbon per gram is Pt > Pt-Sn > Pt-Sn-K. It has been found that the areas of the TPO peaks increase with the amount of carbon deposition for the Pt-based catalysts.

On the other hand, Fig. 1B exhibits spectra of TPO on the acidic sites of Pt, Pt-Sn and Pt-Sn-K catalysts. It is observed that a single peak appears on the spectra of TPO for the modified catalysts. Coke burns off at higher temperature, about 525°C, compared with coke on the metal sites. This implies that the peak shifts to a higher temperature because of a larger degree of polymerization of coke [14]. Moreover, the TPO area of the Pt catalyst is diminished by the addition of Sn and especially in combination with K. As presented above, it is relevant to note that the surface coverage has different compositions, which is summarized in Table 1. The amount of coke on both the metal sites and support sites decreased significantly by the addition of Sn and/or K.

As mentioned above, carbonaceous materials deposit either on the active metal sites or on the acidic alumina support surface. The migration of coke precursor from one type of sites to another may possibly occur. Hence, a model of coking is proposed in Fig. 2. Hydrocarbons first undergoes dehydrogenation and cracking on the active metal surface to form precursors of coke deposits. In general, unsaturated reaction intermediates such as monocyclic diolefins are formed and then reversibly adsorbed to form coke on the metal and in its direct vicinity. However, they can migrate to acid sites and become polymerized to the more graphite-like material. Additionally, when comparing the amount of coke on the metal sites and the support sites as shown in Table1, it is obvious that a small part of coke is located on the metal sites whereas the major fraction is accumulated on the acidic sites. These results imply that coke deposits on the metal sites is less dehydrogenated and corresponds to species rich in hydrogen in accordance with the literature reviews [15,16]. Accordingly, the H/C ratio of coke deposits on metal sites is higher than that of the coke deposits on acidic support sites. It displays the different nature of coke between

the metal sites and alumina. Finally, the modifications of Pt catalyst by addition of Sn and K are able to reduce the amount of coke on both sites.

Carbon radicals of coke on the metal sites and the acidic sites of the Pt, Pt-Sn and Pt-Sn-K catalysts

In order to examine the effect of Sn and K addition on coke formation with both sites in more detail, Electron Spin Resonance (ESR) has long been an effective technique to estimate the radical density of coke. ESR spectra are obtained by measuring the intensity vs. wavelength (or frequency) of a beam of electromagnetic radiation as it passes through a sample of matter, which is presented in a derivative trace of absorption curve. Then, the radical density can be computed from the integrated area of the spectra obtained [17,18]. Further coke radicals are representative of the overall coke, for both its nature and its amount because the amount of olefin or allylic radicals are characteristic of carbonaceous matter as introduced elsewhere [19-23]. In an earlier study, H.G. Karge *et al.* [19,20] investigated low temperature coke (below about 500 K) and high temperature coke radicals (above about 500 K). They found that olefinic or allylic oligomeric species were low-temperature coke radicals while highly unsaturated species were high-temperature coke radicals. Consequently, the formation of radicals enable us to discriminate between individual coke of various catalysts including coke on the metal sites and the support surface. In this study, Fig. 3A shows the ESR spectra of coke radicals for various catalysts on the metal sites. The carbon radicals density computed form the total peak area is given in Table 2. The g value of coke radicals is estimated to be 2.003 in agreement with earlier literature [22,24]. It is found that the modification of catalysts displays a dominant role in reducing the intensity of

carbonaceous radicals as well as reducing the amount of coke precursors. Interestingly, the K-doped sample has a sharply lower amount of radicals of coke, by 27 times, compared with the Pt catalyst resulting in the lowest amount of coke shown in Table 1. Another modification of the Pt catalyst diminishes carbonaceous radicals about 1.7 times. A comparison between ESR results and TPO results, which are described above, exhibits a good correlation between the number of radicals and the amount of coke.

For the acidic alumina, the ESR spectra of radicals are illustrated in Fig. 3B with the Pt-based catalysts. Table 2 also lists the intensity of them on these sites. This characteristic of carbon radicals is similar to that already reported above. However, the density of coke radicals is greater on the alumina sites than on the active metal sites. It is clear that the amount of radicals compared with the carbonaceous radicals intensity of Pt catalyst is reduced by 1.45 times for Sn modification and 1.65 times for K addition. As mentioned above, it is introduced that the metal sites is relevant to generate coke intermediates, which adsorbed to form coke on this site and can migrate to the acidic support sites. Thus, if the modification of catalysts inhibits the production of coke precursors on the metal sites, then the amount of carbonaceous compounds is consequently decreased. From the result shown in Table 2, it is obvious that the K-doped sample dramatically reduces coke radicals concerned with coke species on the active metal sites. Accordingly, a lower amount of coke deposits is produced as shown by the TPO results.

The changes of textural properties and the dispersion factors of coke on the metal sites and the acidic sites of the Pt, Pt-Sn and Pt-Sn-K catalysts

Coking is claimed to be responsible for a decrease in the specific surface, pore surface and pore volume depending on a limitation of diffusion (dispersion) and nature of coke deposits. As a result, an investigation of texture changes in surface area before and after coke deposition of Pt-based catalysts was carried out. Jovanovic and Putanov [13] introduced the dispersion factor to consider catalyst degradation of Pt/Al_2O_3 and $Pt\text{-}Re/Al_2O_3$. The dispersion factor is the ratio of change of surface area to the quantity of carbon deposits. Higher values of dispersion factor proved that carbon deposited on this catalyst is better dispersed with the fine small grain structure. In this work, the dispersion factor of carbonaceous deposit defined as the ratio of change of surface area to the amount of coke was investigated on Pt, Pt-Sn and Pt-Sn-K catalysts. Table 3 summarizes the textural properties of catalyst samples before and after coking and the dispersion factor, which is separated into the metal sites and the acidic alumina in each catalyst. The change of surface area may be attributed to the blockage of catalysts by coke, though thermal sintering and the other factor except coking should not be ruled out. It has been found that the modified catalyst lost their surface area after the reaction more than the unmodified one containing only platinum. This might be due to the fine structure of coke readily occurred in case of Pt catalysts with the presence of Sn and/or K, which easily block the existing porous area of the catalyst. The obtained results were consistent with the report of fine small grain structure of coke deposits for the modification catalysts suggested in literature reviews [21,25,26]. Moreover, noticeably higher values of dispersion factors are obtained from the Pt-Sn and particularly Pt-Sn-K catalysts as illustrated in Table 3. Comparing with the Pt catalyst, the dispersion factor of the Pt-Sn catalyst is about 1.7

times on the metal sites and about 1.8 times on the acidic sites. In the case of K addition, dispersion factors on the metal sites and on the support sites are about 2.4 times and 4.5 times compared with Pt catalyst, respectively.

The influence of Sn and K addition on coke formation

The main theories put forward to account for the improved properties of multi-metallic catalysts tend to involve either geometric or electronic effects. Coke formation is known to require relatively large clusters or ensembles of adjacent metal atoms. For the Sn addition, the presence of Sn improves the diluting of the active metal surface into smaller ensembles, which enhance the catalysts' resistance to deactivation. The addition of Sn to Pt catalyst forms substitutional surface alloys and it has been shown that Sn interacts with platinum on silica to form a Pt/Sn alloy [1,2,3,27,28]. Thus, carbon intermediates cannot readily form multiple carbon-metal bonds. Furthermore, it inhibits the formation of highly dehydrogenated surface species that are intermediates for coking. According to Padro *et al.* and Larsson *et al.* [14,29], one reason is that coke deposits bind more strongly to the Pt catalyst than to the Pt-Sn catalyst.

From TPO profiles and ESR spectra of the metal sites, that the adsorbed species are attached less strongly to the metal surface would be explained by the significant minimizing of these sites and promotion of the migration of coke precursors to the carrier. These effects are evident by the change in the heights of peaks in the TPO profiles and ESR spectra.

The addition of K into bimetallic Pt-Sn catalyst produces a significant decrease in the catalyst deactivation as shown in Fig. 4 illustrating the conversion of hexane as a function of time. The decline in conversion is slower for catalysts

containing tin and potassium than for catalysts containing platinum only due to less amount of coke was formed on the modified catalysts. In Fig. 4 and Table 1, it is obvious that Pt catalyst deactivates quickly and a considerable amount of coke was formed. It may be related to the incorporation of tin into the surface of platinum through the formation of a substituted alloy, while potassium may be present on top of the platinum surface. As described elsewhere [14,27], it was found that K- doped catalyst significantly decreases the activation energy of CH dehydrogenation which would suggest that K effect diminishes the interaction between Pt and Sn. This modification in the interaction between both metal components could be due either to a direct addition of K on the metal phase or to an indirect effect of the alkali metal addition to support, which could change the metal-support and the metal-metal interactions, as suggested in the literature [27,29,30]. This results in a weakening of Pt-C bond strength to make the catalyst less susceptible to deactivation by deposition of carbonaceous species on both sites as illustrated in Fig. 1, Table 1, Fig. 3 and Table 2. This is known as an electronic effect [1,2,3,30].

CONCLUSION

The addition of Sn and K resists coke formation both on the metal sites and on the support sites. It seems due to the ensemble and electronic effects. They also reduce the density of carbon radicals and affect the nature of coke. For textural properties, noticeably higher values of dispersion factor were obtained on Pt-Sn and Pt-Sn-K catalysts than on Pt catalysts. It can indicate that coke on the Pt-Sn and Pt-Sn-K catalysts has a softer coke nature. Specifically, K addition significantly inhibits coking. Comparing coke on the metal sites and on the support sites, it can be

concluded that coke on the metal is soft in nature, rich in hydrogen and has a lower degree of polymerization.

ACKNOWLEDGEMENTS

The authors would like to thank Thailand Research Fund (TRF) and National Science and Technology Development Agency (NSTDA) for financial support of this project.

REFERENCES

[1] Rostrup-Nielsen, J.R., "Industrial relevance of coking", Catal.Today , 37, 225. (1997).

[2] Trimm, D.L., "Catalysts for the control of coking during steam reforming", Catal. Today, 49,3 (1999).

[3] Trimm, D.L., "Catalyst design for reduced coking", Appl. Catal., 5, 263 (1983).

[4] Lietz, G., and Volter, J., "Initial changes of the catalytic properties of platinum containing catalysts: I. Transformations of mono- and bimetallic Pt/Al_2O_3 catalysts by carbonaceous deposits", Appl. Catal., 13, 77 (1984).

[5] Biswas, J., Bickle, G.M., Gray, P.G., Do, D.D., and Barbier, J., "The role of deposited poisons and crystallite surface structure in the activity and selectivity of reforming catalysts", Catal. Rev.-Sci. Eng., 30 (2), 161 (1988).

[6] Liwu, L., Tao, Z., Jingling, Z., and Zhusheng, X., "Dynamic process of carbon deposition on Pt and Pt-Sn catalysts for alkane dehydrogenation", Appl. Catal., 67, 11 (1990).

[7] Bond, G.C., "Heterogeneous Catalysis: Principles and Application", Clarendon

Press: Oxford (1987).

[8] Afonso, J.C., Schmal, M., and Frety, R., "The chemistry of coke deposits formed on a Pt-Sn catalyst during dehydrogenation of n-alkanes to mono-olefins", Fuel Pro. Tech., 41, 13 (1994).

[9] Barbier, J., "Coking of reforming catalysts", Catalyst Deactivation, 1 (1987).

[10] Biswas, J., Gray, P.G., and Do, D.D., "The reformer lineout phenomenon and its fundamental importance to catalyst deactivation" Appl. Catal., 32, 249 (1987).

[11] Shum, V.K., Butt, J.B., and Sachtler, W.M.H., "The dehydrocyclization-controlling site in bifunctional reforming catalysts", Appl. Catal., 11, 151 (1984)

[12] Inaba, M., Kintaichi,Y., and Hamada, H., "Cooperative effect of platinum and alumina for the selective reduction of nitrogen monoxide with propane", Catal. Lett., 36, 223 (1996).

[13] Jovanovic, M.R., and Putanov, P.S., "Nature and distribution of coke formed on mono-metallic platinum and bimetallic platinum-rhenium catalysts", Appl. Catal., 159,1 (1997).

[14] Padro, C.L., de Miguel, S.R., Castro, A.A., and Scelza, O.A., "Stability and regeneration of supported PtSn catalysts for propane dehydrogenation", Catalyst Deactivation, 191 (1997).

[15] Tao, Z., Jingling, Z., and Liwu, L., "Relation between surface structure and carbon deposition on Pt/Al_2O_3 and $Pt\text{-}Sn/Al_2O_3$ catalysts", Catalyst Deactivation, 143 (1991).

[16] Beltramini, J., and Trimm, D.L., "Activity, selectivity and coking over mono-and bi-metallic reforming catalysts", Appl. Catal., 32, 71 (1987).

[17] Werlz, J.E., and Bolton, J.R., " Electron Spin Resonance: Elementary Theory and Practical Applications", Chapman and Hall Ltd.: New York(1972).

[18] Lunsford, J.H., " Electron Spin Resonance in Catalysis", Advances in Catalysis, 22, 265 (1972).

[19] Butt, J.B., and Peterson, E.E., "Activation Deactivation and Poisioning of Catalysts", Academic Press Inc (1988).

[20] Guisnet, M., and Magnoux, P., "Coking and Deactivation of zeolites: Influence of the pore structure", Appl. Catal., 54, 1 (1989).

[21] Lange, J.P., and Gutsze, A., "Coke formation through the reaction of ethene over hydrogen mordenite: III. IR and 13C-NMR studies", Appl. Catal., 45, 345 (1988).

[22] Lange, J.P., Gutsze, A., and Karge, H.G., "Coke formation through the reaction of olefins over hydrogen mordenite: I. EPR measurements under static conditions", J. Catal., 114, 136 (1988).

[23] Lange, J.P., Gutsze, A., and Karge, H.G., "Coke formation through the reaction of olefins over hydrogen mordenite: II. Insitu EPR measurements under on-stream conditions", J. Catal., 114, 144 (1988).

[24] Gutsze, A., Roland, U., and Karge, H.G., "Evidence for a charge transfer from spilt-over hydrogen to platinum by means of ESR spectroscopy", Spillover and Migration of Surface Species on Catalysts, 417 (1997).

[25] Kirszensztejn, P., Foltynowicz, Z., and Wachowski, L., "Peculiar pore structure of the coke coating formed on Pt-Sn/γ-Al_2O_3 catalysts", Ind. Eng. Chem. Res., 30, 2276 (1991).

[26] Mann, R., "Catalyst deactivation by coke deposition: approaches based on interactions of coke laydown with pore structure", Catal. Today , 37, 331 (1997).

[27] Hill, J.M., Cortright, R.D., and Dumesic, J.A., "Silica- and L-zeolite-supported Pt, Pt/Sn and Pt/Sn/K catalysts for isobutane dehydrogenation", Appl. Catal.,

168, 9 (1998).

[28] Macleod, N., Fryer, J.R., Stirling, D., and Webb, G., "Catal. Deactivation of bi- and multimetall reforming catalysts: Influence of alloy formation on catalyst activity", Catal. Today , 46, 37 (1998).

[29] Larsson, M., Hulten, M., Blekkan, E.A., and Andersson, B., "The effect of reaction conditions and time on stream on the coke formed during propane dehydrogenation", J. Catal., 164, 44 (1996).

[30] Cortright, R.D., and Dumesic, J.A., "Effects of potassium on silica-supported Pt and Pt/Sn catalysts for isobutane dehydrogenation", J. Catal., 157, 576 (1995).

Figure 1A. Temperature Programmed Oxidation of carbonaceous deposits produced on the metal sites with different catalysts

Symbols: ● the Pt catalyst, ▲ the Pt-Sn catalyst and ■ the Pt-Sn-K catalyst

Figure 1B. Temperature Programmed Oxidation of carbonaceous deposits produced on the support sites with different catalysts

Symbols: ● the Pt catalyst, ▲ the Pt-Sn catalyst and ■ the Pt-Sn-K catalyst

Figure 2. Coking mechanism on both sites of catalyst.

Figure 3A. ESR spectra of coke on the metal sites ; (a) reference spectrum before coking reaction (b) coke on Pt-Sn-K catalyst (c) coke on Pt-Sn catalyst and (d) coke on Pt catalyst.

Figure 3B. ESR spectra of coke on the support sites; (a) reference spectrum before coking reaction (b) coke on Pt-Sn-K catalyst (c) coke on Pt-Sn catalyst and (d) coke on Pt catalyst.

Figure 4. %conversion of hexane dehydrogenation for physically mixed catalysts;

Symbols: ● the Pt catalyst, ▲ the Pt-Sn catalyst and ■ the Pt-Sn-K catalyst

Table 1. The amount of carbon deposited on the catalysts

Table 2. The density of carbon radicals of coke per gram catalyst

Table 3. The textural properties of catalysts samples before and after testing and factor of SA change

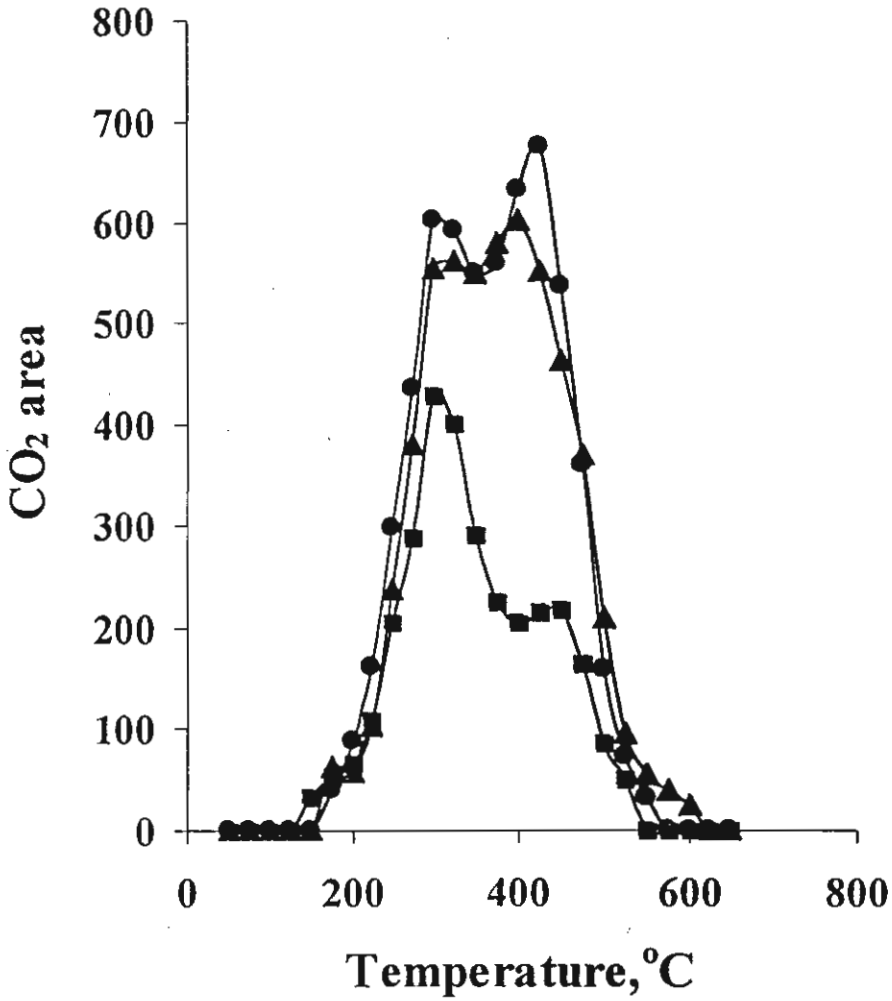

Figure 1A. Temperature Programmed Oxidation of carbonaceous deposits produced on the metal sites with different catalysts

Symbols: ● the Pt catalyst, ▲ the Pt-Sn catalyst and ■ the Pt-Sn-K catalyst.

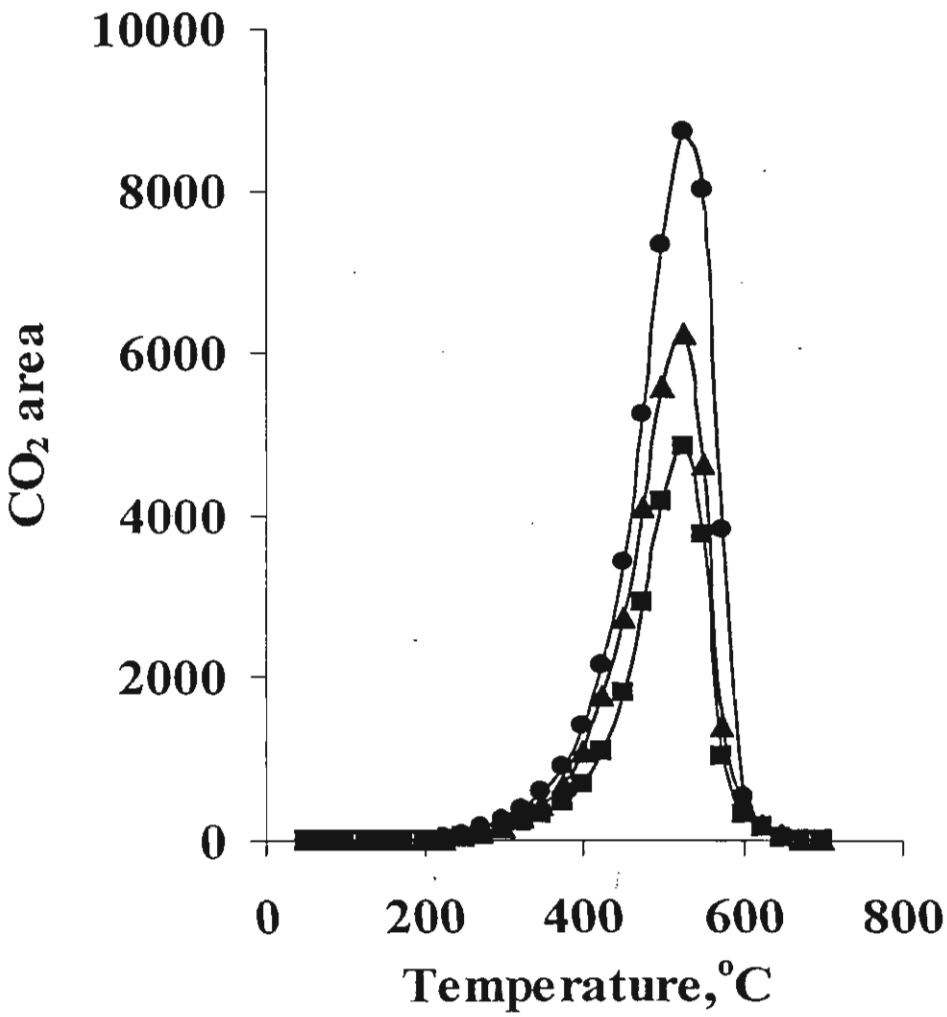

Figure 1B. Temperature Programmed Oxidation of carbonaceous deposits produced on the support sites with different catalysts

Symbols: ● the Pt catalyst, ▲ the Pt-Sn catalyst and ■ the Pt-Sn-K catalyst.

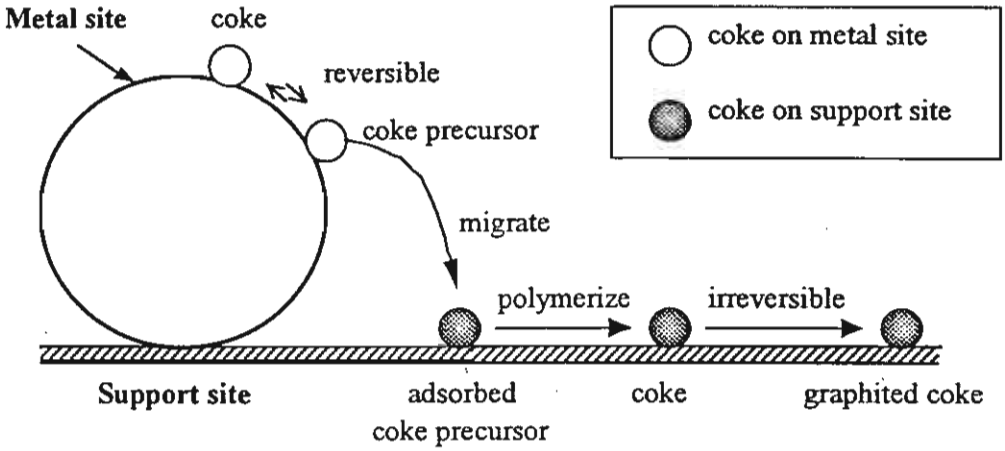

Figure 2. Coking mechanism on both sites of catalyst.

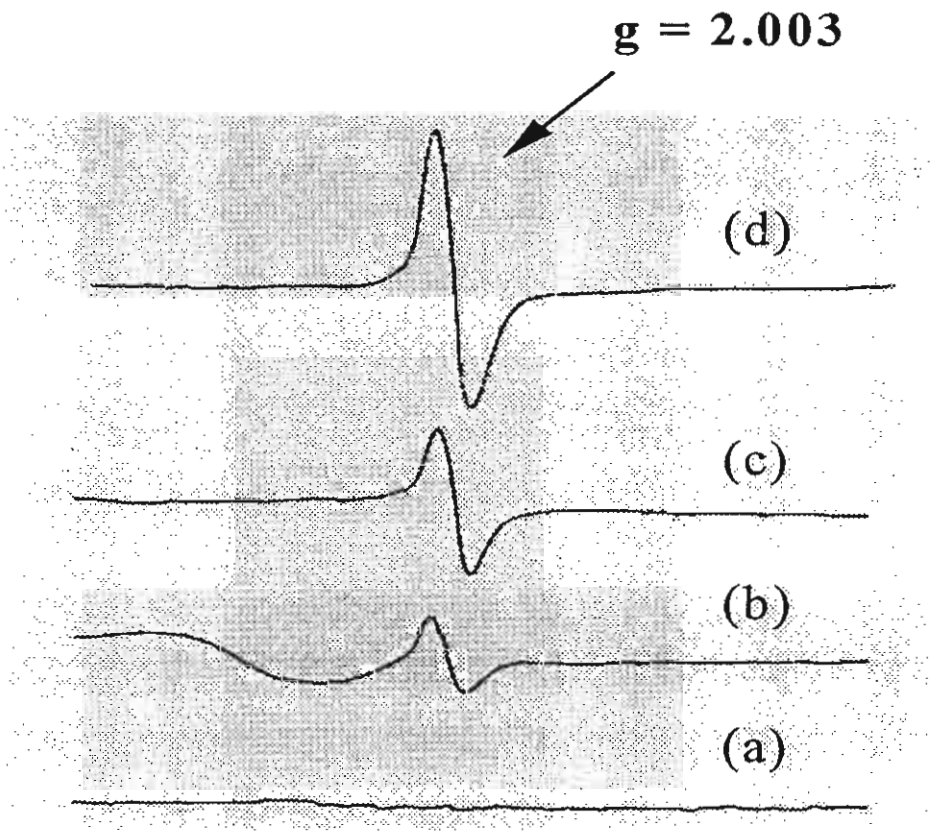

(A)

Figure 3A. ESR spectra of coke on the metal sites ; (a) reference spectrum before coking reaction (b) coke on Pt-Sn-K catalyst (c) coke on Pt-Sn catalyst and (d) coke on Pt catalyst.

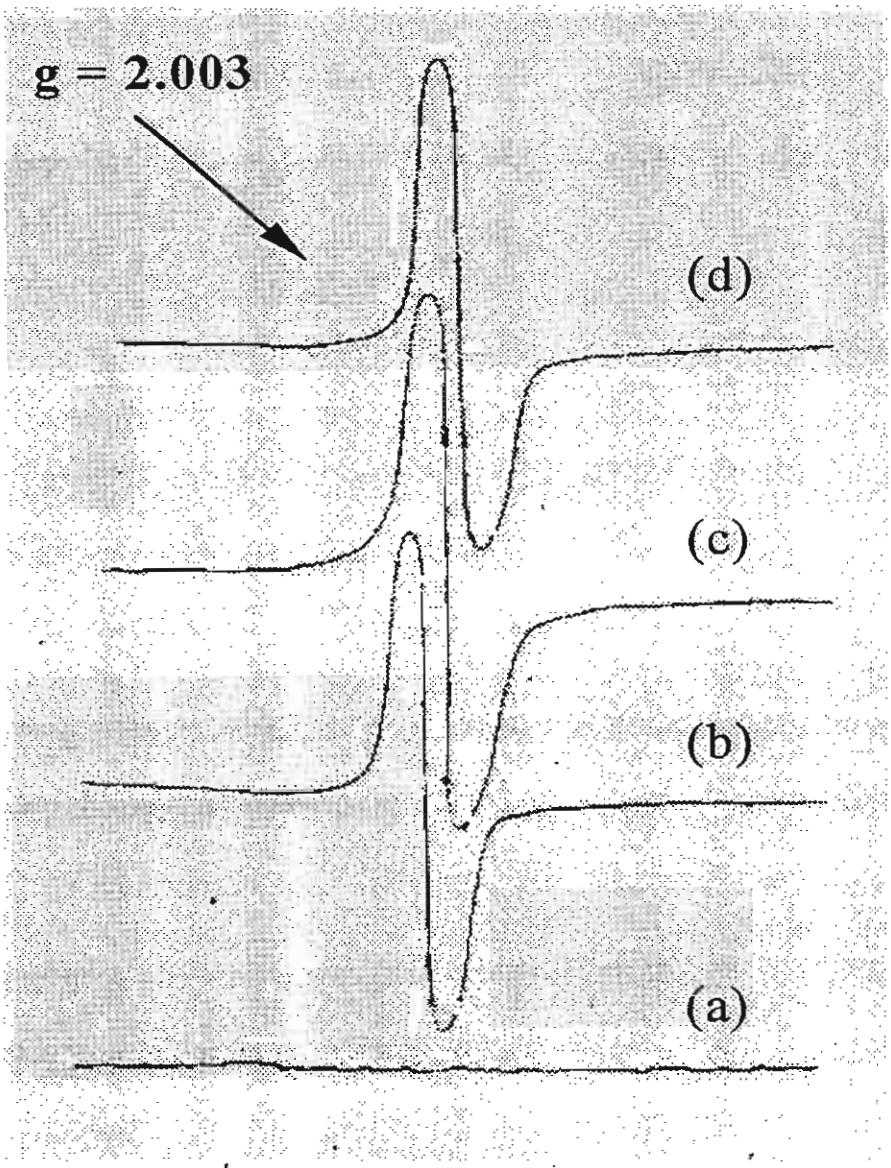

Figure 3B. ESR spectra of coke on the support sites; (a) reference spectrum before coking reaction (b) coke on Pt-Sn-K catalyst (c) coke on Pt-Sn catalyst and (d) coke on Pt catalyst.

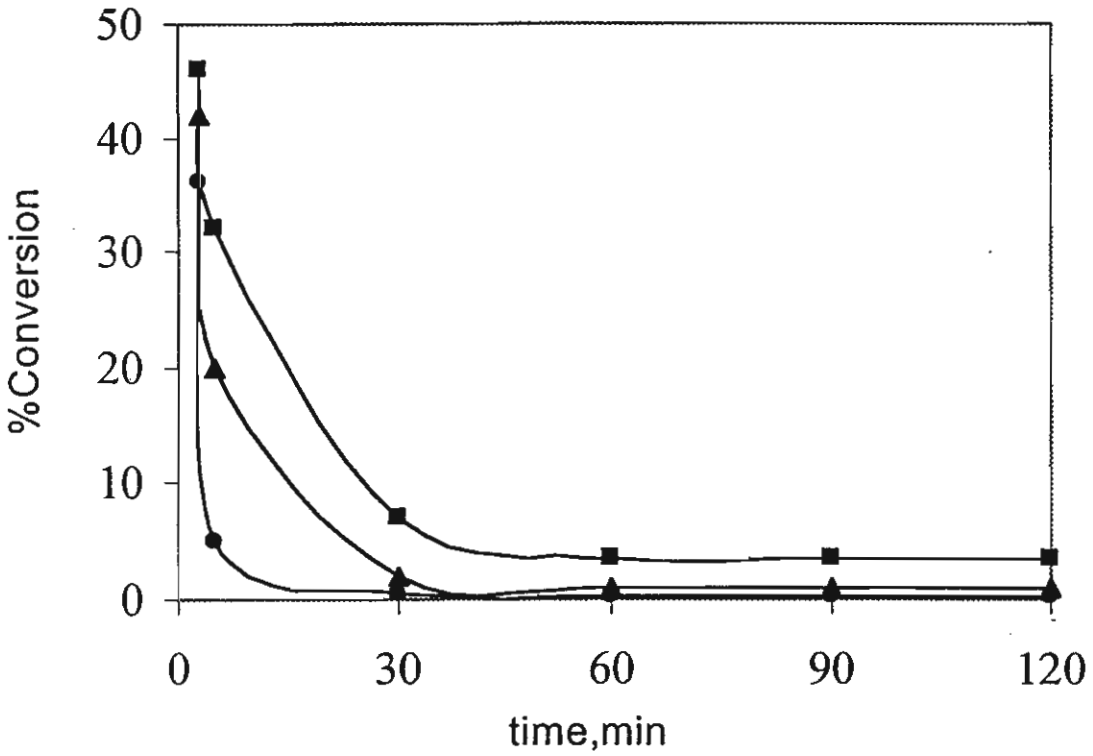

Figure 4 % conversion of hexane dehydrogenation for physically mixed catalysts; Symbols: ● the Pt catalyst, ▲ the Pt-Sn catalyst and ■ the Pt-Sn-K catalyst.

Table 1. The amount of carbon deposited on the catalysts

Catalysts	Coke on the metal sites %C	Coke on the support sites %C
Pt catalyst	0.36	2.50
Pt-Sn catalyst	0.32	1.73
Pt-Sn-K catalyst	0.21	1.26

Table 2. The density of carbon radicals of coke per gram catalyst

catalysts	The metal sites	The support sites
Pt catalyst	8.55×10^5	3.02×10^6
Pt-Sn catalyst	5.18×10^5	2.07×10^6
Pt-Sn-K catalyst	3.17×10^4	1.83×10^6

Table 3. The textural properties of catalysts samples before and after testing and dispersion factor

Catalysts	The metal sites			The support sites		
	SA (m2/g) Fresh	Used	dispersion factor	SA (m2/g) Fresh	Used	dispersion factor
Pt catalyst	447	386	171	390	343	19
Pt-Sn catalyst	417	325	291	390	330	35
Pt-Sn-K catalyst	380	283	462	390	283	85

Activation of Acetylene Selective Hydrogenation Catalysts Using Oxygen Containing Compounds

*Piyasan Praserthdam, Suphot Phatanasri, Jumpod Meksikarin

Petrochemical Engineering Research Laboratory, Department of Chemical Engineering, Chulalongkorn University, Bangkok 10330, Thailand

Abstract

Hydrogenation of acetylene in the presence of a large excess of ethylene has been investigated on the Pd-Ag catalyst at 60°C with a space velocity of 2,000 h^{-1}. It was found that an enhancement in the performance of Pd-Ag catalyst can be obtained by pretreatment with N_2O. It is suggested that a certain amount of N_2O added to the catalyst before use not only augments the sites associated with ethylene production from acetylene but also depletes the sites responsible for direct ethane formation. Upon aging, the pretreated catalyst exhibited good stability.

Keywords: Selective Hydrogenation, acetylene, silver promoted palladium catalyst, N_2O pretreatment

INTRODUCTION

The selective hydrogenation of acetylene over supported palladium catalysts is a process widely used to purify the ethylene produced by steam cracking of hydrocarbons. The ethylene to acetylene ratio in the stream to be treated is generally higher than 70 [1]. Typically the acetylene concentration can be reduced from an initial value in the region of 5,000 to below 5 ppm with hydrogenation of no more than 1% of the ethylene, operating at temperatures in the range of about 60-70°C [2]. At present all such catalysts are based on palladium using alumina as

* Corresponding author. E-mail : Piyasan.p@chula.ac.th

support, and palladium-based catalysts promoted by a second metal are now available [3]. The promoter improves selectivity or stability of the catalyst. A. Sarkany et al. [4] have clearly demonstrated that the addition of copper to palladium causes a significant decrease in the overall rate of ethane formation and at the same time there is a decrease in the catalyst activity as well as a marginal decrease in oligomer selectivity. Recently, it has been discovered that the catalyst comprising elements of group IB and transition metals could be activated with N_2O before use [5]. Thus it is an objective of the study to pretreat the Pd-Ag catalyst before being used for the selective hydrogenation of acetylene.

EXPERIMENTAL

A 0.04 wt% Pd-Ag/γAl_2O_3 (Ag:Pd = 4:1) was prepared via the serial impregnation method. Alumina support was impregnated with palladium first followed by silver. Alumina support was Al_2O_3 (CS-303) supplied by United Catalyst Incorporation (UCI), USA. Palladium nitrate and silver nitrate were used as sources for Pd and Ag, respectively. The calcination temperatures for palladium and silver were 300°C and 370°C, respectively.

A portion of 0.2 g of the catalyst was packed into a 0.6 cm-ID quartz reactor and heated from room temperature to 100°C in Ar. When the temperature reached 100°C, the reduction was made by switching Ar to H_2 and maintained at that temperature for 2 h. After reduction, H_2 was purged with a flow of Ar while the reactor was cooled down to 60°C and held at that temperature for 10 min. Then a gas mixture of 0.3% C_2H_2, 0.8%H_2 and C_2H_4 balanced was switched to replace Ar with a flow rate of 30 ml/min. Consequently, the gas mixture was reacted under catalytic hydrogenation, i.e., C_2H_2 was selectively hydrogenated to C_2H_4.

However, in the case of N_2O treatment, the reactor was cooled down from 100°C to 90°C under Ar flow and held for 10 minutes before N_2O injection. Then the temperature was reduced to 60°C and the reaction was started. The products were analysed by SHIMADZU FID GC 14B equipped with Carbosieve column s-2.

To investigate the effect of carbonaceous deposit on the catalysts, the following experiment was designed: set A was obtained at an early period (5 min on stream) during which the negligible amount of coke was formed, while set B was obtained at 44 h on stream during which the considerable amount of coke was presumably formed though the exact amount of coke deposit was not determined.

The active sites of the catalysts were determined by CO adsorption technique and the BET surface areas by a Micromeritic Surface Area Analyser (model ASAP 2000).

The following terms used herein are defined as:

$$\text{Acetylene conversion (\%)} = \frac{\text{acetylene in feed - acetylene in product}}{\text{acetylene in feed}} \times 100$$

$$\text{Ethylene selectivity (\%)} = \frac{\text{ethylene in product - ethylene in feed}}{\text{acetylene converted}} \times 100$$

Yield per pass (YPP) = (% acetylene conversion)×(%ethylene selectivity)

RESULTS AND DISCUSSION

Figure 1 shows the effect of N_2O addition on the performance of 0.04 wt% Pd-Ag/Al_2O_3 (Ag:Pd = 4:1). Addition of 0.02 to 0.1 cc of N_2O markedly increased the yield per pass (YPP) of ethylene. The best result was obtained with 0.1 cc injection of N_2O while the YPP declined with the amount of N_2O higher than 0.1 cc. It has been suggested that N_2O addition may cause the formation of both silver oxide and palladium

oxide on the surface of Al_2O_3 support [5]. The formation of silver oxide should increase the number of accessible Pd active sites, as shown in Fig. 2, thus promoting the hydrogenation of acetylene to ethylene. The oxidation of active Pd to palladium oxide, however, may possibly cause the loss of active sites also. The maximum YPP of ethylene obtained with 0.1 cc injection of N_2O may be attributed to the simultaneous reproduction and destruction of active sites in which the former is more predominant, particularly the sites responsible for ethylene production from acetylene.

Figures 3 and 4 show the effect of catalyst aging on acetylene conversion and ethylene selectivity, respectively for 0.04 wt% Pd-Ag/Al_2O_3 with and without N_2O treatment. It has been found that both catalysts exhibited similar results in decreasing ethylene selectivity with time on stream, while acetylene conversion was only slightly changed. After 60 h of operation, both catalysts attained an apparent steady state of ethylene selectivity. It has been clearly observed that the N_2O-treated catalyst exerted higher activity and selectivity than the untreated one.

From several previous investigations (Al-Ammar et al. [6-8], Margitfalvi et al. [9,10], Moses et al. [11], and Weiss et al. [12]), it has been generally accepted that four main types of surface sites are involved in the alumina-supported Pd catalyst. Figure 5 illustrates four main types of surface sites; three types of which, located on the Pd metal surface, are responsible for selective conversion of acetylene to ethylene, direct ethane production from acetylene, and oligomer formation from acetylene. Another site located on the alumina support surface involves the hydrogenation of ethylene to ethane. It has been reported from some researchers [3,13] that the decrease in ethylene selectivity (i.e. increase in ethylene hydrogenation) during aging has been related to the amount of carbonaceous adsorbate on the catalyst surface. In other words, the

carbonaceous deposit acts as a hydrogen bridge for the hydrogen spillover from Pd to support.

As shown in Table 1, the substantial amount of ethane obtained for 0.04% Pd/Al_2O_3 of set A should be produced directly frcm acetylene, and the ethylene hydrogenation to ethane should be negligible with the that no carbonaceous deposit bridge was formed. When the base catalyst was promoted with Ag, the amount of ethane significantly decreased and so did the acetylene conversion while the amount of ethylene was almost constant. This implies that the alumina-supported Pd catalyst promoted by Ag may reduce the sites responsible for direct ethane formation from acetylene which is consistent with the previous investigation [13]. In case of the N_2O treatment for set A, both acetylene conversion and ethylene selectivity markedly increased and the amount of ethane was further decreased. This means that the addition of nitrous oxide augments the sites responsible for ethylene formation from acetylene as described above, and advantageously reduces the sites accounting for direct ethane formation as well. As for set B, the amount of ethylene obtained for 0.04% Pd/Al_2O_3 was considerably less than that of the corresponding catalyst for set A, and so did the acetylene conversion. The carbonaceous deposit on the catalyst surface should be responsible for the decrease in acetylene conversion. It is interesting to note that the amount of ethane formed on the base catalyst for set B was higher than that for set A even with less acetylene conversion. This means the substantial amount of ethane was formed via the ethylene hydrogenation on the support sites, with aid of carbonaceous deposit acting as H_2 bridge, rather than the direct ethane formation from acetylene on Pd sites. Sarkany [14,15] has found that the hydrocarbonaceous deposit on Pd/Al_2O_3 catalyst may enhance the over-hydrogenation of 1,3-butadiene and permits the hydrogenation of propene in the presence of 1,3-butadiene due to

transport hindrance of 1,3-butadiene. Thus, the over-hydrogenation of acetylene and hydrogenation of ethylene in the presence of acetylene can also be interpreted by transfer limitation of acetylene caused by the presence of carbonaceous deposits. With the Ag-promoted catalyst, the increase in amount of ethylene and acetylene conversion was obtained while the amount of ethane declined. This also implies that the ethylene hydrogenation was reduced by Ag promotion, and the direct ethane formation from acetylene on Pd sites covered with carbonaceous deposit was negligible. Thus it has been suggested that Ag may hinder the hydrogen spillover from the metal surface to alumina support probably by providing the desorption sites for transferred hydrogen as illustrated in Fig. 5. With the N_2O treatment, both acetylene conversion and ethylene selectivity significantly increased while the amount of ethane was further decreased as similar to those obtained for set A. The improved results achieved on N_2O-treated Pd-Ag/Al_2O_3 catalyst for both sets of data essentially contend that the addition of N_2O increases the sites responsible for ethylene formation from acetylene and decreases the sites involving direct ethane formation as mentioned above. Table 2 shows the results of BET surface area of the catalysts. It has been found that the BET surface area of the N_2O-treated catalyst was slightly higher than that of the untreated one. This reflects that two silver atoms may move closely to one oxygen atom to form Ag_2O. This phenomenon can expose the active palladium sites which normally locate under the surface of metal cluster as modelled in Fig. 2.

Table 3 shows the metal active sites of catalysts measured by co adsorption. It has been found that the Ag-Promoted Pd catalyst exhibited less amount of active sites than that of the unpromoted one. This may be due to the alloy formation between both metals. The addition of N_2O to the silver-promoted catalyst was found to enhance the amount of active

sites which also supported the proposed model as described above. The highest amount of active sites was achieved with the injection of 0.1 cc of N_2O.

CONCLUSION

It might be concluded that N_2O treatment could improve the catalytic performance of the silver-promoted palladium catalyst by enhancing the accessible sites of active Pd responsible for ethylene production from acetylene, and meanwhile decreasing the sites involving the direct ethane formation from acetylene. Furthermore, the N_2O-treated catalyst has the same stability as the untreated one during the aging period.

ACKNOWLEDGEMENTS

The financial support of this research by The Thailand Research Fund (TRF) is gratefully acknowledged.

REFERENCES

1. G.C. Battiston, L. Dallord, G.R. Tauszik: *Appl. Catal.*, **2**, 1 (1982).
2. C.N. Satterfield: *Heterogeneous Catalysis in Practice*, McGraw-Hill, New York, 1980.
3. J.P. Boitianx, J. Cosyn, M. Derrien, and G. Leger: *Hydrocarbon Processing*, March, 51 (1985).
4. A. Sarkany, and L. Guczi: *Appl. Catal.*, **10**, 369 (1984).
5. P. Praserthdam, U.S. Patent 5,849,662 Dec. 15, 1998.
6. Al-Ammar A.S., and G. Webb: *J.C.S. Faraday*, **174**, 195 (1978).
7. Al-Ammar A.S., and G. Webb: *J.C.S. Faraday*, **174**, 657 (1978).

8. Al-Ammar A.S., and G. Webb: *J.C.S. Faraday*, **175**, 1900 (1978).
9. J. Margitfalvi, L. Guczi, and A.H. Weiss, *J. Catal.*, **72**, 185 (1981).
10. J. Margitfalvi, L. Guczi: *React. Kinet. Catal. Lett.*, **15**, 475 (1980).
11. J.M. Moses, A.H. Weiss, K. Matsusek, and L. Guczi: *J. Catal.*, **86**, 417 (1984).
12. A.H. Weiss, S. Leviness, V. Nau, L. Guczi, A. Sakany, and Z. Schay: *Proc. 8th Int. Congr. Catal.*, **5**, 591 (1984).
13. S. Leviness, V. Nau, A.H. Wiess, Z. Schay, and L. Guczi: *J. Mol. Catal.*, **25**, 131 (1984).
14. A. Sarkany: *J. Catal.*, **180**, 149 (1998).
15. A. Sarkany: *Appl. Catal.*, **175**, 245 (1998).

Figure 1 Performance of 0.04 wt% Pd-Ag/Al_2O_3 (Ag:Pd = 4:1) versus the amount of nitrous oxide addition ranging from 0.02 to 0.33 cc
Reaction conditions: 60°C, GHSV 2000 h^{-1}, 5 min on stream

Figure 2 Proposed model illustrating the effect of N_2O addition on enhancing the accessible sites of active Pd responsible for acetylene hydrogenation to ethylene

Figure 3 Effect of catalyst aging on acetylene conversion over untreated and N_2O-treated Pd-Ag/Al_2O_3
Reaction conditions: 60°C, GHSV 2000 h^{-1}

Figure 4 Effect of catalyst aging on ethylene selectivity,over untreated and N_2O-treated Pd-Ag/Al_2O_3
Reaction conditions: 60°C, GHSV 2000 h^{-1}

Figure 5 Conceptual model demonstrating four main types of surface sites on Al_2O_3-supported Pd catalyst and the role of Ag promoter as desorption site for transferred H_2

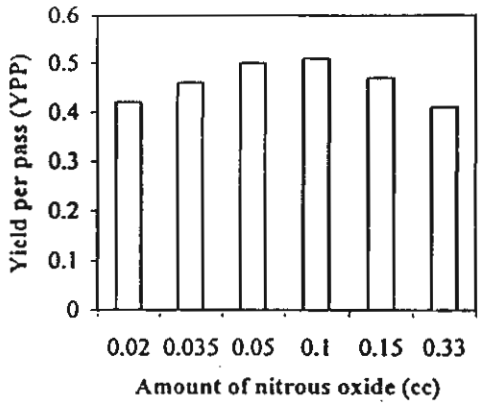
0.6
0.5
0.4
0.3
0.2
0.1
0
Yield per pass (YPP)
0.02 0.035 0.05 0.1 0.15 0.33
Amount of nitrous oxide (cc)

Fig. 1

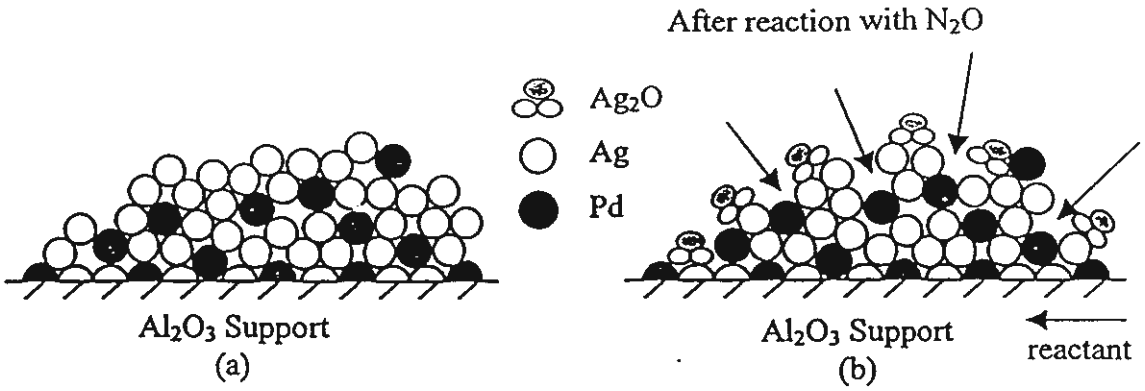
After reaction with N_2O
Ag_2O
Ag
Pd
Al_2O_3 Support
(a)
Al_2O_3 Support
(b)
reactant

Fig. 2

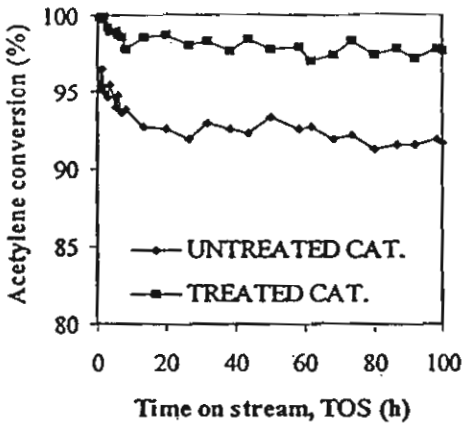
100
95
90
85
80
Acetylene conversion (%)
UNTREATED CAT.
TREATED CAT.
0
20
40
60
80
100
Time on stream, TOS (h)

Fig. 3

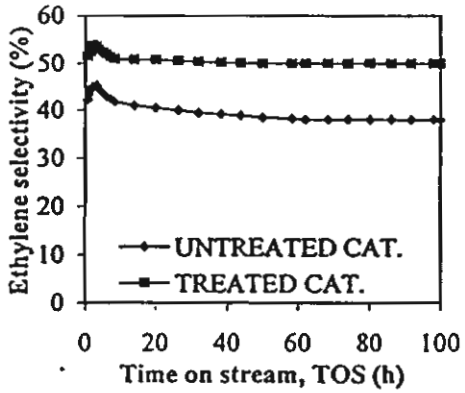
Ethylene selectivity (%)
60
50
40
30
20
10
0
UNTREATED CAT.
TREATED CAT.
0
20
40
60
80
100
Time on stream, TOS (h)

Fig 4

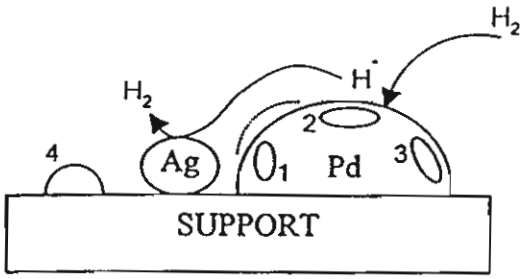

1. site for oligomer formation
2. site for direct ethane formation
3. site for ethylene formation
4. site for ethane production from ethylene

_____ carbonaceous deposit bridges

Fig. 5

Table 1

Product distribution in C wt% of three kinds of catalysts.

Reaction conditions: 60°C, GHSV 2000h^{-1}

Set	Catalyst	TOS	Composition (%)				C_2H_2 Conv.(%)	C_2H_4 Selectivity(%)
			C_2H_2	C_2H_4	C_2H_6	CH_4		
			Feed					
			0.2099	99.7708	0.0121	0.0072		
			Product					
	Base[a]		0.0037	99.8568	0.1321	0.0074	98.23	41.71
A	Untreated[b]	5 min	0.0065	99.8566	0.1294	0.0074	96.90	42.18
	Treated[c]		0.0015	99.8784	0.1126	0.0073	99.28	51.63
	Base[a]		0.0192	99.8338	0.1396	0.0074	90.85	33.04
B	Untreated[b]	44 h	0.0156	99.8465	0.1305	0.0073	92.56	38.96
	Treated[c]		0.0059	99.8731	0.1134	0.0075	97.18	50.15

[a]0.04% Pd/Al_2O_3

[b]0.04% $Pd\text{-}Ag/Al_2O_3$

[c]0.04% $Pd\text{-}Ag/Al_2O_3$ treated with N_2O

Table 2

BET surface area of three catalysts

Catalyst	BET (m^2/g)
0.04% Pd/Al_2O_3	4.74
0.04% $Pd\text{-}Ag/Al_2O_3$ (untreated)	4.36
0.04% $Pd\text{-}Ag/Al_2O_3$ (treated)	4.98

Table 3

The metal active sites of catalysts measured by CO adsorption

Catalyst	Metal active sites (sites/gram of catalyst)
0.04% Pd/Al_2O_3	3.30×10^{17}
0.04% $Pd\text{-}Ag/Al_2O_3$	2.52×10^{17}
0.04% $Pd\text{-}Ag/Al_2O_3$ (0.02 cc of N_2O)	3.14×10^{17}
0.04% $Pd\text{-}Ag/Al_2O_3$ (0.035 cc of N_2O)	3.22×10^{17}
0.04% $Pd\text{-}Ag/Al_2O_3$ (0.05 cc of N_2O)	3.70×10^{17}
0.04% $Pd\text{-}Ag/Al_2O_3$ (0.10 cc of N_2O)	4.04×10^{17}
0.04% $Pd\text{-}Ag/Al_2O_3$ (0.15 cc of N_2O)	3.37×10^{17}
0.04% $Pd\text{-}Ag/Al_2O_3$ (0.33 cc of N_2O)	3.18×10^{17}

Mr. Tharathon Mongkhonsi

Department of Chimical Engineering
Faculty of Engineering
Chulalongkorn University
Bangkok 10330, Thailand

May 25, 2000

Dear Sir:

Re : Manuscript No. CL- 000463

Tharathon Mongkhonsi, Purida Pimanmas, and Piyasan Praserthdam
Selective Oxidation of Ethanol and 1-Propanol over V-Mg-O/TiO_2 Catalyst

As you will see from the enclosed reviews, the referees recommended publication of this paper in Chemistry Letters. However, they made several comments which will merit your consideration. Please send two copies of the revised manuscript, marked REVISED, directly to me, along with a letter indicating what revisions have been made within the next two weeks of receiving this letter. If further delays are necessary, please notify me as soon as possible.

Please keep in mind that the revised manuscript must strictly conform to the format specifications described in Information for Authors, 1998.

Sincerely yours,

PS Please see the FAX version of your manuscript which shows how to modify the format.

朝倉清高

0811
市北区北11条西10丁目
道大学
化学研究センター
委員　朝倉　清高

Kiyotaka Asakura, Associate Editor
Catalysis Research Center
Hokkaido University,
Kita-11-jyo Nishi-10-chome,
Kita-ku, Sapporo 060-0811, Japan

81-11-706-3671　　fax +81-11-706-3671　　email askr@cat.hokudai.ac.jp

Effect of Organic Solvents on the Thermal Stability of Porous Silica-Modified Alumina powders Prepared via One Pot Solvothermal Synthesis

Piyasan Praserthdam[a], Masashi Inoue[b], Okorn Mekasuvandumrong[a], Waraporn Thanakulrangsan[c] and Suphot Phatanasri[a]

[a] Department of Chemical Engineering, Chulalongkorn University, 10330 Thailand E-mail: Okornm@yahoomail.com

[b] Department of Hydrocarbon Chemistry, Faculty of Engineering, Kyoto University, Kyoto 606, Japan

[c] Department of Chemical Engineering, Rajamanggala Institute of Technology, Patumthani 12110 Thailand

Abstract

Mixtures of alumina isopropoxide (AIP) and tetraethyl orthosilicate (TEOS) with weight ratios of AIP/TEOS = 8 in various organic solvents were set in an autoclave and heated at 300 °C for 2 h. The fluid phase was removed at the supercritical temperature. The products were calcined in air to yield silica-modified aluminas. These silica-modified aluminas had different morphology that affected the surface area and thermal stabilities at high temperatures. The reactions of AIP and TEOS in 1-butanol gave substantially the wrinkled sheets morphology having the thermal stability higher than the spherical particles obtained by reaction in toluene.

Introduction

Recently, much attention has been paid to improve the properties of catalyst at high temperatures. Transition aluminas have large surface areas with reasonable mechanical strength and are widely used as catalyst supports in industry. However, because of metastable nature of transition aluminas, they usually transform to α-alumina at around 1100°C which causes a drastic decrease in the surface area. For the purpose of increasing the thermal stability of transition aluminas, the effect of dopants has been investigated and partial success was achieved by incorporation of ThO_2, ZrO_2, SiO_2, etc., in to the alumina matrix.

Iler (1964) found that the addition of silicic acid to fibrillar colloidal boehmite increased the thermal stability of the resultant alumina. Yoldas (1976) examined the thermal stabilities of silica-modified aluminas prepared by a sol-gel method and reported that the alumina doped with 6% silica had the maximum temperature (1380°C) for α-alumina transformation. Murrell and Dispenziere (1988) reported that the alumina doped with 5% silica by reaction with tetraethyl orthosilicate (TEOS) led to marked stabilization against loss of the surface area by vanadium attack at high temperatures. In other papers in this field, Johnson (1990) and Beguin (1991) also prepared silica-modified alumina and confirmed the increase of the thermal stability of the resultant alumina by addition of silica.

For the synthesis of inorganic materials by using organic media, Inoue et al. (1988-1992) found that the glycothermal treatment (the use of glycol instead of water for

hydrothermal treatment) of gibbsite at 250 °C yielded the product having a structure of boehmite with glycol moieties incorporated between the boehmite layers with the covalent bonding. Inoue et al. (1988) also found that treatment of aluminum alkoxide in various glycols at 300 °C yielded the glycol derivatives on boehmite. Inoue et al. (1995) prepared the silica-modified alumina by the reaction of aluminum isopropoxide (AIP) and tetraethyl orthosilicate (TEOS) in 1,4 butanediol at 300°C and found that the product with Al/Si ratio of 8 maintained large surface area even after calcination at high temperatures.

Highly porous solids can be prepared by the removal of solvent from a wet gel at a temperature above the critical temperature of the solvent. In recent years, researchers have built up the strong technical background in such materials. Fanelli and Anthony (1983) found the new polymerization catalyst system comprising an aluminum compound and a transition metal compound on an alumina-based aerogel support. Armor and Carlson (1984) prepared a catalyst composition of a uniform dispersion of individual metallic palladium particles. They (1989) also prepared high pore volume alumina by hydrolysis of AIP followed by supercritical removal of the fluid phase. Aerogel has good properties such as high pore volume, high surface area, and high thermal stability. These properties result from this method that obviates the inherent shrinkage or structural collapse that occurs when precursor gel are conventionally dried to a solid form. Such shrinkage or compaction are brought about by the surface tension of residual liquid trapped within the fragile gel structure.

In the present work, mixtures of AIP and TEOS were treated in 1-butanol, and toluene, and the fluid phase was separated by supercritical drying. In other words, solvothermal synthesis of oxides is combined with the supercritical drying method, which provides a convenient route for the synthesis of powders by using only one reaction vessel. The properties of products are also examined. Then the products are calcined at various temperatures, and thermal stabilities of the resulting silica-modified aluminas are investigated.

EXPERIMENT

In this paper, the products were prepared by three different methods. First, the mixtures of aluminum isopropoxide (AIP, Aldrich) and tetraethyl orthosilicate (TEOS, Aldrich) at weight ratios of 8 were suspended in 100 ml of toluene in a beaker, and then set up in a 300 ml autoclave. In the gap between the beaker and the autoclave wall, 30 ml of toluene was added. After the autoclave was completely purged with nitrogen, the suspension was heated to 300°C at a rate of 2.3°C/min and held at that temperature for 2 h. During the reaction, the autogenous pressure gradually increased to 6-14 MPa. After the reaction, the autoclave valve was opened, and the fluid phase in the autoclave was released at that temperature condensing in a cooling coil. The condensed liquid was collected in another beaker. After the autoclave was cooled, the white powder products were obtained. For the second method, the same procedures as the first one were followed except that 1-butanol was used instead of toluene. In the third preparation, the

same procedures as the first one were followed but a mixture of water and toluene was added instead of toluene in the gap between the beaker and the autoclave wall. Amount of water was varied as 10 and 30 ml.

A part of the product was calcined in a box furnace by heating to the desired temperature (600°C, 1000°C, 1150°C) at a rate of 10 °C/min and holding at that temperature for1 h, and thus silica-modified aluminas were obtained.

The reaction products will be designated by abbreviations T, B and H meaning the solvents that used in the reaction: T means toluene, B means 1-butanol, and H means the mixture of water and toluene in the gap between the beaker and the autoclave wall. The abbreviation was followed by AS, which means the silica-modified alumina. When calcined samples are specified, these abbreviations are followed by calcination temperature in the parentheses. Therefore, TAS(1150) means the silica-modified alumina sample prepared in toluene and calcined at 1150 °C.

Characterization

Powder X-ray diffraction (XRD) was measured on a SIEMENS XRD D5000 using Cu Kα radiation, Infrared (IR) Spectra were recorded on a NICOLET FT-IR Impact 400 spectroscopy using the ex-situ IR technique. Morphologies of the particles were observed by JEOL Transmission Electron Microscope. The BET surface areas were calculated by the BET-single point method on the basis of the nitrogen uptake measured at P/Po = 0.3 using a gas chromatograph. The surface areas calculated by the ordinary

BET method were in good agreement with the surface areas calculated by the single-point method.

Results

The products obtained by one-pot synthesis of mixtures of AIP and TEOS in toluene were colorless powders. The XRD patterns of TAS and TAS calcined at different temperatures are shown in Fig.1a. TAS and TAS(600) exhibited the typical pattern for amorphous product. When the product was calcined at 1000°C and 1150°C, TAS(1000) and TAS(1150) exhibited the characteristic of spinel alumina and some mullite phase was observed from a small peak at $2\theta = 26.5$. When mixtures of AIP and TEOS were allowed to react in 1-butanol, the products were colorless powders. As shown in Fig.1b, BAS exhibited the typical pattern for the mixtures of χ-alumina and pseudoboehmite. BAS (600) exhibited the typical pattern for λ-alumina, while BAS(1000) and BAS(1150) exhibited the typical characteristic for spinel alumina. When the product was prepared by using toluene as the solvent and a mixture of water and toluene was added in the gap between the beaker and the autoclave wall, the XRD patterns of HAS calcined at any temperatures were almost similar to BAS as shown in Fig.1c. This indicates that the water added to toluene according to the third method has the same effect on the reaction as in the case of product preparation in 1-butanol.

IR spectra of the products are shown in Fig.2. Bands characteristics of the boehmite structure were seen at 773, 615 and 478 cm^{-1}, suggesting that BAS had the

layer structure of boehmite and BAS exhibited the small band at 1070 cm^{-1} due to stretching vibration mode of Si-O-Si bond. On the other hand, products obtained in toluene had no adsorption band that indicated the boehmite layer. IR spectra of TAS did not show any band at 1070 cm^{-1}. As for IR spectra of the product prepared via the third preparation, HAS showed the band characteristics of the boehmite structure at 773, 615, 478 cm^{-1} and small band at 1070 cm^{-1}. These adsorption bands were similar to BAS.

Transmission electron micrographs of the calcined silica-modified aluminas at AIP/TEOS ratio of 8 prepared in different solvents are shown in Fig.3. The morphology of BAS(600) seems to be the mixture of wrinkled sheets and spherical particles. When the product was calcined at high temperature, BAS(1150) consists of substantially the wrinkle sheets which are almost the same as BAS(600). However, the wrinkled sheets irregularly twisted in the product became progressively straight as the calcination temperature rose. The morphology of TAS(600) seems to be spherical particles with out any observation of the wrinkled sheets and the particle size increased when the calcination temperature was increased(TAS(1150)). Interestingly enough, when the water was added in the gap between the beaker and autoclave wall (HAS(600)). The wrinkled sheets were observed though these sheets were attached by a number of spherical particles and the morphology of HAS(1150) was not far different from HAS(600).

The BET surface areas of products are summarized in Table1, It has been found that HAS had larger surface area than TAS at each calcination temperature. The results obtained suggest that the mechanism of reaction in toluene was difference from the other

two reactions and comparison of the results between HAS and BAS suggests that these reactions took place by the same reaction mechanism.

Discussion

The reaction in toluene occurred by thermal decomposition of aluminum isopropoxide. In the first step, aluminum isopropoxide was decomposed yielding Al-O$^-$ and $(CH_3)_2CH^+$ and in the second step nucleophilic attack of Al-O$^-$ on tetraethyl orthosilicate or another AIP molecule took place yielding the Al-O-Si or the Al-O-Al bond. The latter finally gave χ-alumina.

When small amounts of water was added in the gap between the beaker and the autoclave wall, the mechanism was changed. When the reaction temperature was raised, water in the gap was evaporated and dissolved in toluene in the beaker. In the second step, aluminum isopropoxide was hydrolyzed yielding Al-O-H and isopropanol. Al-O-H would react with other AIP molecules finally yielding pseudoboehmite. During this polymerization reaction, the aluminum species might react with TEOS remaining the silicon moiety between the boehmite layers.

When 1-butanol was used as the solvent in the reaction, AIP reacts with 1-butanol yielding aluminum butoxide. Thermal decomposition of aluminum butoxide gave the alkyl (butyl) derivative of boehmite. Because the aluminum butoxide is a primary alkoxide, thermal decomposition of this compound proceeds much more slowly than AIP itself. On the other hand, 1-butanol can be dehydrated to give water which then

hydrolyzes aluminum isopropoxide or butoxide yielding Al-O-H^+ and isopropanol or butanol. Al-O-H^+ finally yields pseudoboehmite. Since direct decomposition of aluminum alkoxide proceeds slowly, a part of reaction took place by this reaction sequence. In the presence of TEOS, Al-O-H^+ species or AL-O^- species formed by thermal decomposition of aluminum alkoxide attacks TEOS yielding Al-O-Si bond. It's well known silica-alumina has strong acidity and therefore the product also has strong acidity. Once a small amount of product having Al-O-Si bond is formed, surface acidity of the product dehydrates the solvent, 1-butanol, yielding water, which then hydrolyzes aluminum alkoxide yielding pseudoboehmite. Therefore addition of a small amount of TEOS in the starting mixture completely altered the reaction sequence.

From TEM data, the above mechanism of the reaction in each solvent can be proved. The wrinkled sheets found in the third preparation indicated that the water added in the gap between a beaker and the autoclave wall had the effect on the presence of the wrinkled sheets. This suggests that the hydrolysis of AIP gave the boehmite structure having the morphology of wrinkled sheets. Thus the mechanism of the reaction in 1-butanol occurred through the dehydration of 1-butanol to give water, and then the hydrolysis of AIP eventually yielding pseudoboehmite having the wrinkled sheets structure can be predicted.

From BET surface areas of the products shown in Table1, the products obtained in toluene had lower surface area at high calcination temperature than the products obtained in the presence of water in the gap between the autoclave wall and the beaker. This indicates the effect of water on the reaction. However the surface areas were far

lower than that of the product obtained in 1-butanol, the results suggests that the reaction in toluene having water in the gap proceeds by two routes: water dissolved in toluene hydrolyzes AIP, while thermal decomposition of AIP could occur. High thermal stability of product obtained in 1-butanol suggests that the hydrolysis of AIP substantially occurred.

It is generally accepted that α-alumina transformation starts from the contact between particles. Tucker (1985) found that crystallization of α-alumina started from the contact of polycrystalline spherical particles and single crystal are formed. He explained that mechanical strain caused by the thermal expansion concentrating at the contact point of spherical particle and caused tetragonal closest packing of oxygen atom to hexagonal closet packing, which acted as the nuclei of α-alumina. Taking into account of this explanation, the thermal stability of the present products can be elucidated. From BET surface area, the decreasing order of thermal stability of products prepared in each solvent is 1-butanol>toluene+water in the gap>toluene. From the morphological viewpoint, the thermal stability of the products increased with the increase of the content of wrinkled sheets. Since the wrinkled sheets have the limited number of contact points in the unit volume, the nucleation frequency of α-alumina, and hence the α-alumina transformation is reduced. On the other hand, the spherical particles have a large number of contact points between the primary particles which α-alumina transformation can occur much more easily.

Conclusion

The reaction of AIP and TEOS in toluene gave products having the spherical particles. When water was added in the gap between the beaker and the autoclave wall the product was seem as the mixture of wrinkled sheets and spherical particles which was the same as product synthesized in 1-butanol, however, the content of wrinkled sheets in BAS was higher than HAS. The thermal stability of products also increased with the increasing content of the wrinkled sheets. The wrinkled sheets occurred by the hydrolysis of aluminum alkoxide in the reaction system comprise the as-synthesis structure of boehmite, which had the limited number of contact point in the product morphology. BAS sample possessing substantially the wrinkle sheets had the highest thermal stability. The surface area of which is 169 m^2/g even after calcination at 1150 °C

Acknowledgements

The authors would like to thank the Thailand Research Fund (TRF) for their financial support of this project.

Reference

1. Armor, J. N., Carlson, E. J. US Patent 4469816 (1984)
2. Armor, J. N., Carlson, E. J. Variables in synthesis of unusually high pore volume aluminas, J. Mater. Sci. 22,2549-2556 (1989)
3. Beguin, B., Garbowski, E., Primet, M. Stabilization of alumina toward thermal sintering by silicon edition. . J. Catal. 127,595-604 (1991)
4. Fanelli, A. J., Burlew, J. V. US Patent 4387085 (1983)
5. Fanelli, A. J., Burlew, J. V. Preparation of fine alumina powder in alcohol, J. Mater. Sci. 23,2897-2904 (1989)
6. Gani, M. S. J., Mcpherson, R. Glass formation and phase transformation in plasma prepared Al_2O_3-SiO_2 powders. J. Mater. Sci.12, 999-1009 (1977)
7. Iler, R.K. Effect of Silica on transformations of fibrillar colloidal boehmite and gamma alumina. J. Am. Ceram. Soc. 47, 339-341 (1964)
8. Inoue, M., Kondo, Y. An ethylene glycol derivative of boehmite, Inorganic Chemistry 27, 215-221 (1988)
9. Inoue, M., Tanino, H. Formation of microcrystalline α-alumina by glycothermal treatment of gibbsite, J. Am. Cerm. Soc. 72, 352-353 (1989)
10. Inoue, M., Kominami, H. Thermal transformatiom of χ-alumina formed by thermal decomposition of aluminum alkoxide in organic media, J. Am. Cerm. Soc. 75, 2597-2598 (1992)

11. Inoue, M., Otsu, H. Kominami, H. Synthesis of thermally stable, porous silica-modified alumina via formation of a precursor in an organic solvent, Ind Eng Chem Res 35, 295-306 (1995)

12. Johnson, M. F. L. Surface areas stability of aluminas. J. Catal.123, 245-259 (1990)

13. Murrell, L. L., Dispenziere, N. C. Jr. Silica -stabilized aluminas resistance to vanadium attack under severe high temperature condition. J. Catal. 111, 450-452 (1988)

14. Tucker, D. L. Gamma-to-Alpha transformation in spherical aluminum oxide powders. J. Am. Ceram. Soc. 68, C163-164 (1985)

15. Yoldas, B. E. Thermal stabilization of an active alumina and effect of dopants on the surface area. J. Mater. Sci. 11, 465-470 (1976)

Table 1 : BET surface area of products calcined at various temperatures

AIP/TEOS of 8 in each solvents	BET surface areas (m^2/g)		
	600	1000	1150
TAS	244.2	92.4	74.7
BAS	210.6	190.5	168.4
HAS	208.7	182.7	110.8

Figure 1a: XRD patterns of precursor gel obtained by the reaction of AIP and TEOS in toluene at every calcination temperatures

Figure 1b: XRD patterns of precursor gel obtained by the reaction of AIP and TEOS in 1-butanol at every calcination temperatures

Figure 1c: XRD patterns of precursor gel obtained toluene, which the addition of water in the gap at every calcination temperatures

Figure 2: IR spectra of precursor gels for silica-modified aluminas obtained by the reaction of AIP and TEOS in every preparation

Figure 3: TEM image of precursor gel obtained by the reaction of AIP and TEOS in every preparation

Figure 4a: BET surface area of silica-modified aluminas prepared in toluene and calcination at various temperatures

Figure 4b: BET surface area of silica-modified aluminas prepared in 1-butanol and calcination at various temperatures

Figure 5a : TEM image of BAS(600)(*150,000)

Figure 5b : TEM image of BAS(1150)(*150,000)

Figure 5c : TEM image of TAS(600)(*150,000)

Figure 5d : TEM image of TAS(1150)(*150,000)

Figure 5e : TEM image of HAS(600)(*150,000)

Figure 5f : TEM image of HAS(1150)(*150,000)

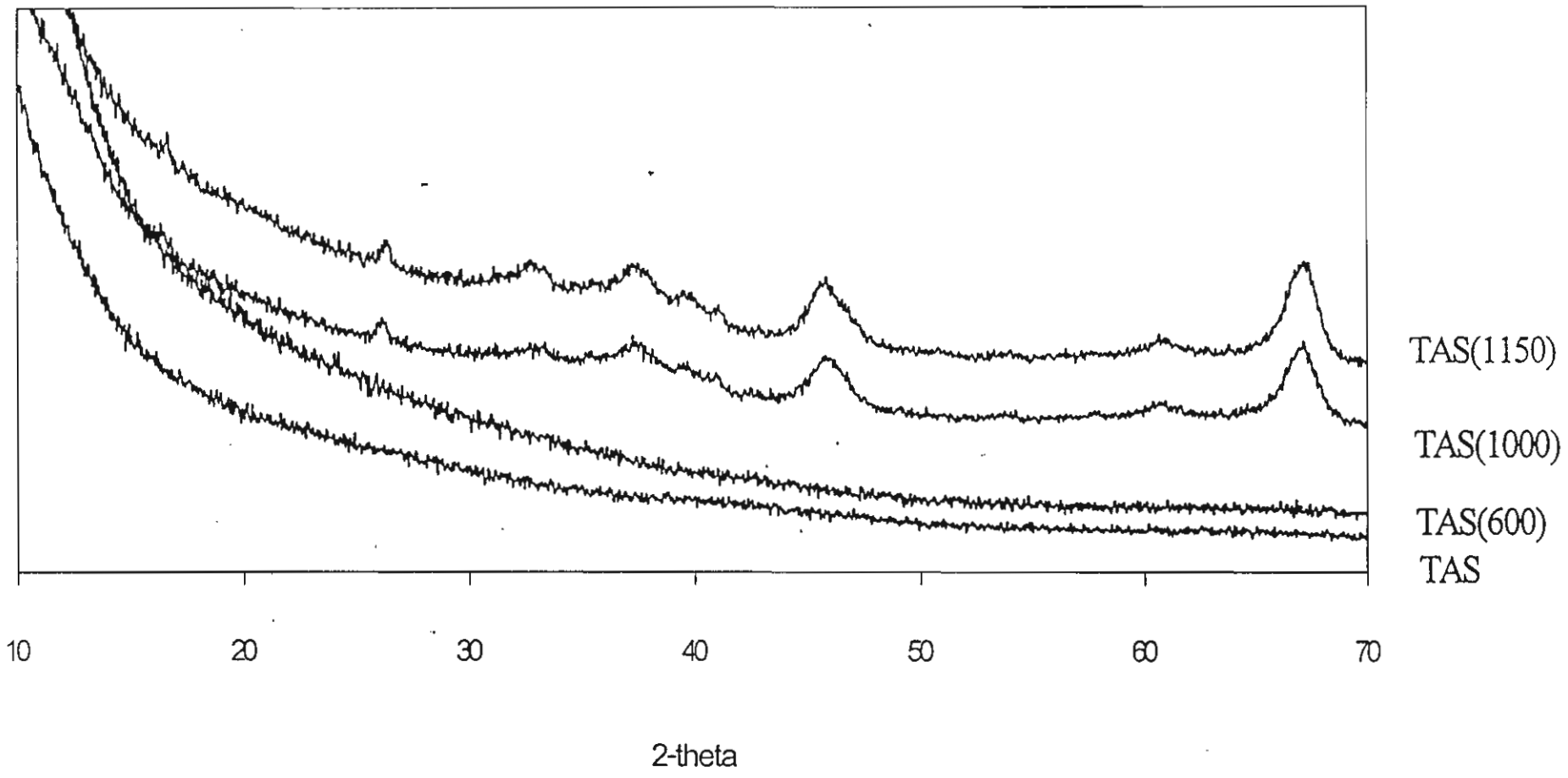
TAS(1150)
TAS(1000)
TAS(600)
TAS
10
20
30
40
50
60
70
2-theta

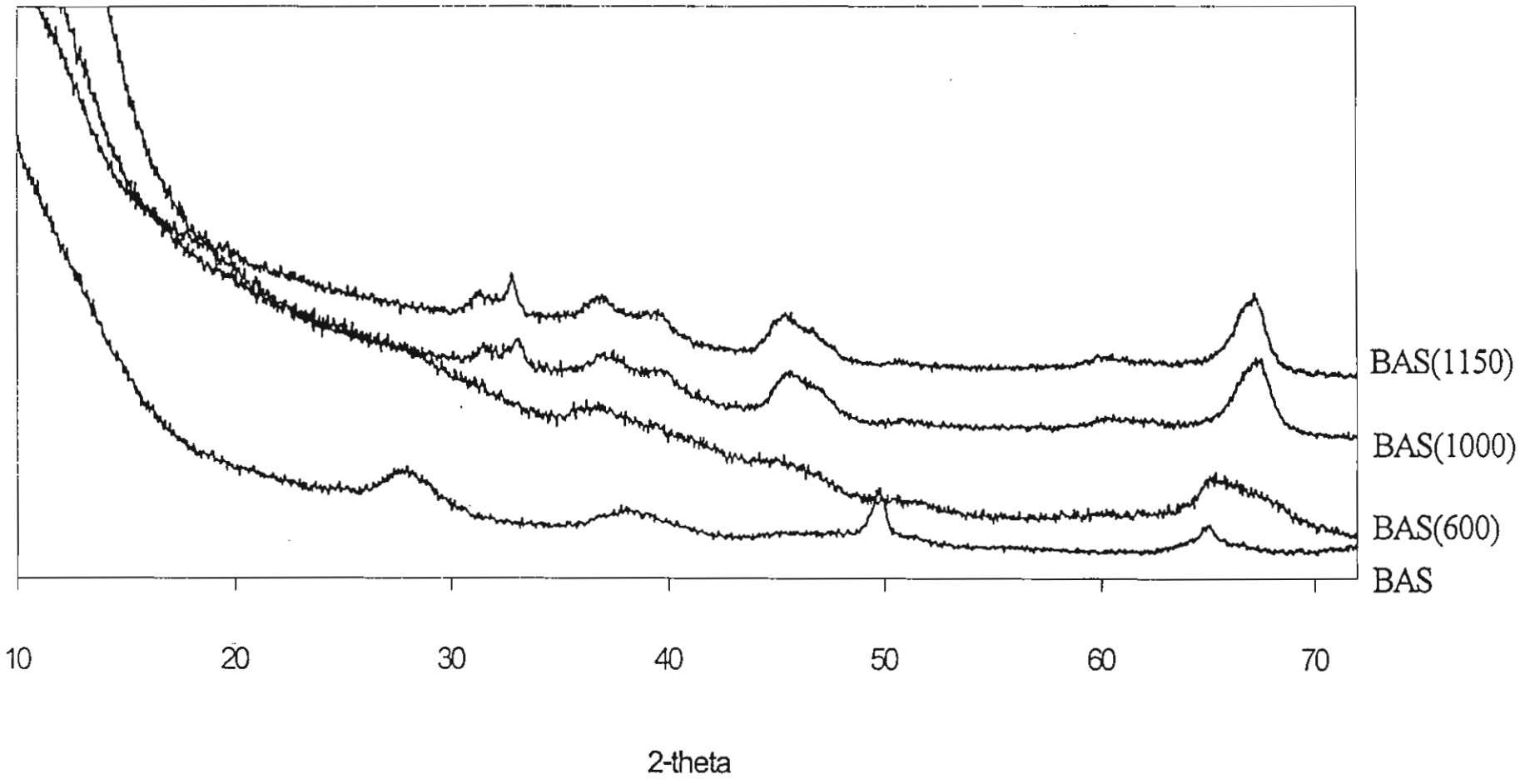
BAS(1150)
BAS(1000)
BAS(600)
BAS
10
20
30
40
50
60
70
2-theta

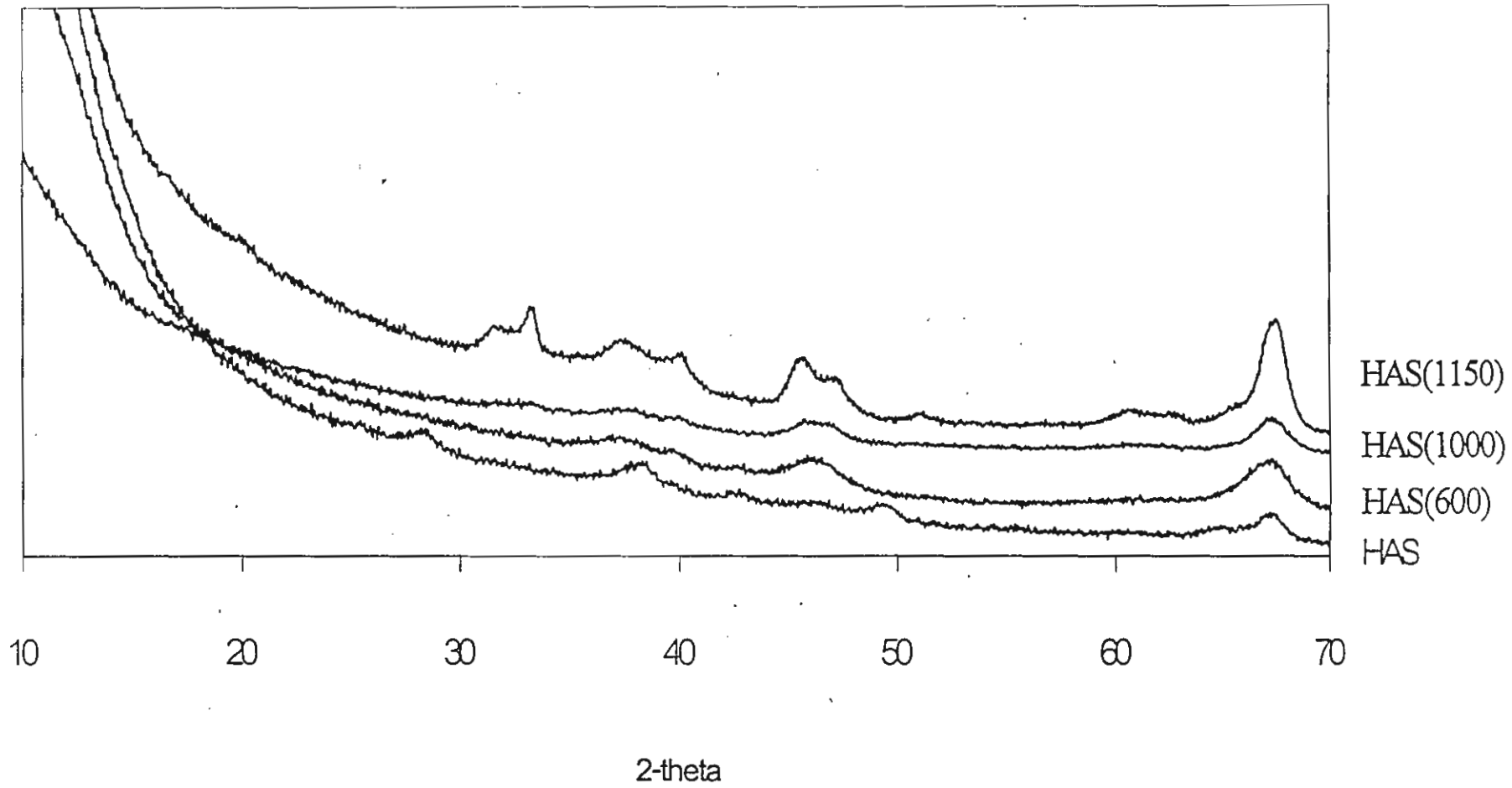
HAS(1150)
HAS(1000)
HAS(600)
HAS
10
20
30
40
50
60
70
2-theta

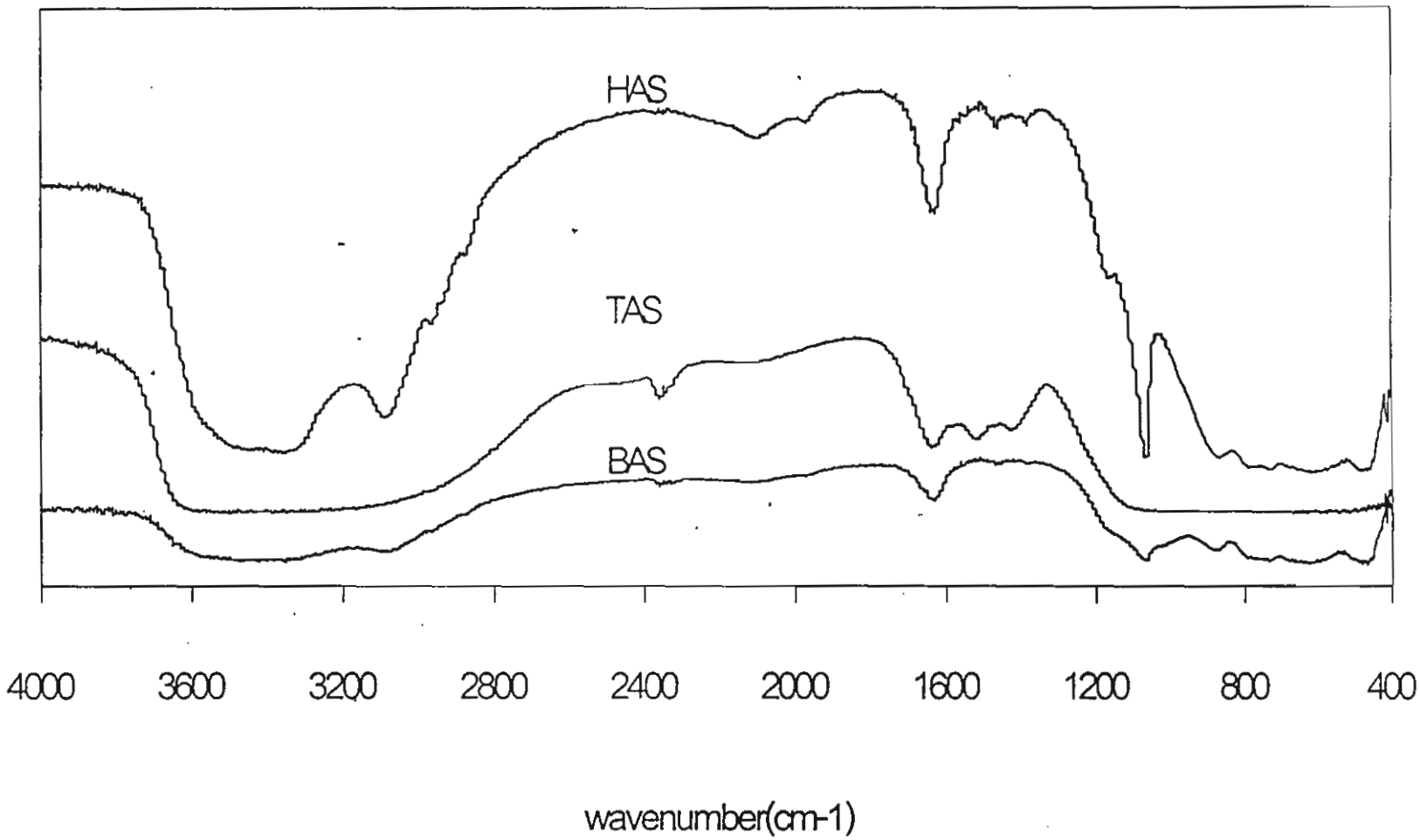
HAS
TAS
BAS
4000
3600
3200
2800
2400
2000
1600
1200
800
400
wavenumber(cm-1)

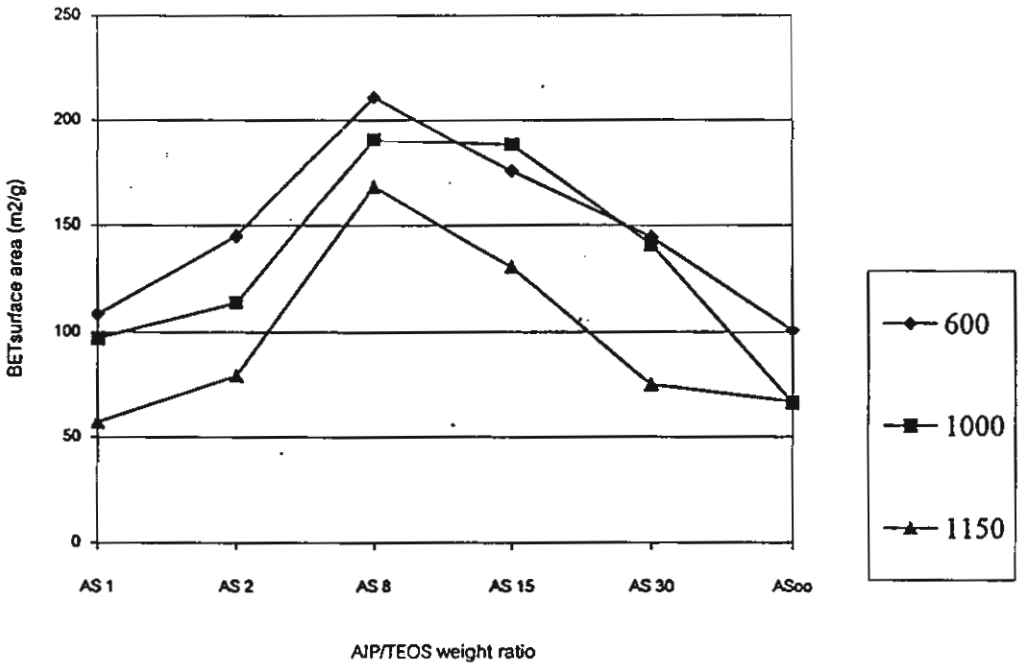
250
200
150
100
50
0
BETsurface area (m2/g)
AS 1
AS 2
AS 8
AS 15
AS 30
ASoo
AIP/TEOS weight ratio
600
1000
1150

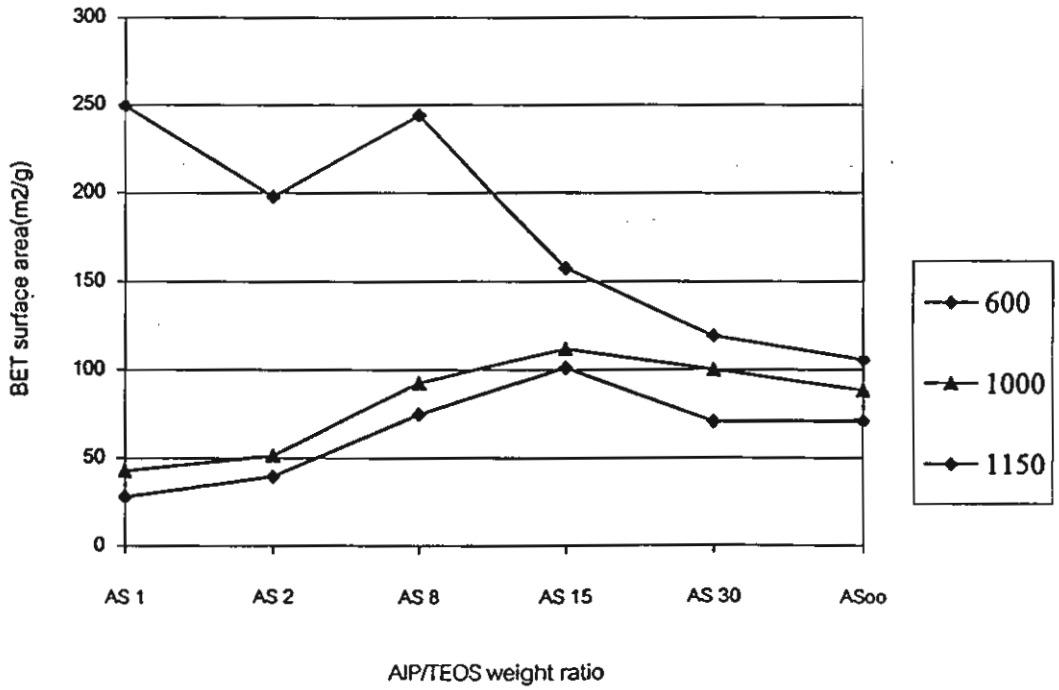
300
250
200
150
100
50
0
BET surface area(m2/g)
AS 1
AS 2
AS 8
AS 15
AS 30
ASoo
AIP/TEOS weight ratio
600
1000
1150

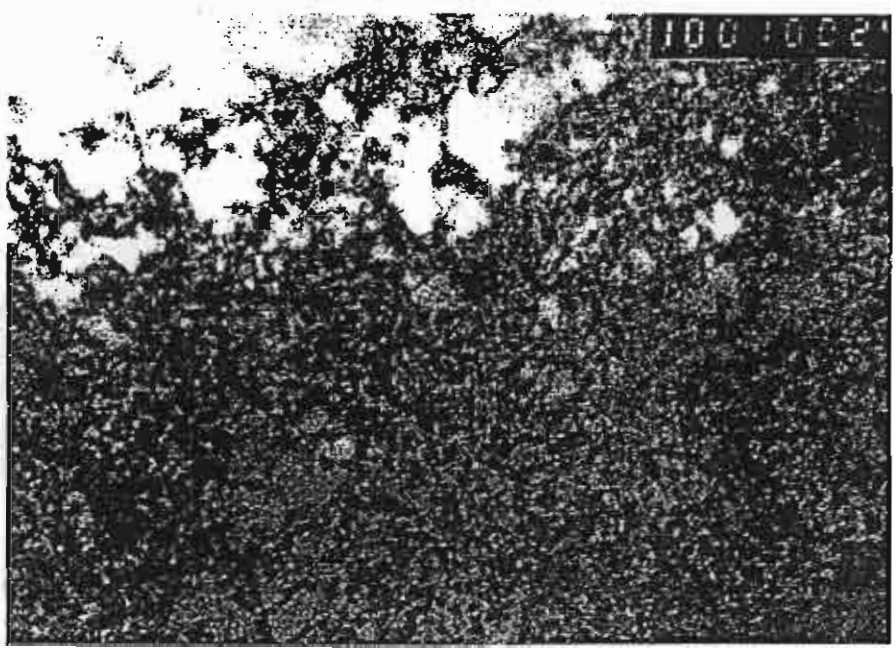

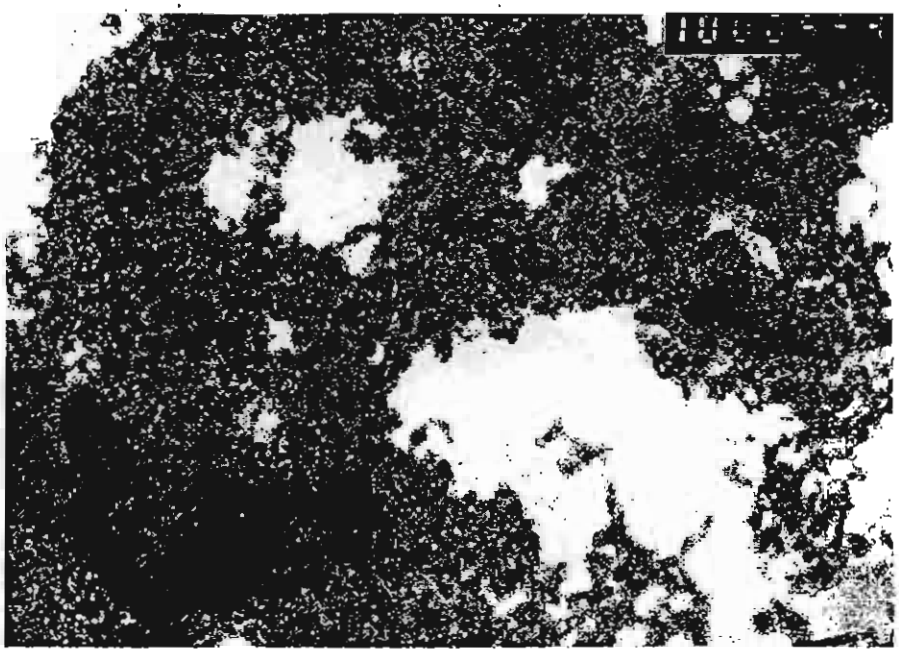

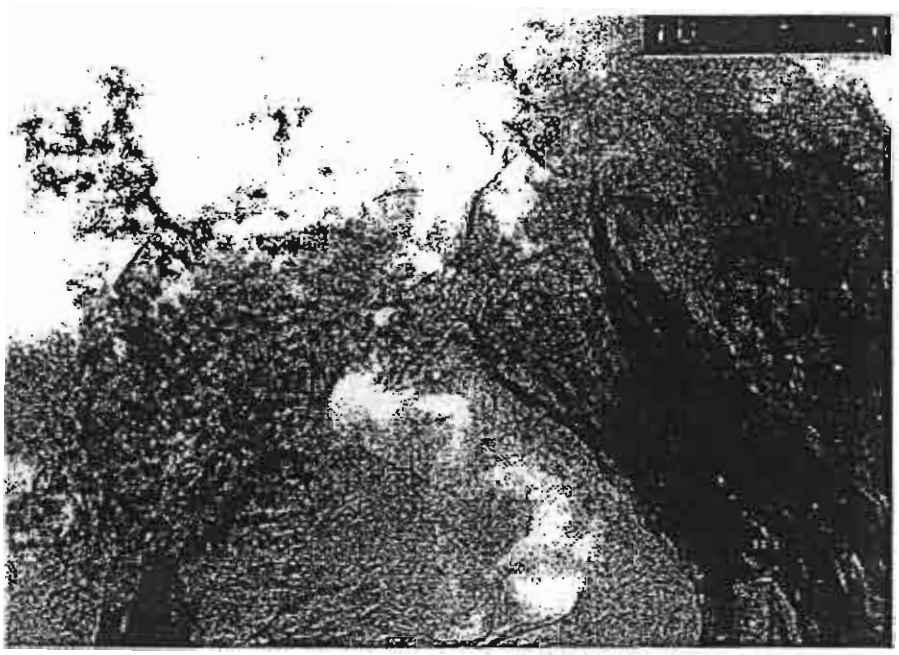

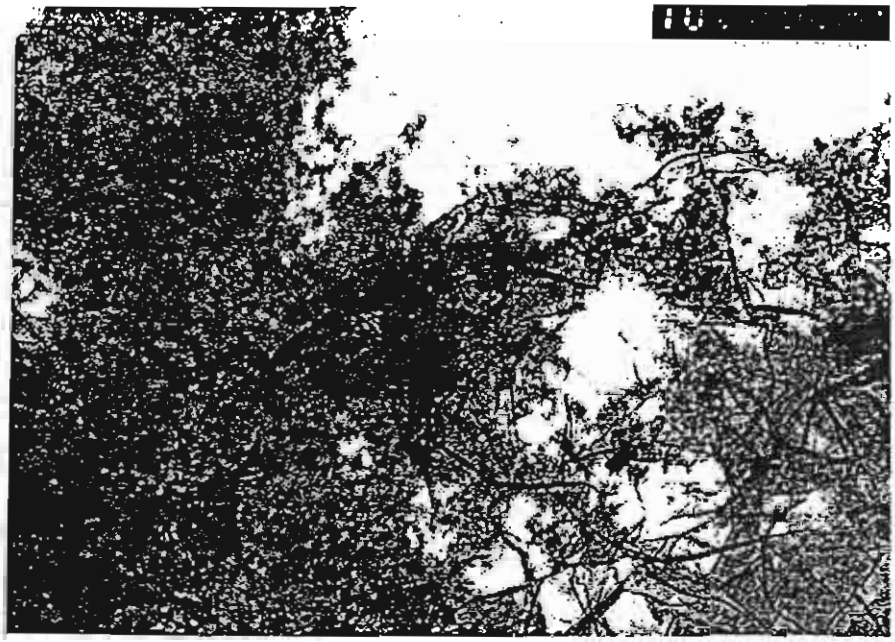

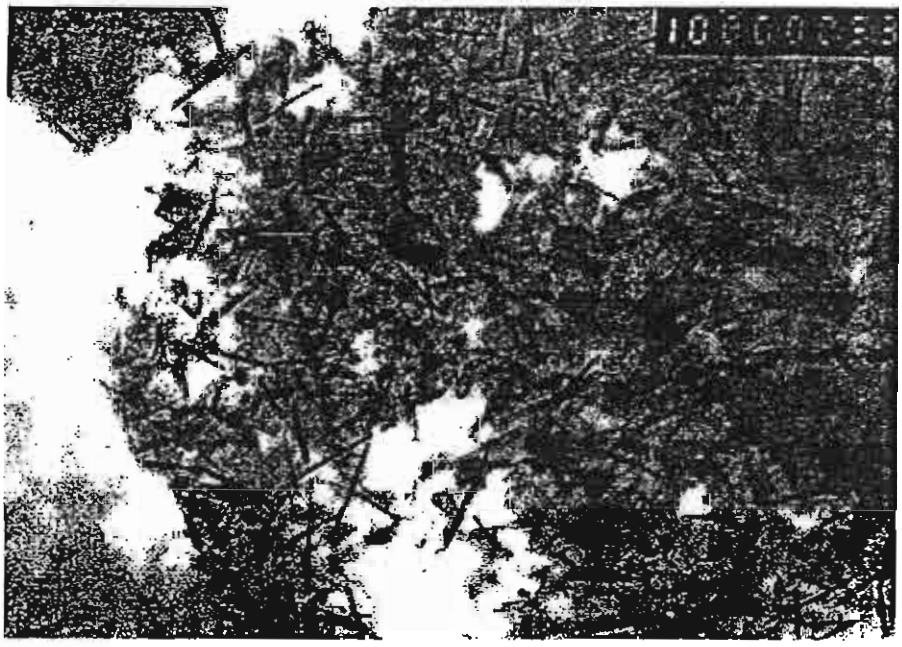

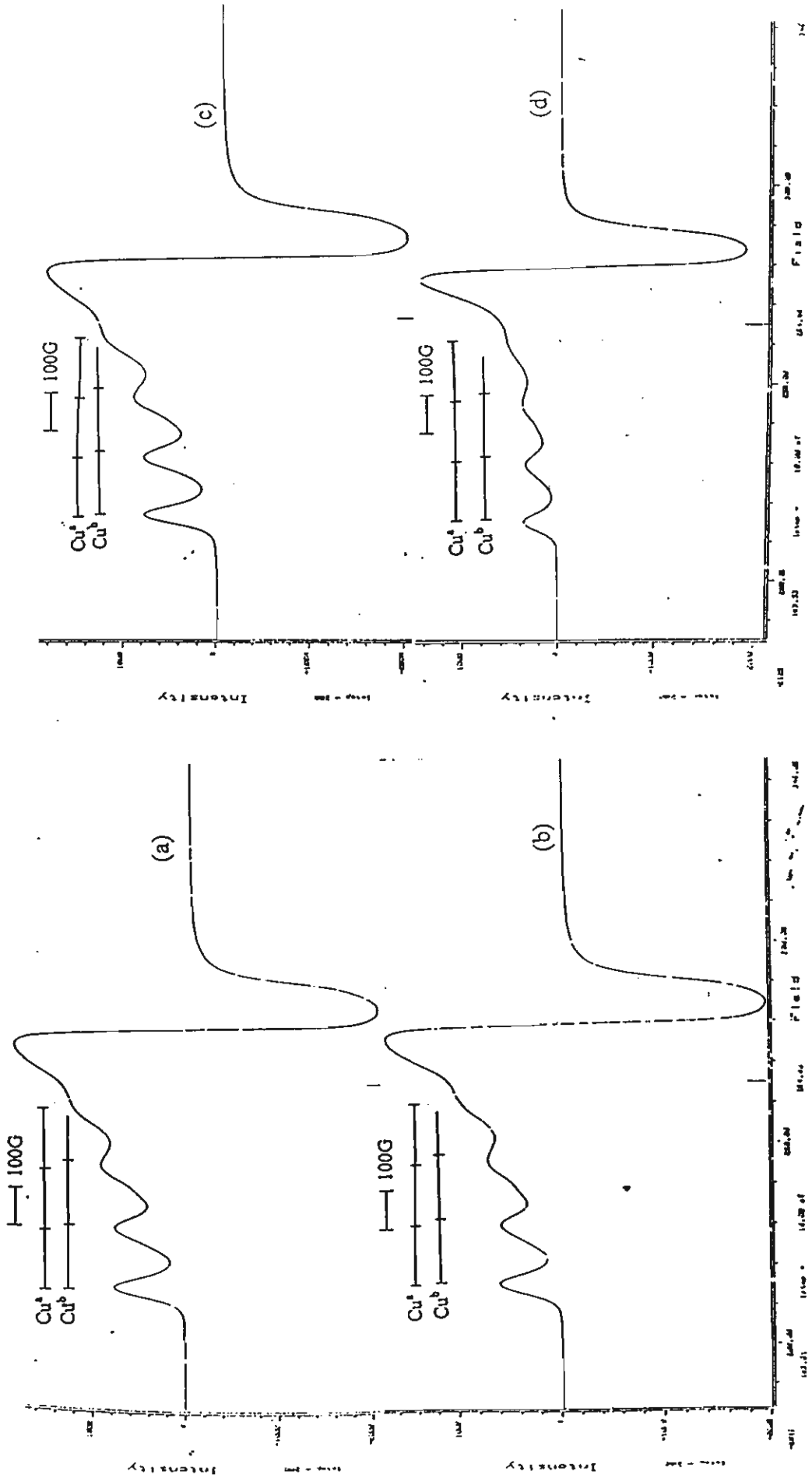

Figure 2.3

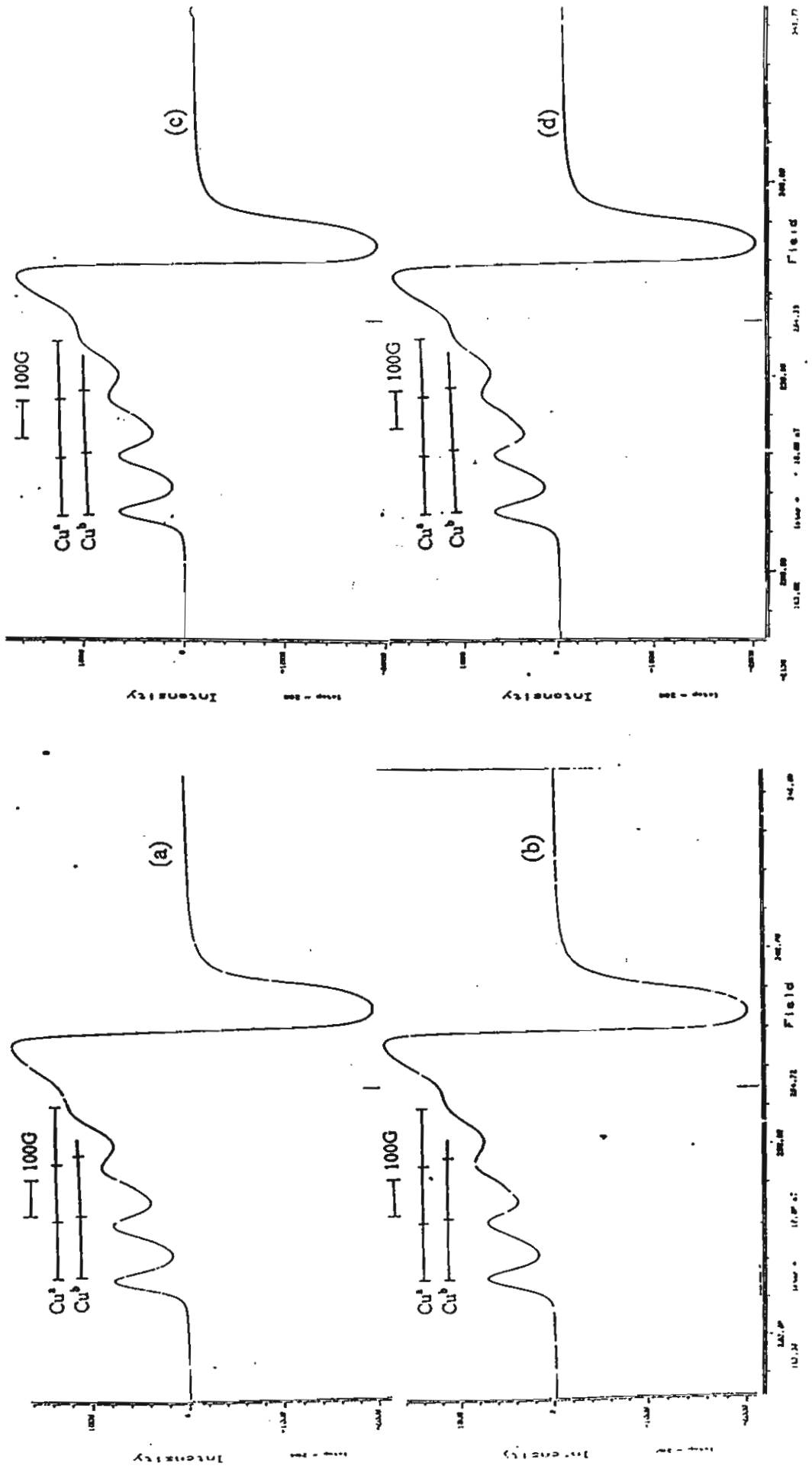

Figure 2.4

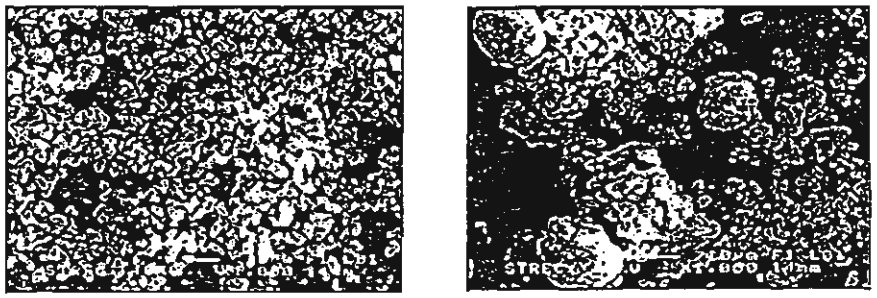

Cu/H-MFI

0.1%Pd/Cu/-MFI

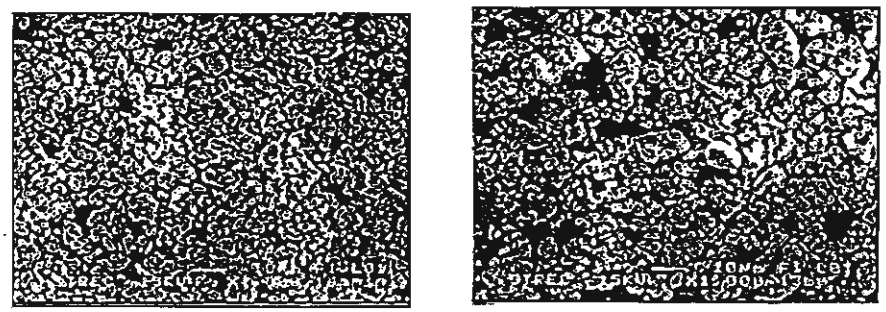

0.2%Pd/Cu/H-MFI

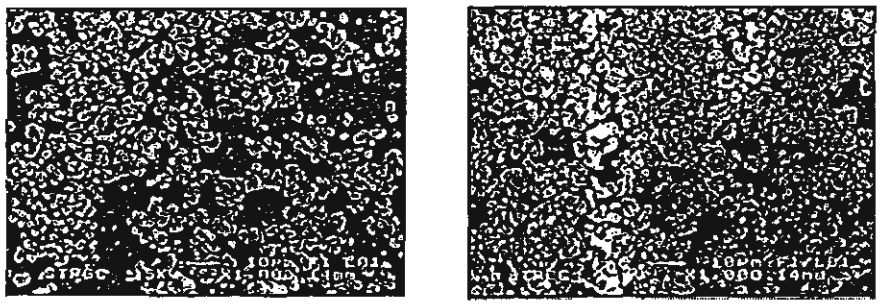

0.3%Pd/Cu/H-MFI

(a) (b)

Figure 3.1

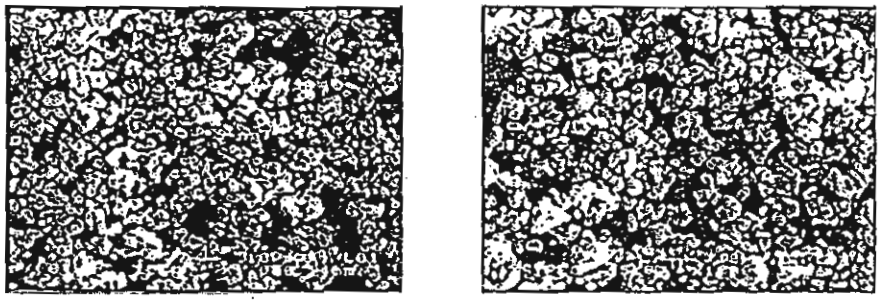

0.4%Pd/Cu/H-MFI

0.6%Pd/Cu/-MFI

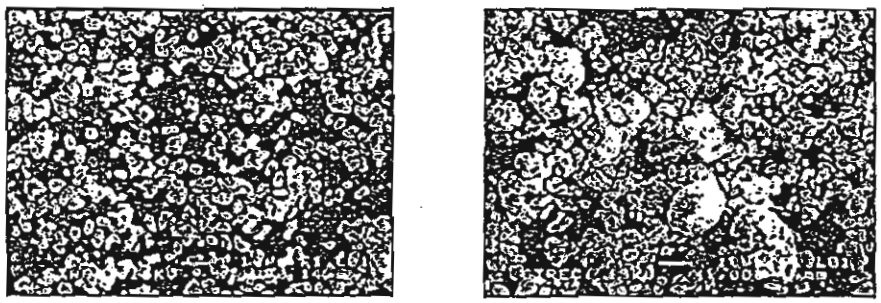

0.8%Pd/Cu/H-MFI

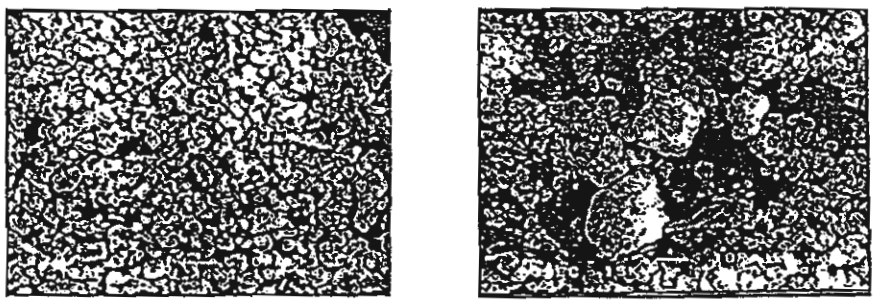

1.0%Pd/Cu/H-MFI

(a) **(b)**

Figure 3.2

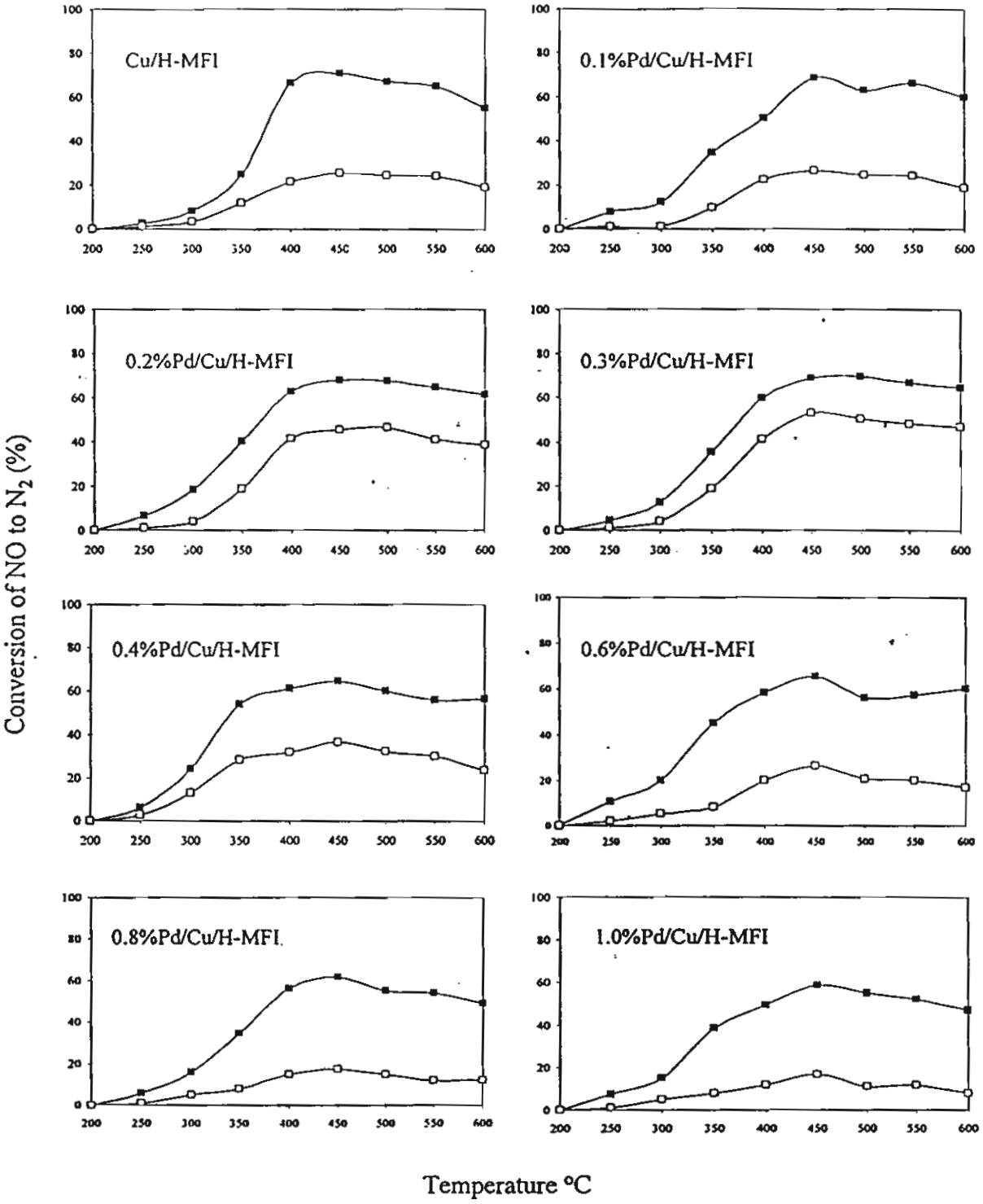
Cu/H-MFI
0.1%Pd/Cu/H-MFI
0.2%Pd/Cu/H-MFI
0.3%Pd/Cu/H-MFI
0.4%Pd/Cu/H-MFI
0.6%Pd/Cu/H-MFI
0.8%Pd/Cu/H-MFI
1.0%Pd/Cu/H-MFI
Conversion of NO to N_2 (%)
Temperature °C

Figure 4

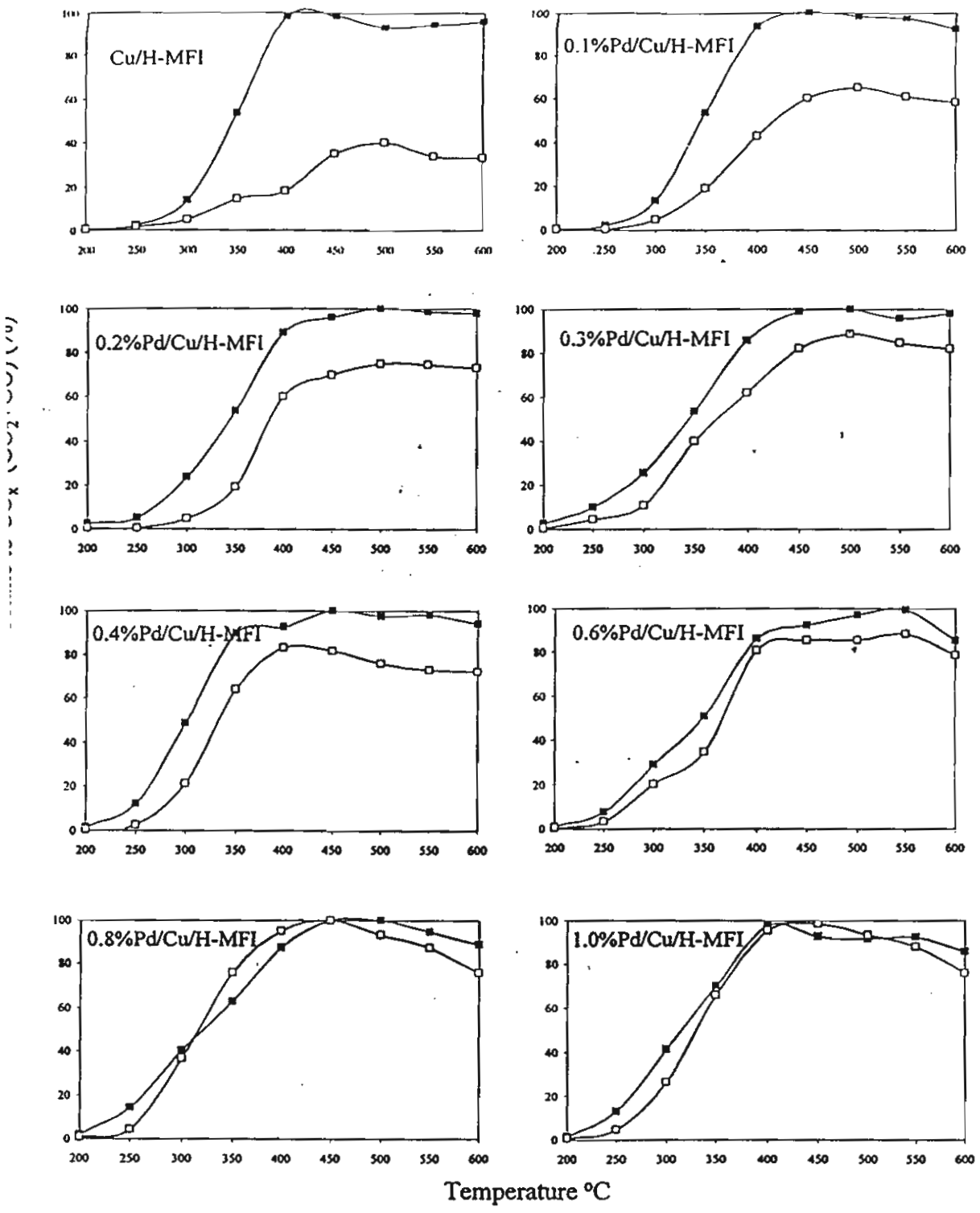
Cu/H-MFI
0.1%Pd/Cu/H-MFI
0.2%Pd/Cu/H-MFI
0.3%Pd/Cu/H-MFI
0.4%Pd/Cu/H-MFI
0.6%Pd/Cu/H-MFI
0.8%Pd/Cu/H-MFI
1.0%Pd/Cu/H-MFI
Temperature °C

Figure 5

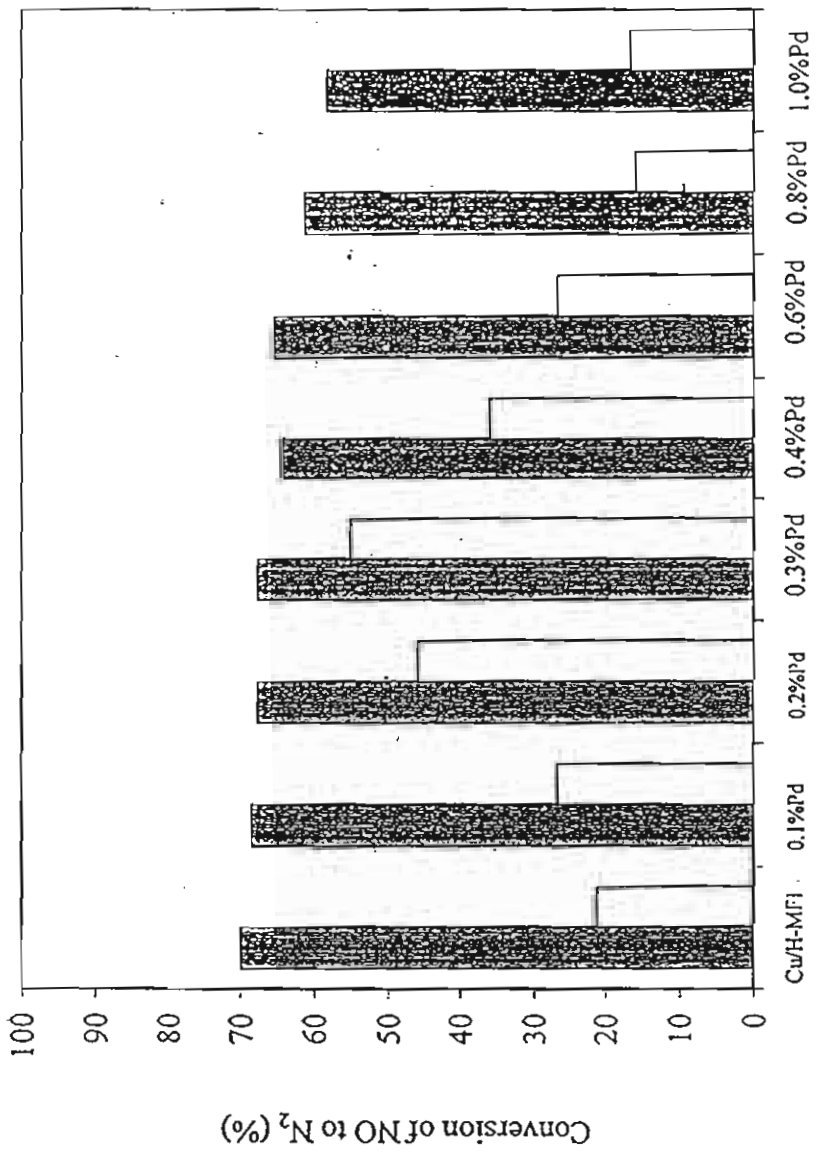
Conversion of NO to N_2 (%)
100
90
80
70
60
50
40
30
20
10
0
Cu/H-MFI
0.1%Pd
0.2%Pd
0.3%Pd
0.4%Pd
0.6%Pd
0.8%Pd
1.0%Pd
fresh catalyst
pretreated catalyst

Figure 6

Table 1. Data for bulk composition, BET surface area and crystallinity of catalysts

Figure 1 ^{27}Al MAS-NMR spectra of fresh (a) and severe steamed (b) catalysts.

Figure 2.1 ESR spectra of high spin Cu^{2+} of Cu/H-MFI and Pd/Cu/H-MFI with and without pretreatment at 800°C 10% H_2O a) fresh Cu/H-MFI, b) severe steamed Cu/H-MFI, c) fresh 0.1%Pd/Cu/H-MFI, d) severe steamed 0.1%Pd/Cu/H-MFI

Figure 2.2 ESR spectra of high spin Cu^{2+} of Cu/H-MFI and Pd/Cu/H-MFI with and without pretreatment at 800°C 10% H_2O a) fresh 0.2%Pd/Cu/H-MFI, b) severe steamed 0.2%Pd/Cu/H-MFI, c) fresh 0.3% Pd/Cu/H-MFI, d) severe steamed 0.3%Pd/Cu/H-MFI

Figure 2.3 ESR spectra of high spin Cu^{2+} of Cu/H-MFI and Pd/Cu/H-MFI with and without pretreatment at 800°C 10% H_2O a) fresh 0.4%Pd/Cu/H-MFI, b) severe steamed 0.4%Pd/Cu/H-MFI, c) fresh 0.6% Pd/Cu/H-MFI, d) severe steamed 0.6%Pd/Cu/H-MFI

Figure 2.4 ESR spectra of high spin Cu^{2+} of Cu/H-MFI and Pd/Cu/H-MFI with and without pretreatment at 800°C 10% H_2O a) fresh 0.8%Pd/Cu/H-MFI, b) severe steamed 0.8%Pd/Cu/H-MFI, c) fresh 1.0% Pd/Cu/H-MFI, d) severe steamed 1.0%Pd/Cu/H-MFI

Figure 3.1 Scanning electron micrograph of catalysts.(a) fresh and (b) severe steamed catalysts

Figure 3.2 Scanning electron micrograph of catalysts.(a) fresh and (b) severe steamed catalysts

Figure 4 The effect of hydrothermal-treatment on the activity of NO conversion of Cu/H-MFI, Pd/Cu/H-MFI. Close symbol: fresh catalysts, Open symbol: pretreated catalysts

Figure 5 The effect of hydrothermal-treatment on the activity of n-Octane conversion of Cu/H-MFI, Pd/Cu/H-MFI. Close symbol: fresh catalysts, Open symbol: pretreated catalysts

Figure 6 Maximum NO conversion of catalysts

Effect of Pd on the Stability Improvement of Cu/H-MFI for NO removal under Hydrothermal Pretreatment Conditions

P.Praserthdram, S.Phatanassri and J.Rungsimanop

Petrochemical Engineering Laboratory, Department of chemical Engineering,

Faculty of Engineering, Chulalongkorn University, Bangkok 10330,Thailand

Tel: +(662) 218-6711, Fax: +(662) 218-6769, E-mail: Piyasan.P@chula.ac.th

Abstract

The effect of Pd-modification of Cu ion-exchanged H-MFI (Pd/Cu/H-MFI) on its performance for removal was studied. The stability of the catalysts subjected to hydrothermal treatment with a He stream containing 10% stream at 800 °C was investigated. The Cu/H-MFI catalyst markedly lost its activity for NO conversion after the hydrothermal pretreatment. The Pd-modification of the Cu/H-MFI resulted in improved stability against the hydrothermal treatment with the presence of Pd loading amount approximately 0.2 to 0.3 wt%. The dealumination of tetrahedral Al in MFI framework was completely prevented with the Pd loading amount of 0.3% or higher. Further loading of Pd higher than 0.3% caused the larger crystallite size upon pretreatment as seen from the Scanning Electron Micrographs (SEM). It has been suggested that there may be some changes in Pd and Cu on H-MFI, such as alloying and/or palladium oxides formation, loading to some lost of Cu^{2+} active species for NO

removal. This results in the limitation of NO conversion improvement for the pretreated Pd/Cu/H-MFI with the loading amount of Pd higher than approximately 0.3%.

Keywords: Copper ion-exchanged MFI, Pd-modification, stability improvement, NO removal, Hydrothermal pretreatment

* To whom correspondence should be directed

1. Introduction

The environmental problems caused by emissions from stationary sources and transportation vehicles are still using despite of the recent advance in catalytic technologies base on NH_3-reduction and the use of three-way catalysts. NO emitted from combustion facilities and diesel engines causes acid rain and photochemical smog [1]. A number of studies concerning various types of catalyst for NO removal have been investigated. Cu ion-exchanged MFI type zeolite (Cu/MFI) proposed by Iwamoto et al. is effective for NO removal under the excess oxygen condition [2,3]. Other kinds of metal ion-exchanged MFI such as gallium [4,5], ion [6,7], cobalt [8-10], cerium [11,12], platinum [13], palladium [14] were also studied for the reaction. In addition, other groups of active catalysts such as transition metal and/or metal oxide (Cu, Co, Mn, Fe, Cr, V, Ag) were also concerned [15-19]. Nevertheless, any types of catalyst referred above suffer from the deactivation under the condition of high temperature and the presence of

stream possibly occurred in practical use [20-22]. On the other hand, platinum group metal catalysts have also been studied for NO conversion [23,24] and it is known that platinum group metal catalysts are highly resistant to large amounts of steam [25]. Based on these reasons, therefore, this work aims to investigate the influence of severe condition on the activity of Cu ion-exchanged MFI. The effect of Pd on the stability improvement of the catalyst for NO removal under such severe condition was also studied.

2. Experimental

2.1 Catalyst Preparation

MFI zeolite with Si/Al ratio of 50 in Na form supplied by ALSI-PENTA ZEOLITE SM-55 was made by ion exchange with ammonium nitrate solution to obtain NH_4-MFI. It was then washed, dried and calcined at 540 °C for 3.5 h in air to convert it the protonated from (H-MFI), Cu ion-exchanged H-MFI and Pd ion -exchanged H-MFI, designated as Cu/H-MFI and Pd/H-MFI were prepared using an ion-exchange procedure at 80 °C and 90 °C, respectively. They were washed, dried and calcined at 540 °C for 3.5 h in air. For Pd/Cu/H-MFI, successive ion-exchange of H-MFI with palladium was made first and then copper was carried out using the method described above. The amount of palladium was varied in the range of 0.1-1 wt% Pd. In order to investigate the stability of the catalyst under severe condition, the catalysts were heated in a He stream while elevating the temperature from room temperature to 600 °C and 600 to 800 °C with

constant heating rate of 10 and 1.67 °C /min, respectively. The catalyst samples were then kept at 800 °C for 12 h while adding 10 mol% of water vapor. The catalysts were then cooled down to room temperature in the He stream. The catalysts thus obtained were in powder form, and were tableted, crushed and sieved to 12-22 mesh to provide the reaction.

2.2 Characterization

The bulk composition and BET surface area of the samples were measured by Inductively Coupled Plasma analysis (ICP JOBIN YVON model JY 2000 S) and surface area analyzer (ASAP 2000, Micromerities) using liquid nitrogen as a probe molecule, respectively. The crystallinity of MFI was estimated by using a SIEMENS D 5000 diffractometer with CuKα radiation. Quantitative analysis of tetrahedral alumina in zeolites was conducted by Al Magnetic Angle Spinning Nuclear Magnetic Resonance (^{27}Al MAS NMR). The ^{27}Al MAS NMR spectra were obtained using a BRUKER DPX-300 spectroscopy operating at 78.2 MHz. The morphology of the catalysts was observed using a Scanning Electron Microscope (JEOL, JSM-35). To determine the state of Cu^{2+} of catalysts, ESR measurements were obtained, an exact weight of catalyst was calcined at 500°C for 2 h. to remove adsorbed species.

2.3 Reaction Method and Analysis

The catalytic reaction test was performed using a tubular flow reactor at atmospheric pressure. A 0.25 g portion of the catalyst was packed into a quartz tube reactor of 6 mm.

inner diameter. It was heated from the ambient temperature to 600°C in a He flow at a constant heating rate of 10°C/min, and maintained at that temperature for 30 min. A feed gas composed of 1000 ppm NO, 1000 ppm n-C_8H_{18}, 2 mol% O_2 and 10 mol% H_2O balanced with He was then introduced into the reactor with a GHSV of 30,000 h^{-1}. Every 30 min, after the catalytic activity was at steady state, the effluent gas composition was analyzed using gas chromatographs (SHIMADZU GC-8ATP with MS-5A column and SHIMADZU GC-8AIT with porapak Q column) equipped with integrators. The reactor temperature was then cooled down from 600 to 200°C with a constant cooling rate of 10 °C/min. After every 50 °C drop in temperature effluent gas was analyzed using the same method. The catalytic activities of NO reduction and n-octane combustion were investigated as the amount of nitrogen and carbon oxides (CO_X: CO + CO_2) produced, respectively.

3. Results and discussion

3.1 Changes in Physical properties upon pretreatment

Table 1. shows the physical properties of the catalysts before and after pretreatment. Crystallinity, as determined by XRD profiles, was calculated using the intensity of diffraction line at 23.5° 2θ, which was compared with that of H-MFI as a reference. As shown in Table 1. H-MFI and Cu/H-MFI considerably lost their crystallinity after pretreatment due to the structural collapse. Such tendency of lost in crystallinity and BET surface area was reduced with the presence of Pd, and no significant lost of

crystallinity was observed on Pd/Cu/H-MFI catalysts with amount of Pd up to 0.2% or more. This suggests the stabilization effect of Pd on MFI framework structure. It should be noted that though some lost of structure occurred after pretreatment particularly the catalysts without Pd, the content of Cu or Pd loaded was not significantly affected by the pretreatment as can be seen from the ICP data. This indicated that there was no significant loss of metal species such as evaporation of metal due to the hydrothermal treatment. The result of ^{27}Al MAS NMR of the catalysts before and after pretreatment is shown in Fig. 1. The fresh catalysts exhibited only one sharp signal at ca. 50 ppm, which is assigned to the tetrahedral aluminum in the zeolite lattice [26-28]. Hydrothermal treatment of H-MFI, Cu/H-MFI and 0.1% Pd/ Cu/ H-MFI at 800 °C caused the appearance of a new ^{27}Al MAS NMR signal at 0 ppm assigned to extra-framework Al atoms in octahedral coordination [26-28]. This is consistent with the report somewhere else of loss in activity and stability after steam pretreatment due to framework dealumination of the zeolite [27]. However, only one signal of ^{27}Al MAS NMR at around 50 ppm was observed on Pd/Cu/H-MFI with the amount of Pd 0.3% or higher even after pretreatment and no peak relating to octahedral aluminum was noticed. This suggests that the presence of a certain amount of Pd, approximately 0.3% loading as observed here, could stabilize the MFI framework structure by preventing the occurrence of dealumination.

Figure 2.1-2.4. shows the ESR spectra of Cu/H-MFI and 0.3% Pd/Cu/H-MFI. The spectra of both fresh catalysts were similar in shape which indicated the presence of two Cu^{2+} species located in two different coordination (i.e. a square pyramidal environment

with $g_{\|} = 2.31\text{-}2.33$, $A_{\|} = 149$ G (Cu^{A}) and a square planar one with $g_{\|} = 2.27\text{-}2.29$, $A_{\|} \sim$ 157 G (Cu^{B})), as is typically found in the literature [29-32]. Shelef [33] proposed that Cu^{2+} in a square planar configuration is very active for NO removal. Since the features of the Cu^{2+} species were the same for fresh Cu/H-MFI and fresh 0.3%Pd/Cu/H-MFI. it can be suggested that Pd does not have an impact on the configuration of Cu. In addition. the 0.3% Pd/Cu/H-MFI after pretreatment exhibited the same ESR features as the fresh one. Nevertheless, the ESR spectra of pretreated Cu/H-MFI and 0.1%Pd/Cu/H-MFI were different from those of the fresh one. The pretreated Cu/H-MFI and 0.1%Pd/Cu/H-MFI not only lost the intensity of the ESR spectra, but the shape of signal also changed. This means that the amount of Cu^{2+} species in both the square pyramidal and square planar coordination was diminished due to pretreatment. Additionally, a new spectrum with $g_{\|} = 2.30$, $A_{\|} = 160$ G (Cu^{C}) appeared indicating a change in the coordination of Cu^{2-} although part of the two old Cu^{2+} species remained. This new signal may be attributed to the migration of Cu ions to the locations near 5-membered oxygen rings as suggested by Iwamoto et al. [34]. On the other hand, the pretreated catalysts with 0.8-1.0 wt.% Pd *loading did not* show any change of coordinated Cu^{2+} species; however some lost of the intensity of ESR has been observed. This means that the amounts of two Cu^{2+} species in both square pyramidal and square planar coordination are diminished due to some change in Pd and Cu on H-MFI such as alloying and/or oxides formation.

The scanning electron micrographs (SEM) of the catalysts before and after hydrothermal treatment are shown in Fig.3.1-3.2. Cu/H-MFI showed an obvious agglomeration after pretreatment. As or Pd/Cu/H-MFI, such agglomeration seems to be

prevented considerably especially for the samples with the Pd loading amount ranging between 0.3 to 0.6%. However, the larger crystallite size was clearly observed on the samples with Pd loading amount 0.8 and 1.0%. This suggests that there should be some change in the Pd and Cu on the H-MFI, such as alloying, due to the hydrothermal treatment provided that the amount of Pd present is higher than a certain level. It is interesting to note that an optimum amount of Pd is necessary to stabilize the crystal morphology of Cu/H-MFI subjected to hydrothermal treatment the temperature as high as 800 °C.

3.2 Catalytic Performance

NO conversion reactions were carried out on the catalysts both with and without pretreatment. The effect of reaction temperature on NO conversion to N_2 for Cu/H-MFI and Pd/Cu/H-MFI with different amount of Pd is shown in Fig.4. The conversion of n-octane to carbon oxides (CO and CO_2) is also demonstrated. It has been found that the conversion of NO markedly decreased at any reaction temperatures after hydrothermal treatment. However, the margin difference in catalyst activity before and after pretreatment was alleviated with the presence of a certain amount of Pd (ca. 0.2-0.3% loading). When the amount of Pd was raised higher than 0.3%, such beneficial effect on the stabilization of Cu/H-MFI was surprisingly lost. As for the conversion of n-octane to carbon oxides shown in Fig. 5, Cu/H-MFI also exhibited a substantial decrease in n-octane conversion upon pretreatment. The presence of Pd improved the n-octane

conversion of the pretreated catalysts similar to NO conversion. Nevertheless, while the improvement of NO conversion for the pretreated catalysts was limited by a certain amount of Pd present, the n-octane conversion was almost continuously improved with the increasing amount of Pd. Pd/Cu/H-MFI catalysts with 0.8 and 1.0% loading of Pd, in particular, exerted more or less conversion of n-octane at the reaction temperatures higher than 400 °C after hydrothermal treatment. This indicates that n-octane would not be effective for use in NO conversion Pd/Cu/H-MFI with the high loading amount of Pd. Therefore, this should be one of the reasons for the limitation of NO conversion improvement on Pd/Cu/H-MFI after hydrothermal treatment by an optimum amount of Pd. In addition, the possibility of any changes in Pd and Cu on H-MFI such as alloying and/or the formation of palladium oxides in case of high loading amount of Pd should not be ruled out.

4. Conclusion

The MFI framework stability of Cu/H-MFI was maintained after pretreatment at 800 °C in a He stream with 10 mol% H_2O by the presence of Pd. The dealumination of tetrahedral Al in MFI framework was completely prevented when the amount of Pd loading was 0.3% or higher. The stabilization effects of Pd are due to the prevention of dealumination and the ability to maintain the active Cu^{2+} species. The optimum amount of Pd, approximately 0.2-0.3% loading, present in Pd/Cu/H-MFI improved the catalysts stability for NO removal under hydrothermal treatment conditions as concluded in Fig. 6.

Further loading of Pd higher than 0.3% may cause some changes in Pd and Cu on H-MFI, such as alloying and/or palladium oxides formation, leading to some lost of Cu^{2-} active species for NO removal. This results in the limitation of NO conversion improvement for the pretreated Pd/Cu/H-MFI with the loading amount of Pd higher than approximately 0.3%.

Acknowledgement

The authors wish to express their deep appreciation to the Thailand Research Fund (TRF) for the financial support to this work.

References

1. Impens, R., Stud. Surf. Sci. Catal., 1987, 30, 11.
2. Iwamoto, M., Yahiro, H., Tanda, K., Mizuno, N., Mine, Y. and Kagawa, S., J. Phys. Chem., 1991, 95, 3727.
3. Iwamoto, M., Yahiro, H., Mizuno, N., Zhang, W., Mine, Y., Furukawa, H. and Kagawa, S., J. Phys. Chem., 1992, 96, 9360.
4. Burch, R., Scire, S., Appl. Catal. B, 1994, 3, 295.
5. Yogo, K., Tanaka, S., Ihara, M., Hishiki, T. and Kikuchi, E., Chem. Lett., 1992, 1025.
6. Tabata, T., Kokitsu, M. and Okada, O., Appl. Catal. B, 1993, 2, L1.
7. Iwamoto, M., Yahiro, H., Shundo, S., Yu, Y. and Mizuno, N., Appl. Catal., 1991,69, L15.

8. Sato, S., Hirabayashi, H., Yahiro, H., Mizuno, N. and Iwamoto, M., Catal. Lett., 1992,12, 193.

9. Li, Y. and Armor, J. N., Appl. Catal. B, 1993,2, 239.

10. Li, Y. and Armor, J. N., Appl. Catal. B, 1993,3, 55.

11. Aylor, A.W., Lobree, L. J., Reimer, J. A. and Bell, A. T., Stud. Surf. Sci. Catal., 1996, 101, 661.

12. Yokoyama, C. and Misuno, M., Catal. Lett., 1994, 29, 1.

13. Kintaichi, Y., Hamada, H., Tabata, M., Sasaki M. and Ito T., Catal. Lett., 1990, 6, 239.

14. Hirabayashi, H., Yahiro, H., Mizuno, N. and Iwamoto, M., Chem. Lett., 1992, 2235.

15. Hamada, H., Kintaichi, Y., Sasaki, M., Ito, T., Appl. Catal., 1990, 64, L1.

16. Tabata, M., Tsuchida, H., Miyamoto, K., Yoshinari, T., Yamazaki, H., Hamada, H., Kintaichi Y., Sasaki, M. and Ito, T., Appl. Catal. B, 1995, 6, 169.

17. Hamada, H., Kintaichi, Y., Sasaki, M., Ito, T. and Tabata, M., Appl. Catal., 1991, 75, L1.

18. Miyadera, T., Appl. Catal. B, 1993, 2, 199.

19. Ukisu, Y., Sato, S., Abe, A. and Yoshida, K., Appl. Catal. B, 1993, 2, 147.

20. Burch, R., Ramli, A., Appl. Catal. B, 1998, 15, 49.

21. Kharas, K.C.C., Robota, H. J. and Liu, D. J., Appl. Catal. B, 1993, 2, 225.

22. Martinez, A., Gomez, S. A. and Fuentes, G. A., Catalyst Deactivation, 1997, 225.

23. Burch, R., Scire, S., Appl. Catal. B, 1994, 3, 295.

24. Burch, R., Ramli, A., Appl. Catal. B, 1998, 15, 49.

25. Hirabayashi, H., Yahiro, H., Mizuno, N. and Iwamoto, M., Chem. Lett., 1992, 2235.

26. Tanabe, T., Iijima, T., Kaiwai, A., Mizuno, J., Yokota, K. and Isogai, A., Appl. Catal. B, 1995, 6, 145.

27. Budi, P., Hyde, E. C. and Howe, R. F., Catal. Lett., 1996, 41, 47.

28. Tanabe, T., Kokitsu, M., Okada, O., Nakayama, T., Yasumatsu, T. and Sakane, H., Stud. Surf. Sci. Catal., 1994, 88, 409.

29. Matsumoto, S., Yokota, K., Doi, H., Kimura, M., Sekizawa, K. and Kasahara, S., Catal. Today, 1994, 22, 127.

30. Grunert, W., Hayes, N. W., Joyner, R. W., Shpiro, E. S., Siddiqui, M. R. H. and Baeva, N., J. Phys. Chem., 1994, 98, 10832.

31. Kucherov, A. V., Shigapov, A. N., Ivanov, A. A. and Shelef, M., J. Catal., 1999, 186, 334.

32. Tapanee, D., Piyasan, P., Kim, J. B., Inui, T., Advances in Environmental Research, 2000, 3, 450.

33. Shelef M., Catal. Lett., 1992, 15, 305.

34. Iwamoto, M., Wang, J., Sperati, K. M., Sajaki, T., and Misono, M., Chem. Lett., 1997, 1281.

Table 1. Data for bulk composition, BET surface and crystallinity of catalysts

Catalyst	BET surface area (m^2 /g. catalyst)		Me/Al atomic ratio		Me/Al atomic ratio		Crystallinity[a] (%)	
			Cu/Al		Pd/Al			
	fresh	severe steamed	fresh	severe steamed	fresh	severe steamed	fresh	severe steamed
H-ZSM-5	350	295	-	-	-	-	100	48
Cu/HZSM-5	326	286	0.911	0.913	-	-	100	85
0.1% Pd/Cu/HZSM-5	310	275	0.890	0.892	0.012	0.012	99	87
0.2% Pd/Cu/HZSM-5	310	289	0.901	0.892	0.023	0.022	99	97
0.3% Pd/Cu/HZSM-5	302	290	0.865	0.863	0.035	0.034	99	98
0.4% Pd/Cu/HZSM-5	300	289	0.864	0.860	0.042	0.048	98	98
0.6% Pd/Cu/HZSM-5	298	280	0.849	0.850	0.072	0.074	97	98
0.8% Pd/Cu/HZSM-5	298	288	0.827	0.824	0.088	0.089	97	97
1.0% Pd/Cu/HZSM-5	298	286	0.821	0.821	0.112	0.110	98	97

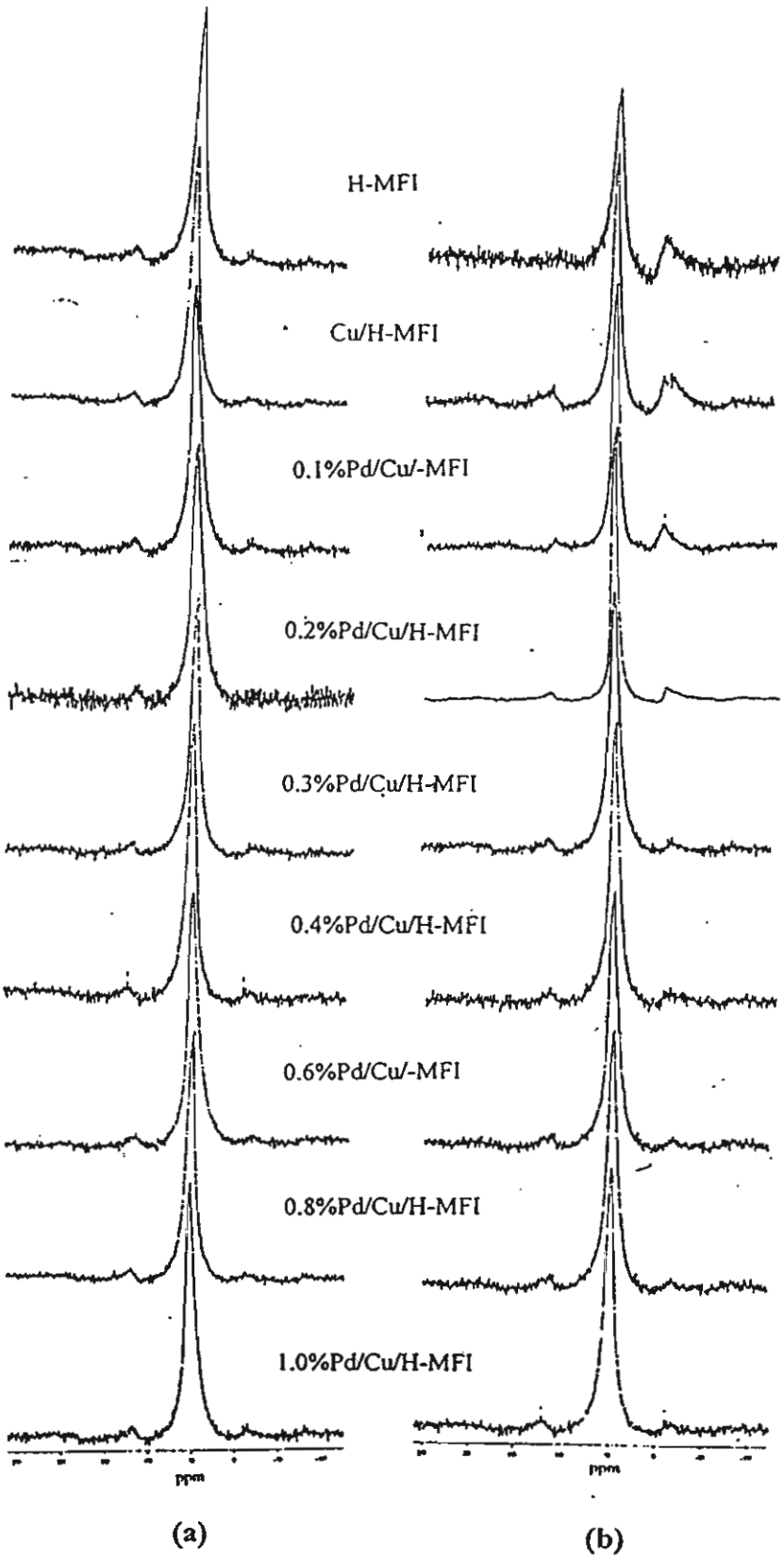
H-MFI
Cu/H-MFI
0.1%Pd/Cu/-MFI
0.2%Pd/Cu/H-MFI
0.3%Pd/Cu/H-MFI
0.4%Pd/Cu/H-MFI
0.6%Pd/Cu/-MFI
0.8%Pd/Cu/H-MFI
1.0%Pd/Cu/H-MFI
ppm
ppm
(a)
(b)

Figure 1.

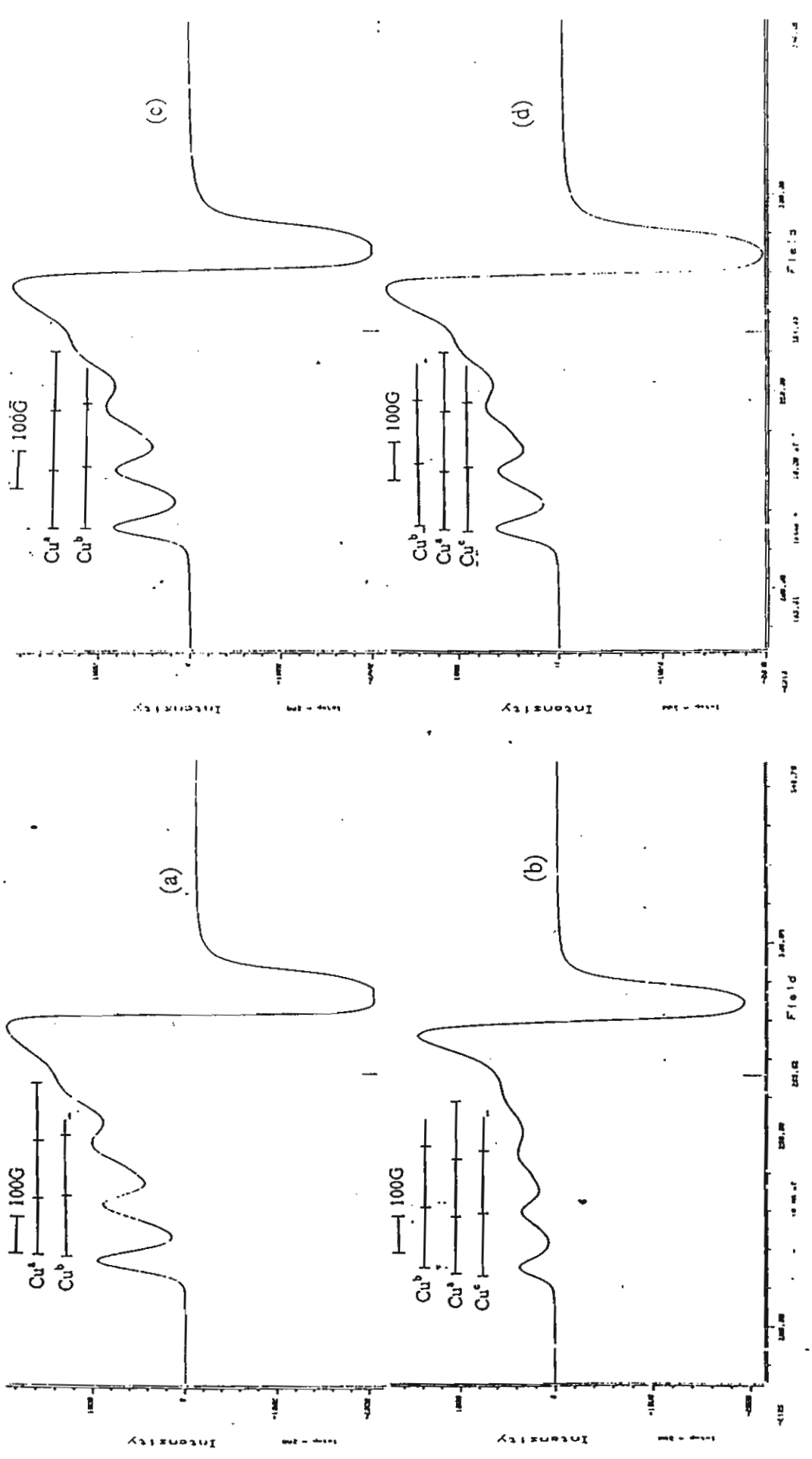

Figure 2.1

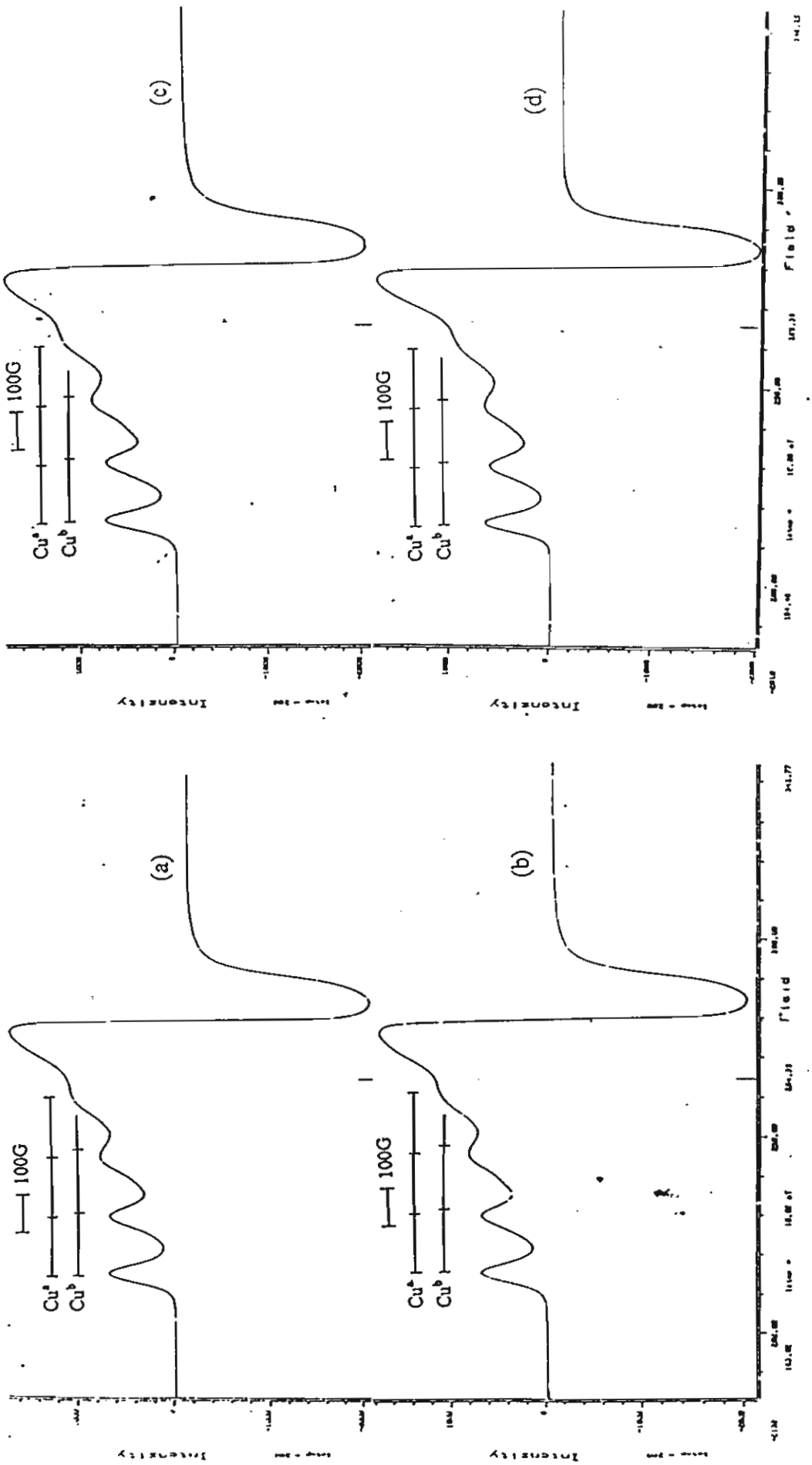

Figure 2.2

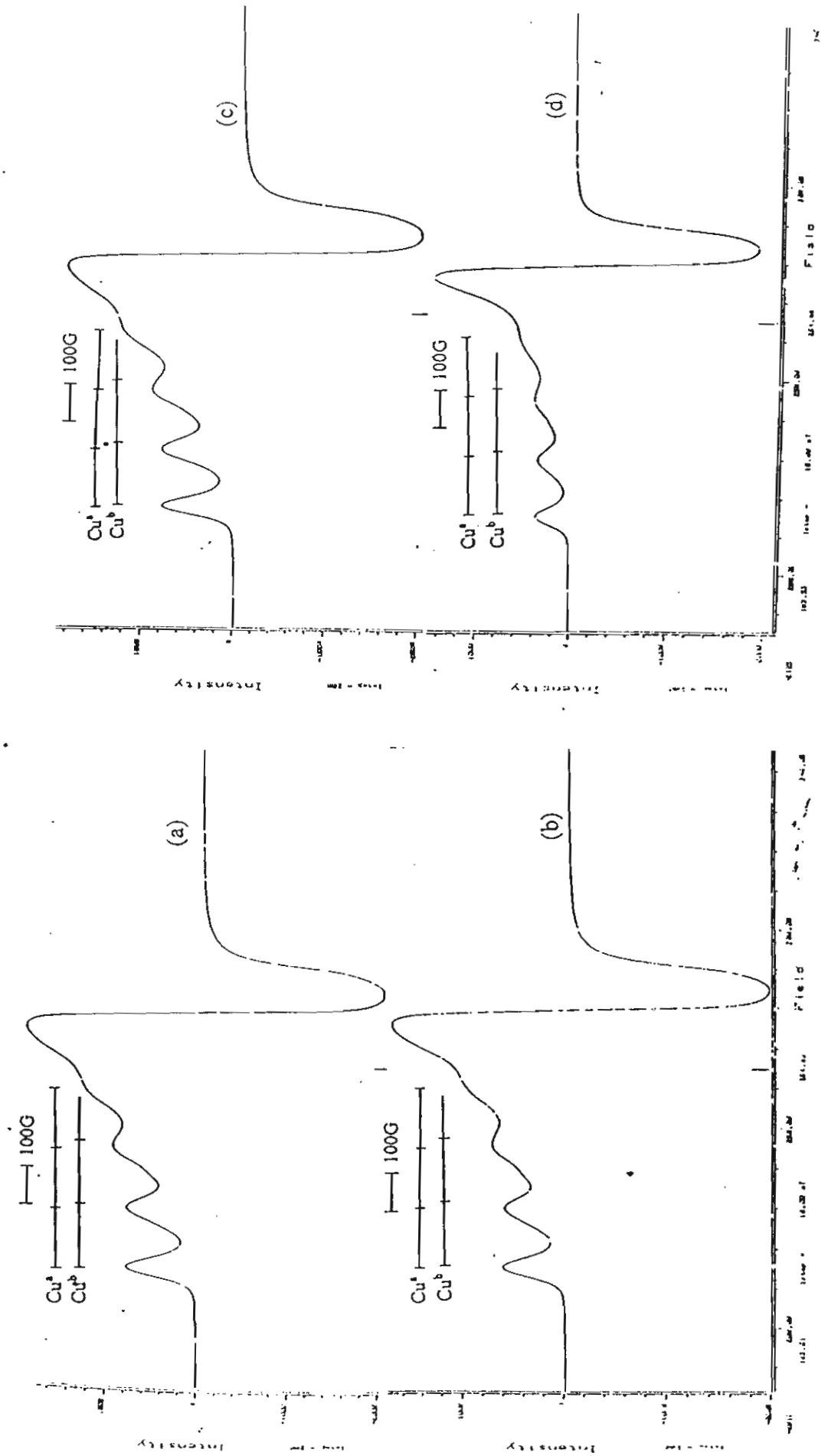

Figure 2.3

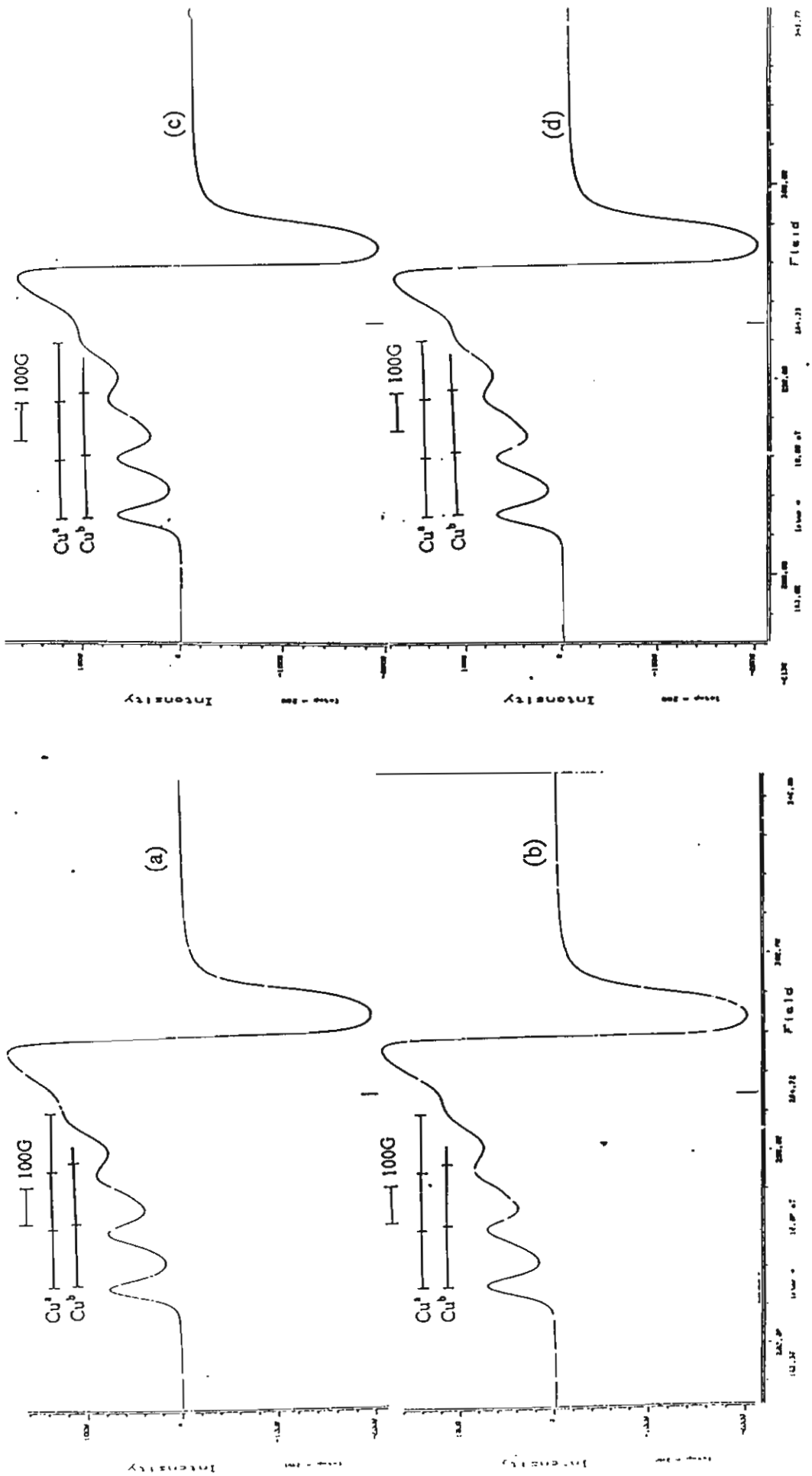

Figure 2.4

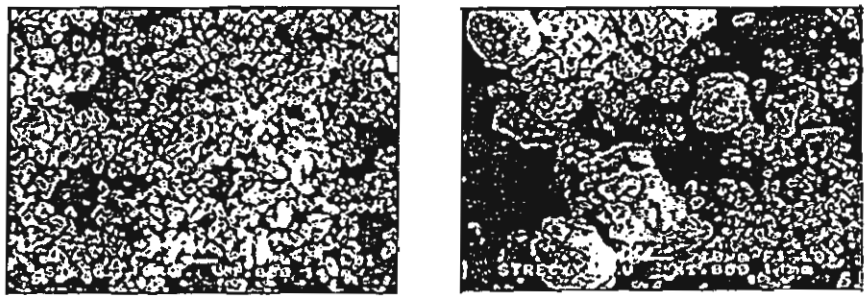

Cu/H-MFI

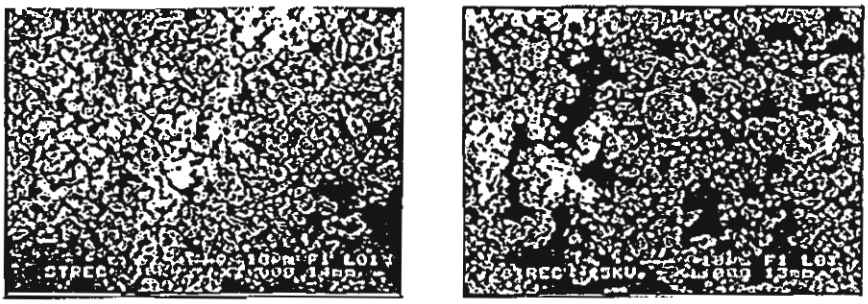

0.1%Pd/Cu/-MFI

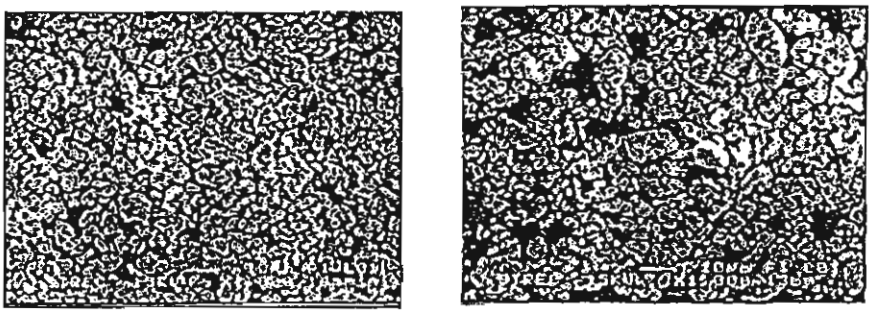

0.2%Pd/Cu/H-MFI

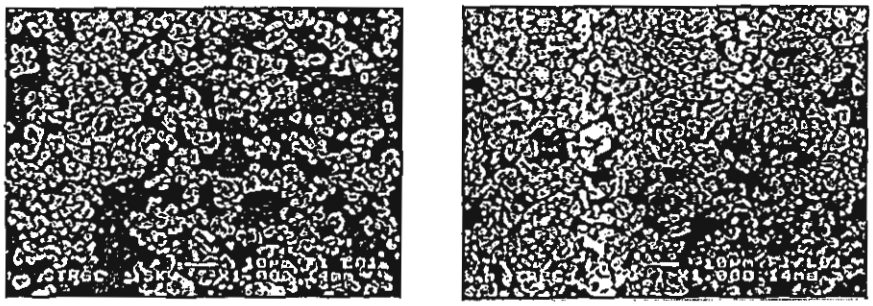

0.3%Pd/Cu/H-MFI

(a) (b)

Figure 3.1

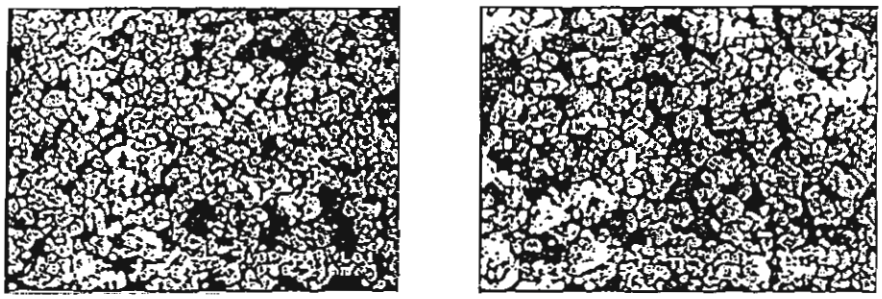

0.4%Pd/Cu/H-MFI

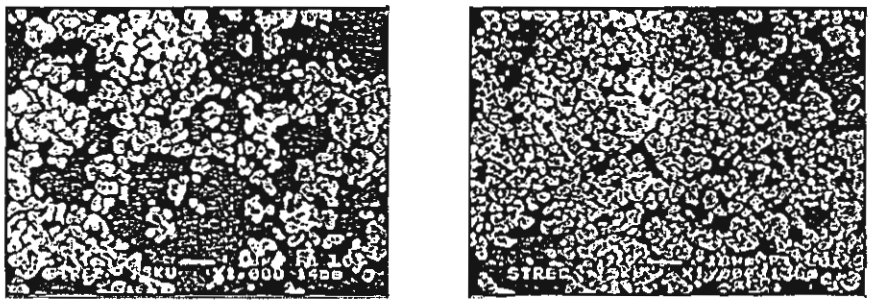

0.6%Pd/Cu/-MFI

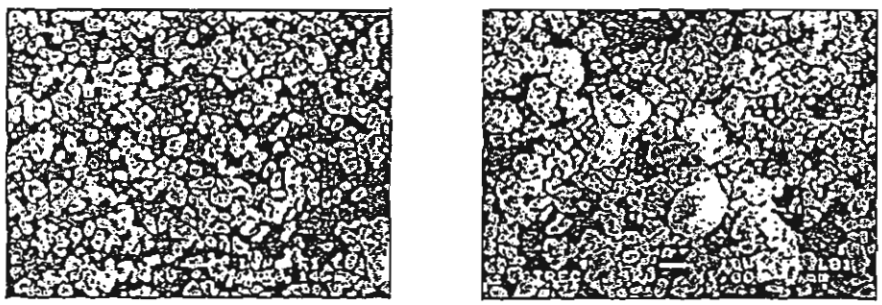

0.8%Pd/Cu/H-MFI

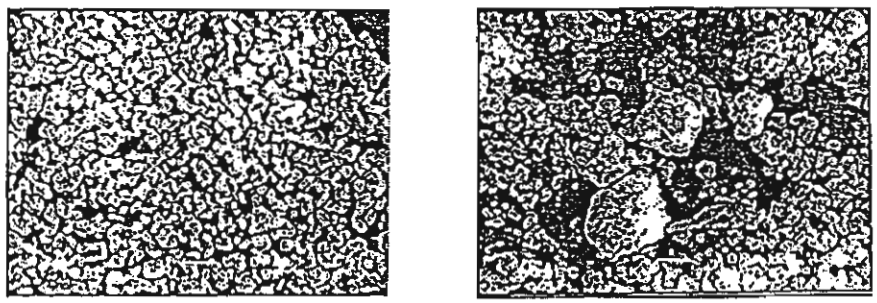

1.0%Pd/Cu/H-MFI

(a) (b)

Figure 3.2

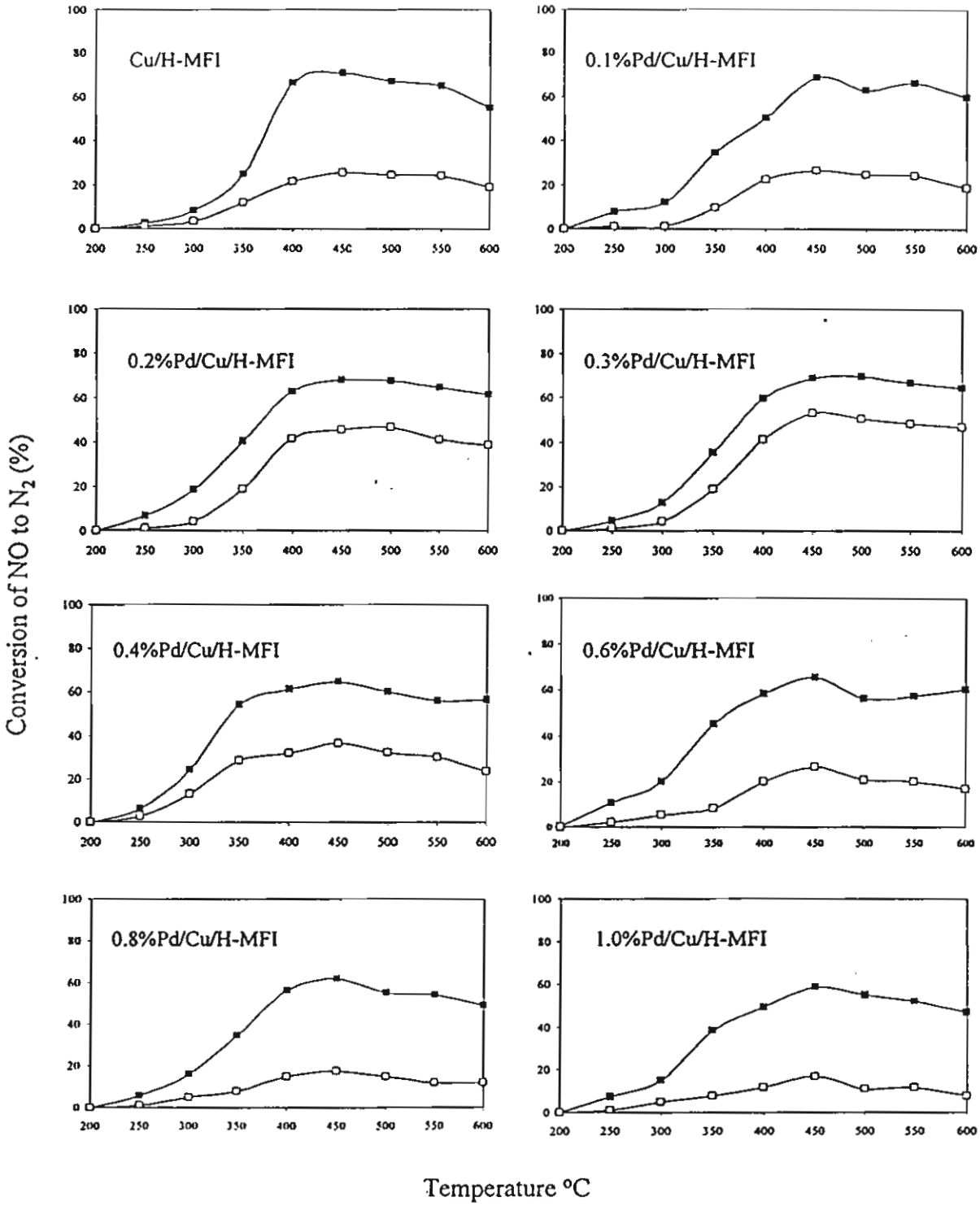
Cu/H-MFI
0.1%Pd/Cu/H-MFI
0.2%Pd/Cu/H-MFI
0.3%Pd/Cu/H-MFI
0.4%Pd/Cu/H-MFI
0.6%Pd/Cu/H-MFI
0.8%Pd/Cu/H-MFI
1.0%Pd/Cu/H-MFI
Conversion of NO to N_2 (%)
Temperature °C

Figure 4

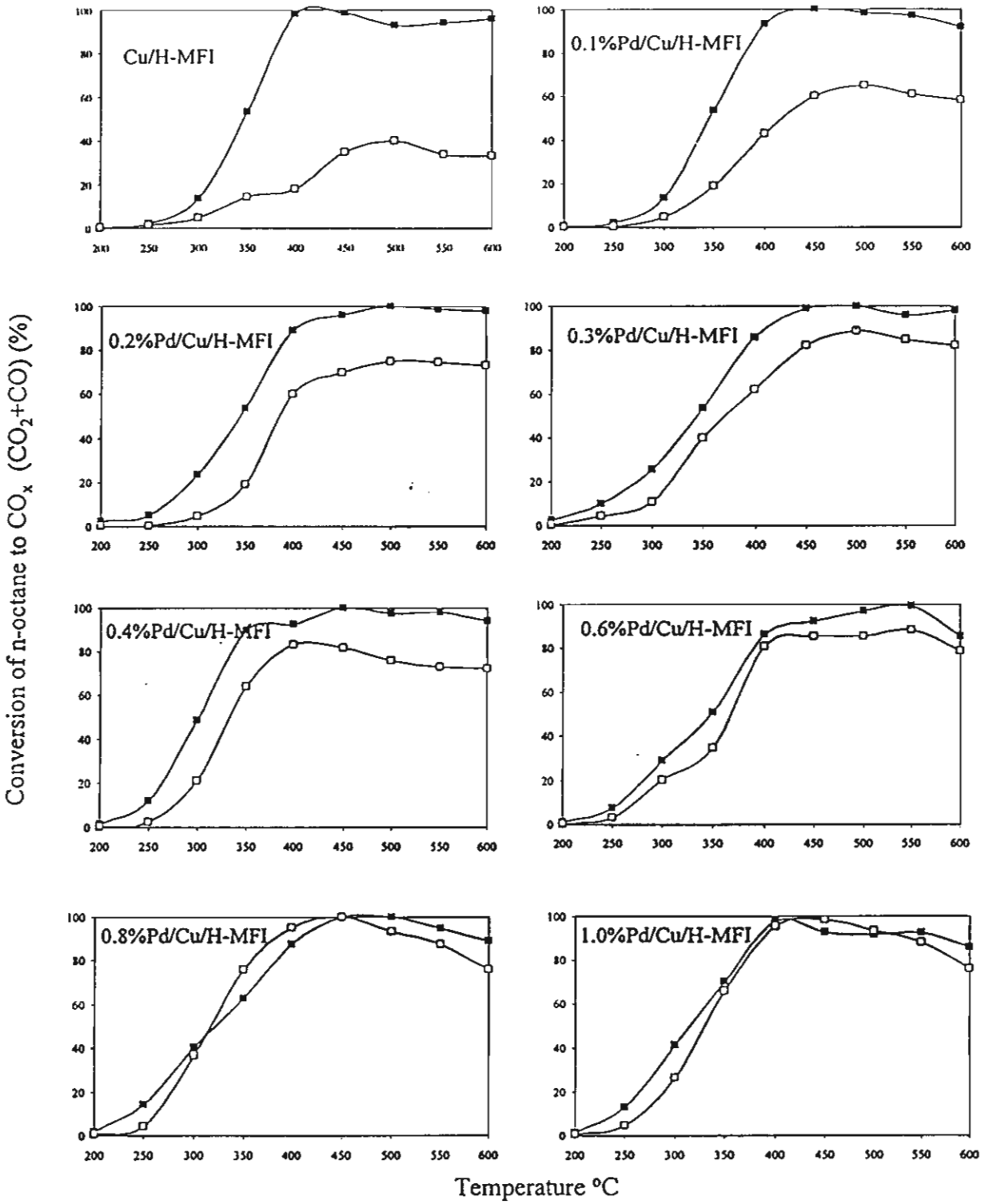
Cu/H-MFI
0.1%Pd/Cu/H-MFI
0.2%Pd/Cu/H-MFI
0.3%Pd/Cu/H-MFI
0.4%Pd/Cu/H-MFI
0.6%Pd/Cu/H-MFI
0.8%Pd/Cu/H-MFI
1.0%Pd/Cu/H-MFI
Conversion of n-octane to CO_x (CO_2+CO) (%)
Temperature °C

Figure 5

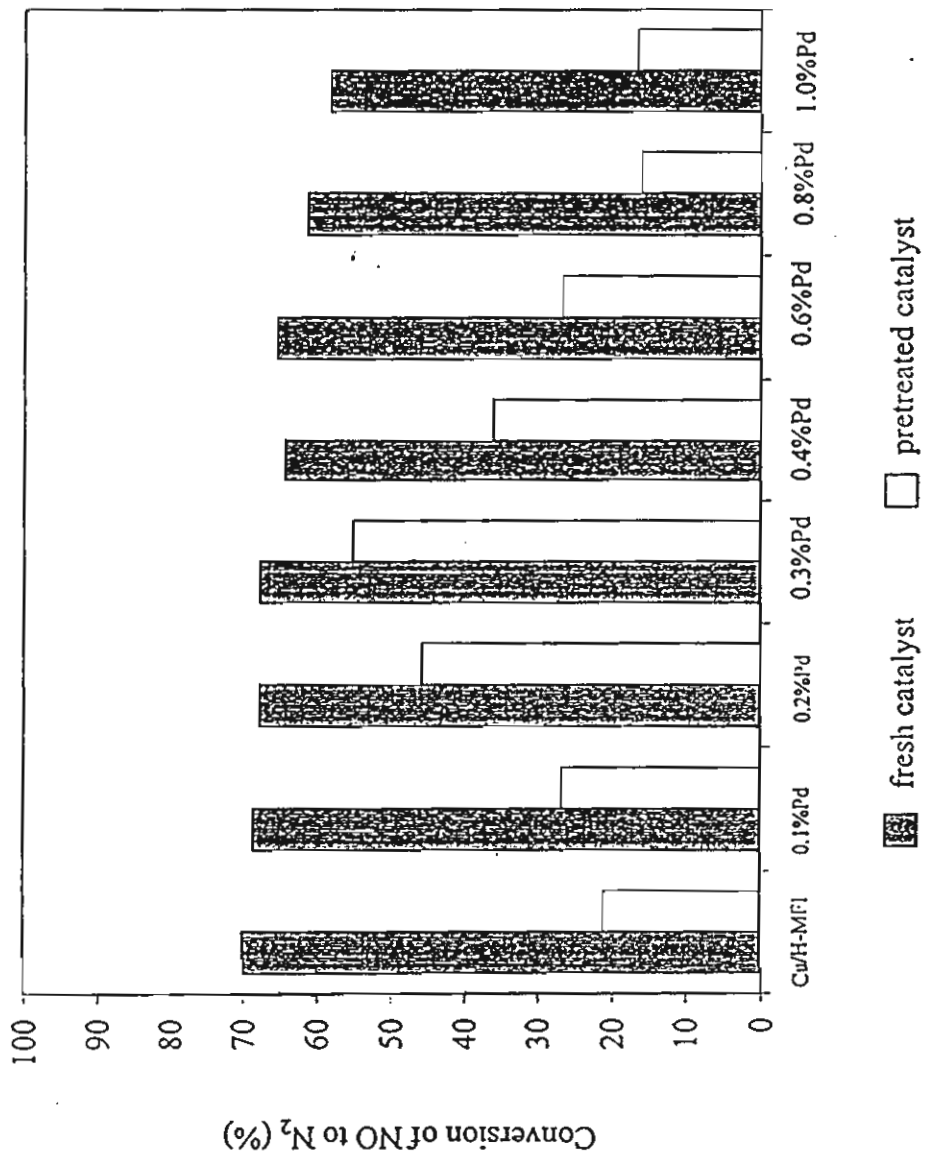
Conversion of NO to N_2 (%)
100
90
80
70
60
50
40
30
20
10
0
Cu/H-MFI
0.1%Pd
0.2%Pd
0.3%Pd
0.4%Pd
0.6%Pd
0.8%Pd
1.0%Pd
fresh catalyst
pretreated catalyst

Figure 6

Table 1. Data for bulk composition, BET surface area and crystallinity of catalysts

Figure 1 ^{27}Al MAS-NMR spectra of fresh (a) and severe steamed (b) catalysts.

Figure 2.1 ESR spectra of high spin Cu^{2+} of Cu/H-MFI and Pd/Cu/H-MFI with and without pretreatment at 800°C 10% H_2O a) fresh Cu/H-MFI, b) severe steamed Cu/H-MFI, c) fresh 0.1%Pd/Cu/H-MFI, d) severe steamed 0.1%Pd/Cu/H-MFI

Figure 2.2 ESR spectra of high spin Cu^{2+} of Cu/H-MFI and Pd/Cu/H-MFI with and without pretreatment at 800°C 10% H_2O a) fresh 0.2%Pd/Cu/H-MFI, b) severe steamed 0.2%Pd/Cu/H-MFI, c) fresh 0.3% Pd/Cu/H-MFI, d) severe steamed 0.3%Pd/Cu/H-MFI

Figure 2.3 ESR spectra of high spin Cu^{2+} of Cu/H-MFI and Pd/Cu/H-MFI with and without pretreatment at 800°C 10% H_2O a) fresh 0.4%Pd/Cu/H-MFI, b) severe steamed 0.4%Pd/Cu/H-MFI, c) fresh 0.6% Pd/Cu/H-MFI, d) severe steamed 0.6%Pd/Cu/H-MFI

Figure 2.4 ESR spectra of high spin Cu^{2+} of Cu/H-MFI and Pd/Cu/H-MFI with and without pretreatment at 800°C 10% H_2O a) fresh 0.8%Pd/Cu/H-MFI, b) severe steamed 0.8%Pd/Cu/H-MFI, c) fresh 1.0% Pd/Cu/H-MFI, d) severe steamed 1.0%Pd/Cu/H-MFI

Figure 3.1 Scanning electron micrograph of catalysts.(a) fresh and (b) severe steamed catalysts

Figure 3.2 Scanning electron micrograph of catalysts.(a) fresh and (b) severe steamed catalysts

Figure 4 The effect of hydrothermal-treatment on the activity of NO conversion of Cu/H-MFI, Pd/Cu/H-MFI. Close symbol: fresh catalysts, Open symbol: pretreated catalysts

Figure 5 The effect of hydrothermal-treatment on the activity of n-Octane conversion of Cu/H-MFI, Pd/Cu/H-MFI. Close symbol: fresh catalysts, Open symbol: pretreated catalysts

Figure 6 Maximum NO conversion of catalysts

Isomerization of n-Hexane over Platinum Ion-Exchanged Zeolite Beta

*S. Phatanasri, P. Praserthdam, S. Kularbkeaw , and S. Panichsarn

Petrochemical Engineering Laboratory, Department of Chemical Engineering, Faculty of Engineering, Chulalongkorn University, Bangkok 10330, Thailand Tel: +(662) 218-6890 Fax: +(662) 218-6877

Abstract - Zeolite Beta was synthesized from appropriate gels and crystallized under the controlled temperature and pressurized conditions. For isomerization of n-hexane, platinum ion-exchanged zeolite Beta exhibited high activity and selectivity for 2,2-Dimethylbutane (2,2-DMB), 2,3-dimethylbutane (2,3-DMB), 2-Methylpentane (2-MP) and 3-Methylpentane (3-MP). As high as 72% of n-hexane conversion and 98% of product selectivity were obtained at 250°C, 1600 h^{-1} for 20 min on stream. The influences of reaction temperature, space velocity, as well as the catalyst stability were also studied. Pt/H-Beta zeolite was recommended as one of the promising catalyst for n-hexane isomerization due to its high activity and stability. The combined effect of the stronger acidity possessed by H-Beta and the dehydrogenation role played by Pt was believed to be responsible for the good catalytic performance of Pt/H-Beta.

Key word: isomerization, n-hexane, zeolite beta, Pt-ion-exchanged zeolite beta

INTRODUCTION

Zeolite Beta is a 12-member ring (12MR) tridirectional zeolite, with two different types of channels having about 7.0 and 5.5 A°[1]. It can be synthesized within a wide range of silica-to-alumina ratio (12-200) [2]. This zeolite may offer interesting opportunities as a catalyst for the isomerization and transalkylation of xylenes[2,3], the alkylation of

* To whom correspondence should be made

toluene by methanol[4], and the condensation of benzene and formaldehyde[5]. Furthermore, the isomerization processes were run over bifunctional zeolite Beta consisting of highly dispersed metals[2,3].

Therefore, this work aims to investigate the synthesis of zeolite Beta and the performance of zeolite Beta for isomerization of n-hexane.

EXPERIMENTAL

Catalyst Preparation

Zeolite Beta was synthesized by hydrothermal technique under autogenous pressure following the procedure reported earlier [1]. The synthesis batch consists of K_2O : $2Na_2O$: 12.5 $(TEA)_2O$: $0.5Al_2O_3$: $40SiO_2$: $700H_2O$: 0-3HCl.

The crystallization period was for 40 hours at 135°C. After the crystallization the solid material thus obtained was separated by centrifugation and decantation, dried in an oven at 110°C overnight. The as-synthesized zeolite Beta was calcined at 773 K and repeatedly ion exchanged with 1 M ammonium nitrate solution. Another calcination again at 773 K converted the NH_4-Beta to its proton form, H-Beta. The Pt ion-exchange was conducted by adding 1 g of catalyst in 40 ml of distilled water. The mixture was heated from room temperature to 98°C, then $Pt(NH_3)_4Cl_2$ solution was added into the mixture and heated at 98°C for additional 6 h. The sample was dried overnight at 110 °C. Dry crystals were heated to 350°C in 50 ml/min of air stream with a constant heating rate of 3°C/min and maintained at that temperature for 10 min. The amount of Pt loading in the catalyst was 0.6 wt%. The catalysts were tableted, crushed and sieved to the range of 8-16 mesh to provide the reaction.

APPARATUS AND REACTION METHOD

The isomerization of n-hexane was carried out by using a conventional flow tubular reactor. A 0.3 g portion of the catalyst was packed in the quartz tubular reactor. The reaction was carried out under the following conditions: atmospheric pressure; gas hourly space velocities (GSHV), 380-3200 h^{-1}; reaction temperatures, 150-350°C.

RESULTS AND DISCUSSION

Effect of reaction temperatures

The reaction temperatures of n-hexane conversion were varied as 150, 200, 250, 300 and 350°C. The reaction was carried out over Pt/H-Beta (Si/Al = 40, 0.6%wt Pt loaded by ion exchange) at GHSV of 650 h^{-1} for 20 min on stream by using hydrogen as carrier gas.

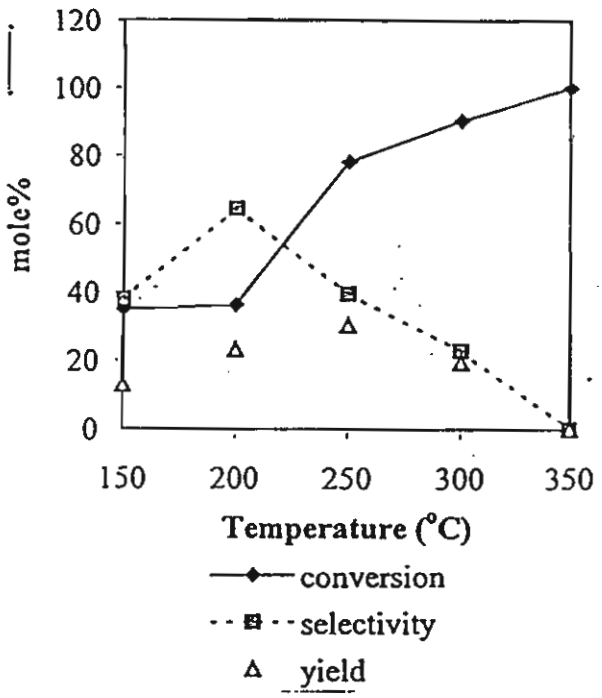

Fig.1 Isomerizationof n-hexane on Pt/H-Beta at various temperatures reaction conditions: 650 h^{-1}, 20 min on stream.

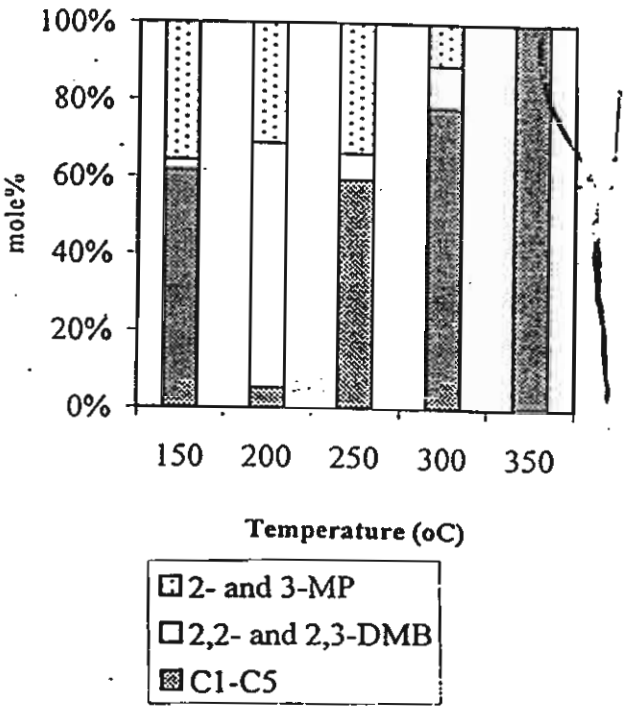

Fig.2 Product distribution of n-hexane isomerization of Pt/H-Beta.

The conversion and selectivity of n-hexane isomerization are shown in Figs. 1 and 2. It has been found that the hexane conversion increased with the increasing temperature and nearly complete conversion was obtained at 350°C. The isomers selectivity (2,2-DMB, 2,3-DMB, 2-MP, 3-MP) was high at the reaction temperatures of 200-250°C. The maximum yield, defined as the product of conversion and selectivity, was obtained at reaction temperature of 250°C. At temperatures higher than 250°C, much C_1-C_5 amount was formed probably due to the catalytic cracking.

Effect of GHSV

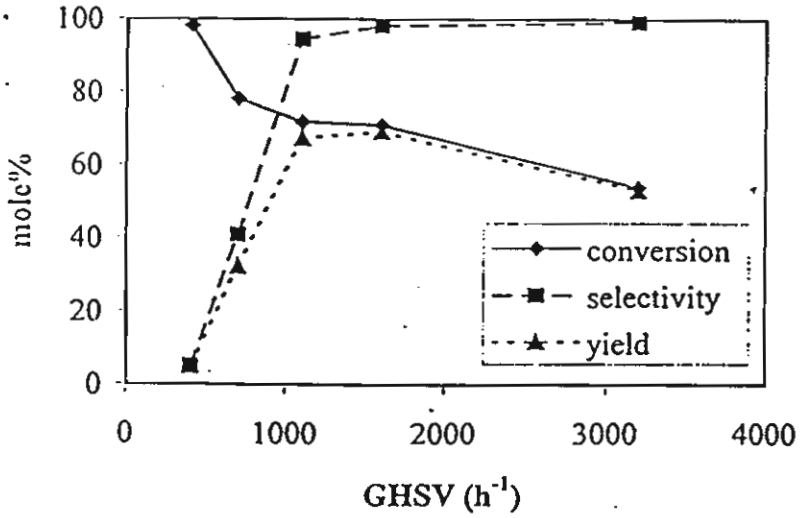

Fig.3 Isomerization of n-hexane on Pt/H-Beta at different space velocities reaction conditions: 250°C, 20 min on stream.

Figure 3 shows the conversion and selectivity of n-hexane isomerization over Pt/H-Beta with space velocities (GHSV) ranging from 400 to 3200h^{-1}. The reaction was carried out at 250°C for 20 minutes on stream by using hydrogen as carrier gas. At higher GHSV the contact time between hexane and catalyst was shortened and thus the conversion decreased; however, the amount of C_6 isomers (2,2-DMB, 2,3-DMB, 2-

MP, 3-MP) was markedly increased. It should be noted that at low GHSV especially 380 h^{-1}, the main product was C_1-C_5 fraction. It has been suggested that C_1-C_5 should be formed through catalytic cracking of C_6 isomer during the long contact time. Therefore at high GHSV, the formation of C_1-C_5 was substantially prevented and thus the high yield of isomer products was obtained.

Prolonged operation test

The catalyst stability was tested by prolonged operation at 250°C and GHSV of 1600 h^{-1} for 13 h as shown in Fig. 4. The conversion and selectivity of n-hexane isomerization were almost constant throughout the period. It has been generally accepted that Pt on the catalyst may act as hydrogen porthole to transfer hydrogen to the adsorbate species on the catalyst surface, and thus the coke formation was significantly suppressed.

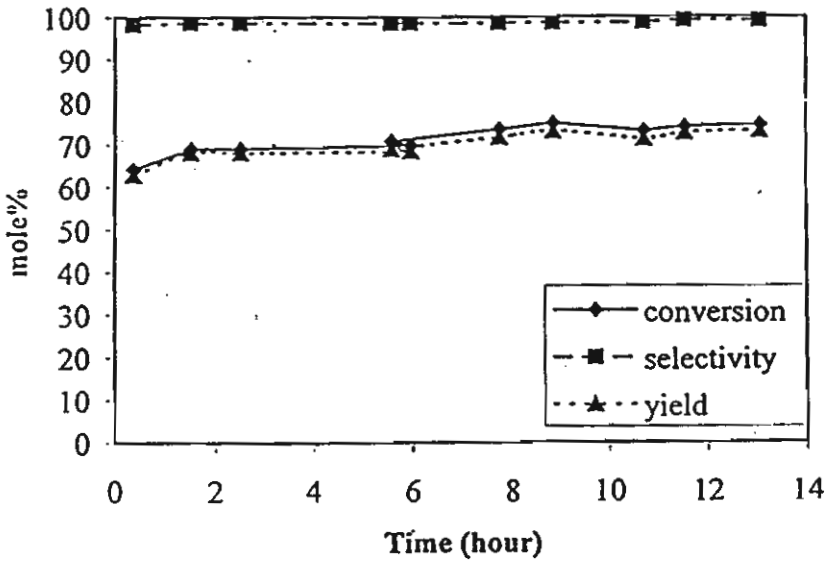

Fig.4 Prolonged operation of n-hexane isomerization on Pt/H-Beta
reaction conditions: 250°C, 1600 h^{-1}.

Comparison of Pt/H-Beta and Pt/H-Y

From Figs. 5 and 6, the conversion and selectivity of n-hexane isomerization was compared when using Pt/H-Beta and Pt/H-Y as the catalysts with the same amount of platinum loading (0.6%wt). It has been found that the Pt/H-Beta gave much higher conversion than did Pt/H-Y zeolite. It has been realized that Pt/H-Beta and Pt/H-Y have substantially

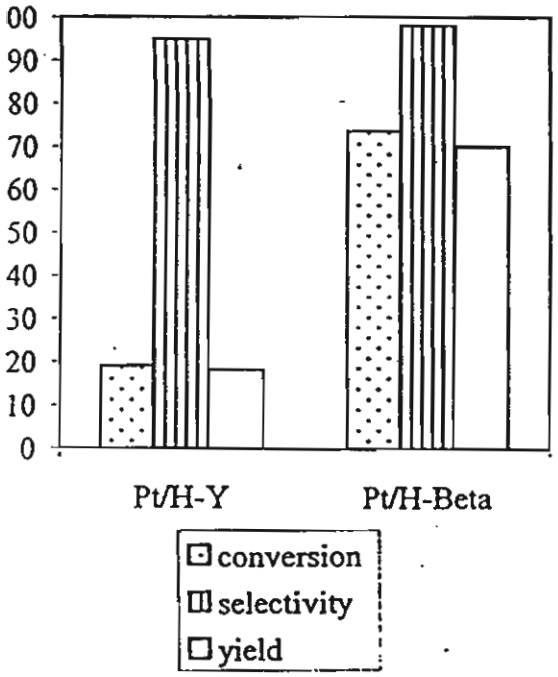

Fig. 5 Isomerization of n-hexane on Pt/H-Y and Pt/H-Beta
reaction conditions: 250°C, 1600 h^{-1}, 20 min on stream.

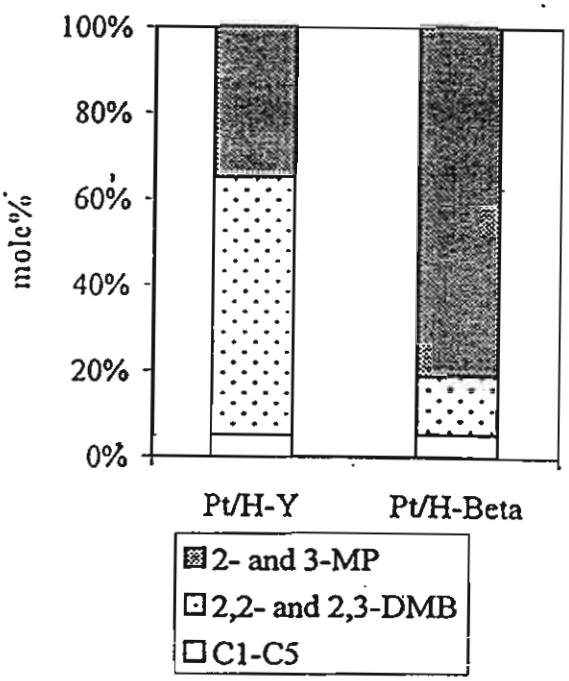

Fig.6 Product distribution of n-hexane isomerization on Pt/H-Y and Pt/H-Beta.

similar pore size and shape with the average pore diameters of 15.69 Å for Pt/H-Beta and 15.57 Å for Pt/H-Y [6,7]. To gain further insight, the pyridine adsorption technique on in-situ FTIR was adopted for the assessment of Brönsted and Lewis acidities. The bands at about 1540 cm^{-1} and 1450 cm^{-1}(not shown here) were reportedly assigned to pyridine adsorbed on Brönsted and Lewis acid sites, respectively [8,9,10]. The Brönsted and Lewis acid site concentrations, defined as A_B and A_L, of H-

Beta and H-Y were determined by measurement of peak areas of these bands at the reference temperature of 150°C while the relative acid strengths of Brönsted and Lewis types were determined by measurement of the temperature required for reduce a half of pyridine adsorbed, defined as $T_{B/2}$ and $T_{L/2}$, respectively. Thus, the higher temperature means the stronger acid strength. As shown in Table 1, H-Beta zeolite contains smaller amount of acid sites but stronger acid strengths than H-Y. Therefore, though the selectivities for C_6 isomers obtained on both catalysts were almost the same due to their similar pore size and shape, the stronger acidities possessed by Pt/H-Beta should be responsible for the higher n-hexane conversion.

Table 1: Brönsted and Lewis acidities on H-Beta and H-Y catalysts

Catalyst	A_B	A_L	$T_{B/2}$(°C)	$T_{L/2}$ (°C)
H-Beta	150.9	106.3	434.5	247.1
H-Y	206.0	287.4	369.3	156.3

CONCLUSIONS

Beta zeolite has been found to be a promising catalyst for n-hexane isomerization. The products obtained include 2,2-Dimethylbutane(2,2-DMB); 2,3-Dimethylbutane (2,3-DMB); 2-Methylpentane (2-MP); and 3-Methylpentane (3-MP). The optimum catalyst composition was zeolite Beta with Si/Al ratio of 40 loaded with 0.6 wt% of Pt by ion-exchange. The optimum reaction conditions were as follows: reaction temperature of 250°C; GHSV of 1600 h^{-1} with the presence of H_2.

ACKNOWLEDGEMENT

This research has been partly supported by the Thailand Research Fund (TRF). The authors would like to express their deep appreciation herein.

REFERENCES

1. R. L. Wadlinger, G. T. Keer, and E. J. Rosinski, US. Patent 3308069 (1967).
2. J. Perez-Pariente and E. Sastre: *Appl. Catal.*, **69**, 125 (1991).
3. P. Ratnasamy, R.N. Bhat, S.K. Pokhrrigal, S.G. Hegde, and R. Kumar: *J. Catal.*, 65, 199 (1989).
4. C. Marcilly, J. Deves, and F. Raatz, Eur. Pat. Appl., EP 278839 (1988).
5. M.J. Climent, A. Corma, H. Garcia, S. Iborra, and J. Primo, Heterogeneous Catalysis and Fine Chemicals II, *Studies in Surface Science and Catalysis*, **59**, 557 (1991).
6. Li-Jen Leu, L.Y. Hou, and B.C. Kang: *Appl. Catal.*, **69**, 49 (1991).
7. L. Beranek and M. Kraus, Comprehensive Chemical Kinetics (C.H., Banford and C.F.H., Tipper, eds.), VI. 20, Chapter 3, Elsevier, New York (1978).
8. J. Connerton, R. Joyner, and M. Padley: *J.C.S. Faraday*, **91**, 1841 (1995).
9. M. Campbell, M. Bibby, M. Coddington, F. Howe, and H. Meinhold: *J. Catal.*, **161**, 358 (1996).
10. H.G. Karge: *Microporous Materials*, **22**, 547 (1998).